Addis Ababa University

Addis Ababa Institute of Technology

School of Electrical and Computer Engineering

Electrical Power Engineering

MODELING OF GIRD CONNECTED SOLAR, WIND AND FUEL CELL DISTRIBUTED GENERATION UNITS AND POWER FLOW CONTROLLING SYSTEM FOR INTERFACING

(CASE STUDY: MODEL COMMUNITY IN ADAMA CITY)

A thesis Submitted to Addis Ababa Institute of Technology, School of Graduate Studies, Addis Ababa University In partial Fulfillment of the Requirement for the Degree of Master of Science in Electrical Engineering (Electrical Power Engineering)

By: GIRMA MOGES TADESSE

Under the Supervision of

Dr. GETACHEW BEKELE BEYENE

Addis Ababa, Ethiopia, **March 2018**

Addis Ababa University

Addis Ababa Institute of Technology

Department of Electrical and Computer Engineering

MODELING OF GIRD CONNECTED SOLAR, WIND AND FUEL CELL DISTRIBUTED GENERATION UNITS AND POWER FLOW CONTROLLING SYSTEM FOR INTERFACING

(CASE STUDY: MODEL COMMUNITY IN ADAMA CITY)

By: GIRMA MOGES TADESSE

APPROVED BY BOARD OF EXAMINERS

Mr. Dawit Habtu	_____	_____
Chairman, Department of Graduate Committee	Signature	Date
Dr.Getachew Bekele	_____	_____
Advisor	Signature	Date
Dr.Dereje Shiferaw	_____	_____
Internal Examiner	Signature	Date
Mr.Kiros Tesfay	_____	_____
External Examiner	Signature	Date

Declaration

I, the undersigned, declare that this thesis is my own work, has not been presented for fulfillment of a degree or otherwise in this or any other university, and all sources and materials used for the thesis have been acknowledged.

All Advisor's comments are duly incorporated.

Name: Girma Moges Tadesse

Signature: _____

Place: Addis Ababa

Date of submission: _____

This thesis has been submitted for examination as a university advisor.

Dr. Getachew Bekele Beyene _____

Advisor's Name Signature

Dedication

…To

all people who are supporting me in all aspects.

and

…to the following institutions

All Mertulemariam religious schools ,Alusha Primary School, Mertulemariam Secondary School, Adama science and technology University ,Dire Dawa University and Addis Ababa Institute of Technology.

Acknowledgement

First of all, I would like to thank the Almighty God and his mother for his provision of Grace to complete the entire work of this thesis.

Secondly, I wish to express my deepest gratitude to my supervisor Dr.Getachew Bekele Beyene for his patience, guidance, encouragement and support in shaping the outlook of this work. It would have not been possible for me to bring out this thesis without his help and constant encouragement. He provided in valuable insights that have guided my thinking and understanding.

Most important of all, I would like to express my thankfulness to my mother, my brothers, my sister and best of friends for their constant love, affection, endless encouragement and noble devotion to my education.

Finally to those who encouraged me and showed me great affection throughout this thesis work, my sincere thank is here, Thank you all.

Girma Moges Tadesse

Abstract

The popularity of distributed generation system is growing faster in the last few years because of their higher operating efficiency and low emission levels. Distributed generators make use of several micro-sources for their operation like photovoltaic cells, wind generator and fuel cells. All the power generated by each is connected to a micro-grid for DG application. The micro-grid must use an electric inverter for power conditioning and interfacing with the power system. Basically, the micro-grid inverter has two operation modes: Standalone mode and Grid-connected mode.

In this thesis, the modeling of hybrid PV-Wind-FC distributed generation systems are done. Dynamic models for the major system components, namely, wind, PV and fuel cell system modes are developed by using HOMER tool. The simulation and optimization is done based on climatic data sources and economics of the power components in which the Net Present Cost (NPC) has to be minimized to have economically feasible system. Moreover, other parameters like capacity shortage, renewable fraction, excess electricity and Cost of Energy (COE) are also considered to check the technical capability so as to select the best system. HOMER simulation result displays the most economical feasible system sorted by NPC from top to down, the prime system ranked first has renewable fraction of 15 unit wind turbines with 100kW each rating power, 1000kW photovoltaic panel, 500kW fuel cell and 500kW converter are part of the system to fulfill the required 1.3832MW estimated load demand.

Then, a simulation model for the proposed hybrid power system is developed by using Matlab/Simulink environment. This is done by creating a subsystem and masked block sets of the major dynamic component models and then cascading in to a single aggregate model.

The final tasks are control system design and analysis of inverter interfaced micro-grid distributed generations with existing utility- grid system. The analysis of controller is done using the Matlab M-file. For both operation modes, a multi-loop controller is used. The voltage differential feedback inner loop is embedded in the outer voltage loop also an output voltage decoupling and current decoupling are implemented by using the output voltage feedback. The proposed control scheme possess very fast dynamic response at load step change and can also achieve good steady state performance at both linear and nonlinear loads.

Key Words: Distributed Generation, Standalone Operation Mode, Girds Connected Operation Mode, Micro-Gird System, Inverter Interfaced System, Cost Optimization

Table of Contents

List of Figures

List of Tables

List of Acronyms and Abbreviations

AWEA	American Wind Energy Association
CAES	Compressed Air Energy Storage
COE	Cost of Energy
CT	Combustion Turbine
DB	Data Base
DG	Distributed Generation
EEP	Ethiopia Electric Power
FC	Fuel Cell
HAWT	Horizontal Axis Wind Turbine
HOMER	Hybrid Optimization Model for Electric Renewable
IGBT	Insulated Gate Bipolar Transistor
LPF	Low Pass Filter
MT	Micro-Turbine
NASA	National Aeronautics and Space Administration
NPC	Net Present Cost
O&M	Operation and Maintenance
P	Active Power
PCC	Point of Common Coupling
PMSM	Permanent Magnet Synchronous Machine
PR	Proportional Resonance
PS	Pumped Storage
PV	Photovoltaic
PWM	Pulse Width Modulation

Q	Reactive Power
SMES	Superconducting Magnetic Energy Storage
SPWM	Sinusoidal Pulse-Width Modulation
THD	Total Harmonic Distortion
VAWT	Vertical Axis Wind Turbine
VSI	Voltage Source Inverter
WECS	Wind Energy Conversion System

CHAPTER ONE

1. INTRODUCTION

1.1 Background

This thesis presents the use of inverter interfaced micro-grid distribution generation modeling and controlling system design for improving frequent interruption of a distribution system in Adama city. As frequent power interruptions are posing a huge problem to the life of the people and the economy, finding a solution to the problem is very essential. Electric reliability has affected social well-being, public health, water supply, communication service, and economic growth in the country. The average frequency of interruption and average duration of interruption of the city grid have been estimated to be 141 interruptions per customer per year and 177 hours per customer per year respectively. This indicates that there is a high unavailability of electric power in the distribution network. The average unsupplied energy is 14,498,100 kWh per year. This result in a revenue loss of about 350,000 USD per year. The revenue loss of commercial and industrial customers as a consequence of power interruption is also huge [1]. Therefore, in order to alleviate the problems micro-grid distributed generations with controlling system is one way to address the problems.

1.2 Overview of the Thesis

The micro-grid concept: the traditional power system conventional centralized operation for the medium voltage and low voltage distribution levels is defined as a cluster of loads and micro sources operating under a unified controller within a certain local area and is understood as a cluster of loads and paralleled DG systems operating together. Background technologies for proper operation of a micro-grid include generating technologies, storage technologies and control technology. A most distinguishing feature of the micro-gird is its power electronics interfaces. This power electronic interface provides significant flexibilities and permits the micro-grid to function as a semi-automous power system. The requirement and standard of the power electronics interface, there are two basic operation modes for grid-connected inverter as a distributed generation: Grid-connected mode and Standalone mode.

Figure 1.1 shows a general purpose block diagram of DG-grid system with power electronics interface which can be subdivided into five major sections. These include DGs modeling, the AC-DC converter, DC-AC inverter, the output interface and the controller modules. The unidirectional arrows show the power flow path for the distributed energy sources whereas the bidirectional arrows indicate the bidirectional power flows for the distributed energy storages. The input converter module can be either used with alternating current (AC) or direct current (DC) distributed generation (DG) systems and is most likely to be specific for the type of energy source or storage. The DC-AC inverter module is the most generic of the modules and converts a DC source to grid compatible AC power. The output interface module filters the AC output of the inverter. The fourth major module is the monitoring and control module that drives the entire interface and contains protection for both the DG source and the utility at the point of common coupling (PCC) [2]. Generally, this block diagram explains this thesis general objective clearly.

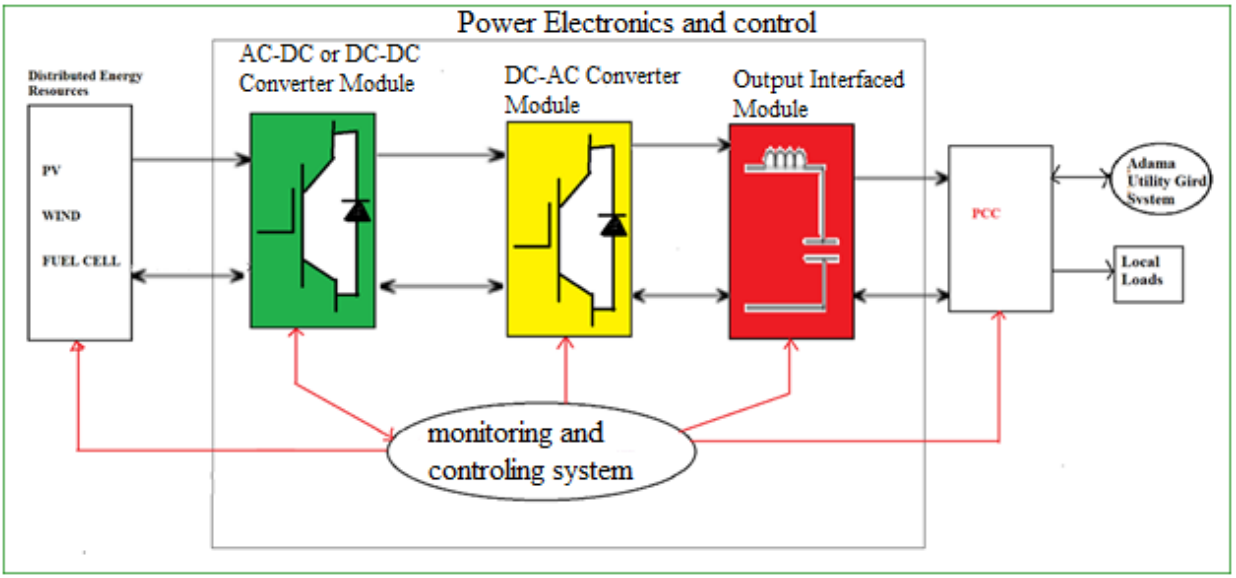

Figure 1.1 General Purpose block diagram of DG-grid system with power electronic interfaced

All the power DC or AC generated by each DG in the micro-grid must use an electric inverter to interface with the electrical power system. This power electronic interface provides significant flexibilities and permits the micro-grid to function as a semi-automous power system. Control of the micro-grid mainly refers to the control of the interfacing power electronic inverters.

1.3 Statement of the Problem

Electricity has become the heart for the sustainable development of the town and nation's economy. Ethiopia electric power system has been increasing from time to time, but the power generated mostly depend on hydro, wind and very few geothermal power plants [3]. These power plants are not sufficient to satisfy the people fundamental services of the country. Certain fundamental services that should be provided to particular community are electricity, water supply, communication, transportation; Health care and education are some mandatory needs for any community to escalate out of poverty. Thus supply of reliable electricity is prerequisite to cater this all services. The demand as well as the energy exploitation is rising in Ethiopia. Despite of the abundant renewable energy resources, many communities still live without access to electricity either from the utility grid or independent renewable and other energy generated electricity. There is a challenge to supply electricity to the population because of three reasons. First, there is no sustainable power generation to fulfill the current power demand. Second, even if there is enough power generation, installation of grid system to each village is challenging due to their geographical locations, controlling system and economic constraints. Third, the life style of the people is changed due to the technological development of the world dynamically. Like, Addis Ababa, Adama, Dire Dawa, Bahar Dar and the like, the people use the electric power based appliances. Thus, in these places the supply power and the power quality are the big issues. Specially, Adama town has affected by shortage of power supply, power interruption as described and poor controlling system of the grid system [4]. It has also no micro-grid DG sources which is installed with utility grid system as alternative energy source that indicates a unidirectional supply is available. Therefore, it requires additional energy generating power plants and smart control system. Adama utility grid system faces different problems due to increasing loads which contain the power electronics devices more than its capacity.

Further tremendous proliferation of power electronics load may produce different power quality. Problems such as harmonics, unbalancing, excessive neutral current, etc. which are some of the power qualities problems .These are seen in the existing system available in Adama town utility grid system [2]. Adama utility grid system has poor controlling system to tackle the problems. To alleviate these problems the only solution that Ethiopia electric power (EEP) authority used, are load shading and supplying the power turn by turn to the customers. These are the poor solution

methods. Therefore, this thesis mainly focuses on model additional energy sources and the control system design analysis to satisfy the needs of the customers by increasing reliable, stable and uninterruptable energy sources.

1.4 Objectives of the Study

1.4.1 General objectives

Modeling of grid connected distributed generations and design the control system between the DGs and the grid system to increase reliability and uninterruptable system in both standalone and grid connected distributed generation (DG) power systems in Adama town.

1.4.2 Specific objectives

This thesis focuses on the following subjects:

- Modeling the micro-grid distributed generation (DG) systems by hybridizing PV, fuel cell stack and windmill system and cost analysis of each distributed generation with the currently market cost of each components using HOMER application software.
- Detail modeling of DG and the mathematical analysis of the hybrid micro-gird based on the estimated loads of the mentioned area using matlab /Simulink.
- Proposes a multi-loop controller with voltage differential feedback, and with output voltage decoupling and output current decoupling by using the output voltage feedback.
- The proposed control scheme is believed to possess very fast dynamic response at load step change and can also achieve good steady state performance at both linear and nonlinear loads.

1.5 Significant of the Study

The result of this study is useful for the Adama town community to increase reliable and uninterruptable power system since the proposed control strategy for standalone mode and grid-connected inverter is capable to achieve high-quality dynamic and steady state performances under both linear and non-linear loads. Additionally, this work introduces the alternative energy sources available in the town. Specially, the wind, solar energy resources are the most widely available in the town due to the geographical area and climatic condition of the location [3].

The study is also useful for EEP to have surplus energy sources for further development of the country. If the system is more reliable, the infrastructures of the town are dramatically increased since Adama is more suitable for infrastructures and nearer to capital city of Ethiopia. The result of the study will be useful for other areas which have similar phenomena and the control system can be applied in other areas since its design is simple and requires only an accurate knowledge of output filter parameters and only the output voltage needs to be sensed provided that dc-link voltage is constant. This avoids the occurrence of total blackout of the country since the controlling mechanism senses the existence of the problem and dismantle from the main grid as well as cover critical load alone.

The design of controller will be useful for Adama power system by showing that the proposed controller can provide seamless transfers between the two operating modes for the inverter, avoiding the temporarily uncontrolled output voltage. Generally, after accomplishing the thesis the, Adama town power system will be more reliable, stable and uninterruptable.

1.6 Overview of the Study Area: Adama

Adama is one of the largest and most populated towns in Oromiya National Regional State in Ethiopia. It is located at 8º33`35``N - 8º36`46`` N latitude and 39º11`57``E – 39º21`15``E longitude with elevation above sea level 1,712 m (5,617 ft). It is about 98 kilometers away from Addis Ababa in southeast direction. Adama has a total area of about 13,000 hectares, which has been subdivided into 14 urban Kebele (least administrative structure) administrations [5]. The current total population of Adama district is 324,000 which is approximately equal percentage of females and males according to the information obtained from Adama administration website

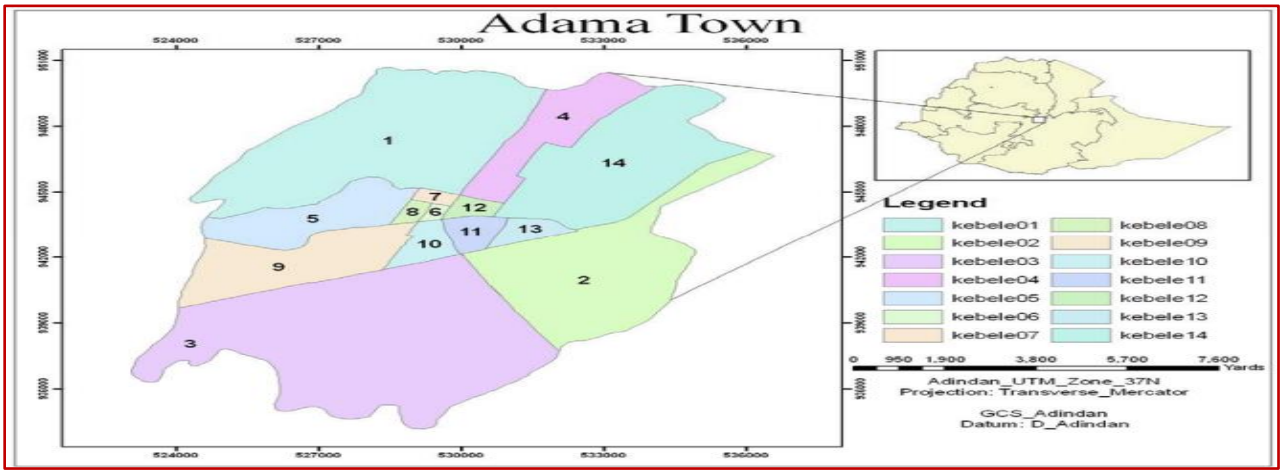

Figure 1.2 Adama Town in its National and Regional Settings *[5]*

1.7 Methodology

- **Literature Review**: the first task of my thesis work is to see the international published papers which are done in similar topic and the way how to model DGs and the method how they solve the problems of the standalone micro-grid system, grid connected system. Specially, I focus on micro-grid system, DG modeling, and inverter interfaced distribution generation. At this time, I prepare the literature review part of my thesis. These resources can get from book, articles, journal papers, thesis, and dissertation
- **Data collection**: the data had been collected from Adama utility office and the distribution system office and the Adama public administration website, EEP report and recently published papers of the area. The data had been focused on the amount of power obtained from the Ethiopia grid system, the average loads which are satisfied by existing system, the problems which face during operation of the systems, the way how to control the problems, the amount of people that satisfied by existing system, the reliability of the system, the available option existing to satisfied the customers etc. These are some of the required information for doing my work.
- **Data analysis**: based on the data obtained from mentioned areas, the analysis and organization for the new modeling of the micro-grid DG systems and analyzed the controller of the grid connected system etc. Additionally, the cost analysis is done using market availability data.

- **Modeling and designing:** based on the data analysis, the modeling is done. Such as micro-grid DGs modeling, designing multi-loop control when the system is grid connected. Then testing the characteristic of each controlling loops of the system using M-file software.
- **Conclusion of the result:** this is the time of conclusion what I has done and I give the conclusion based on the work done. Suggestion and recommendation is included

1.8 Thesis Organization

This thesis is organized into six chapters.

Chapter 1 is background and an introductory part giving overview of the thesis. The basic problem to be investigated is described. The objectives of the thesis work and its significant of study are stated. The overall information about the site is described. Finally, the work flow is explained and the thesis organization is described.

Chapter 2 deals with the theoretical back ground of the thesis work. Under this chapter, DG resource types are discussed. PV, fuel cell (FC), and wind generator are described. Additionally, micro-grid distributed generation control system, grid connected and standalone operation mode general theoretical description are is stated. Finally, Literature review is included.

Chapter 3 covers primarily load estimation, the cost estimation of DGs micro-grid systems with optimized inputs, source overview, electricity load inputs, solar and wind energy sources, cost data and size specifications of each component, solar PV size and cost, wind turbine size and cost, fuel cell size and cost, power converter size and cost. These are analyzed by using HOMER application software.

Chapter 4 covers detail modeling of distributed generation systems, general Simulink model of the hybrid system, PV subsystem model, windmill subsystem model, fuel cell power generation modelling with analysis are combined.

Chapter 5 deals with analyzing of multi-loop control scheme for micro-grid inverter standalone and grid connected operation, system configuration and their prototype picture, controller design outer voltage controller design, output voltage decoupling. Additionally, advantage of analysis, over all simulation of DG-grid connection with different load types are covered.

Chapter 6 deals with the conclusions and relevant recommendations for future work.

CHAPTER TWO

2. BASIC THEORY AND LITERATURE REVIEW

2.1 The Overall Concept of Micro-Grid System

A Micro-grid could be defined as a low-voltage distribution network with distributed energy sources altogether with storage devices and loads. Generally speaking, Micro-grid could be operated in either grid-connected or islanding mode. In [6], the Micro-grid structure assumes an aggregation of loads and micro-sources operating as a single system providing both power and heat. The majority of the micro-sources must be power electronic based to provide the required flexibility to ensure controlled operation as a single aggregated system. This control flexibility allows the micro-grid to present itself to the bulk power system as a single controlled unit, have plug-and play simplicity for each micro-source, and meet the customers' local needs. There are a cluster of radial feeders in the basic Micro-grid architecture. The connection point to utility grid is called point of common coupling. Critical loads on feeders require local generation (PV cell, wind turbine and fuel cell). As local control of distributed generations dominate in power system, the conventional central dispatch is not necessary. During disturbances, the static switch is able to autonomously separate the subsystem from the distribution system to isolate the micro-grid from the disturbance without harming the transmission grid's integrity.

2.2 Distributed Generation (DG) Resource Types

Generally Distributed generation resources are defined as those resources that are directly used in the generation of electric power for connection to distribution system. Sources include traditional and nonrenewable, renewable and energy storage technologies like batteries, flywheels, superconducting magnetic energy storage, to mention but a few as categorized in Figure 2.1 with illustrations of various technologies [7].

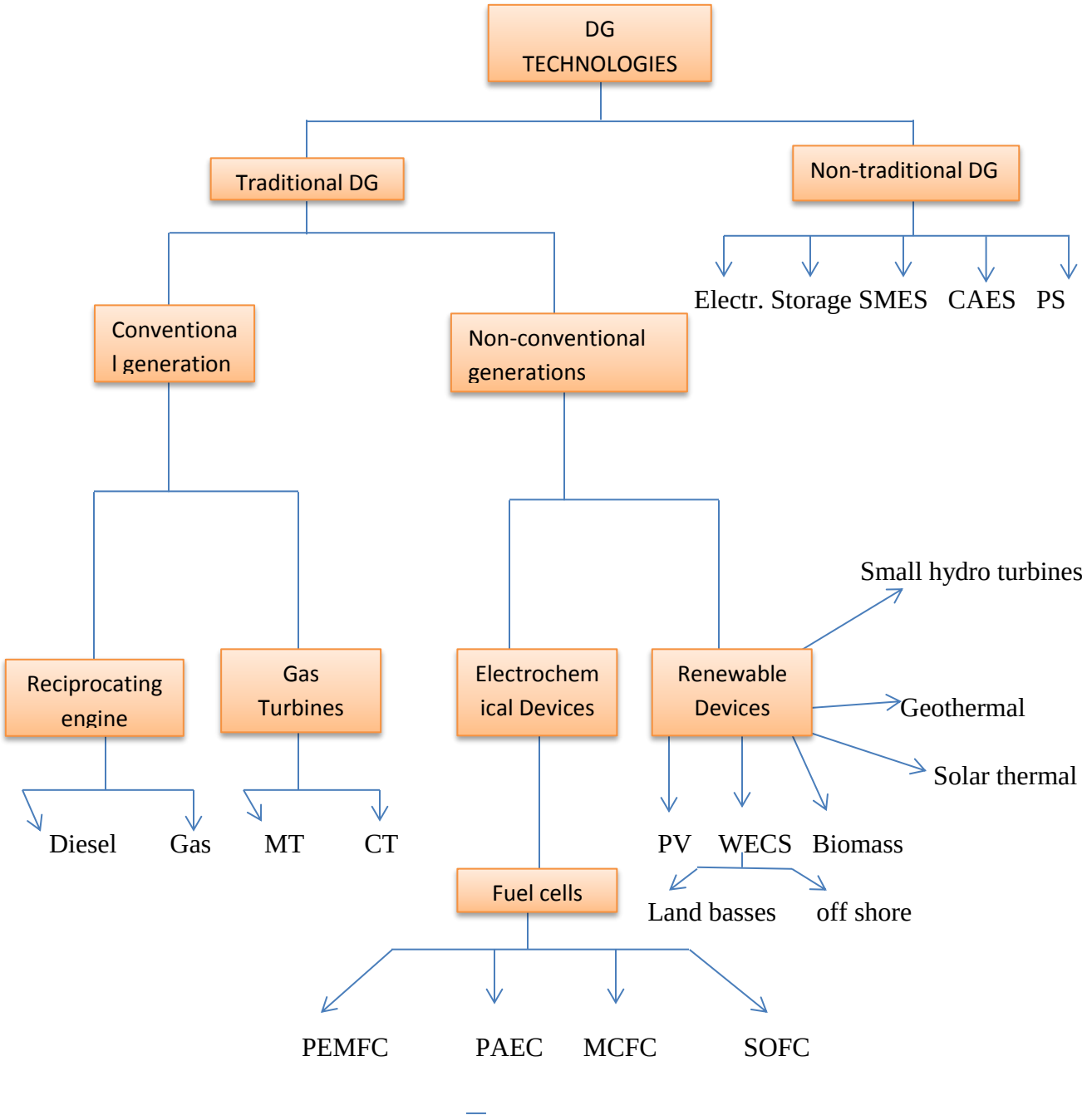
DG TECHNOLOGIES
Traditional DG
Non-traditional DG
Electr. Storage
SMES
CAES
PS
Conventiona l generation
Non-conventional generations
Reciprocating engine
Gas Turbines
Electrochem ical Devices
Renewable Devices
Small hydro turbines
Geothermal
Solar thermal
Diesel
Gas
MT
CT
PV
WECS
Biomass
Fuel cells
Land basses
off shore
PEMFC
PAEC
MCFC
SOFC

(a)

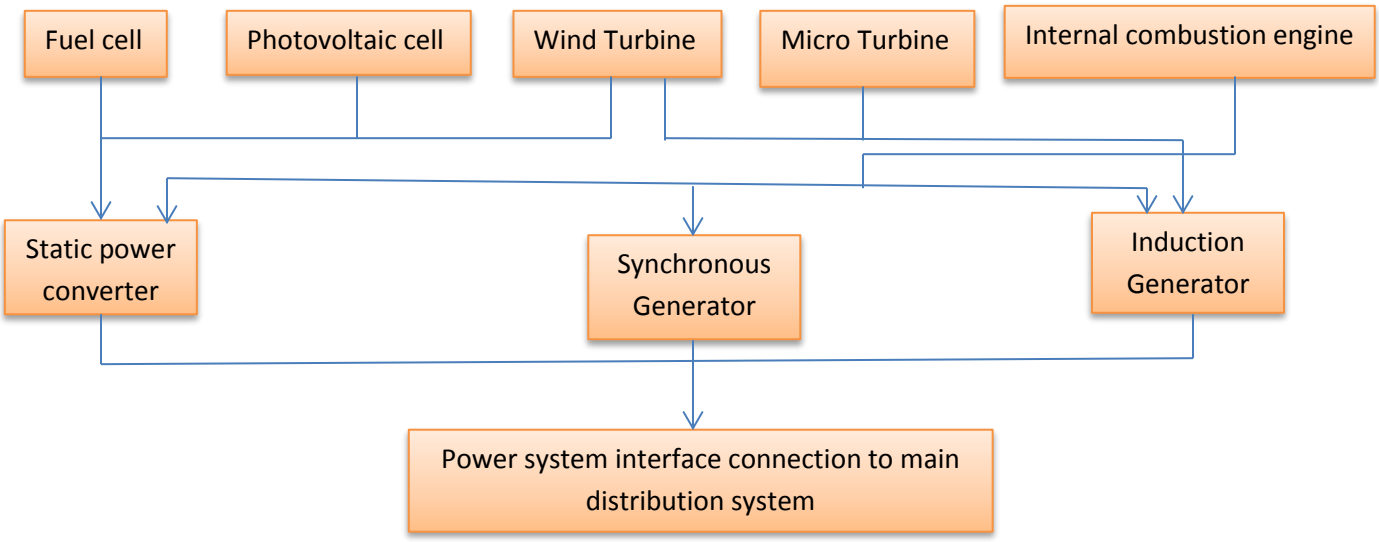

(b)

Figure 2.1 (a) distributed generation technologies *[8]* and (b) DGs and converter circuit's connections for grid interfacing *[9]*

The traditional DGs are those generators that utilize combustion engines such as low speed turbines, reciprocating engine and gas micro-turbine. These resources even through are small in size but are wide spread geographically. On the other hand the Non-traditional DGs are those sources that produce power with zero emissions and are very friendly to environment. Most of these sources usually outputs DC power, therefore conversion to AC power is necessary before integration into an existing AC distribution network. For this reason sources such as photovoltaic and fuel cells uses power electronic converters (inverters) for grid interfacing as shown in Figure 2.1. Some of the distributed generations, which are included in the study, are described below.

2.3 Photovoltaic (PV) system

The PV system is built based on well-known PV models. A PV array consists of many solar cells with each solar cell represented by a current source. The output current normally depends on sunlight and cell temperature. Practically, a solar cell can be modeled as a current source with an anti-parallel diode. A parallel resistor R_p could represent the leakage current inside the cell, and a series resistor R_s could represent the conducting loss.

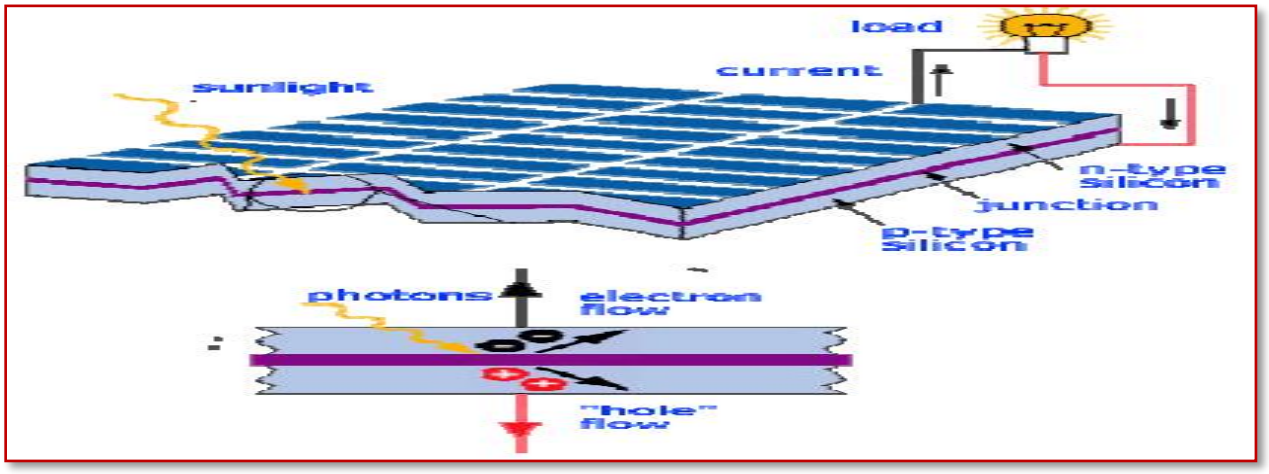

Figure 2.2 Basic structure of PV cell [10]

The basic ingredients of PV cells are semiconductor materials, such as silicon. For solar cells, a thin semiconductor wafer creates an electric field, on one side positive and negative on the other. When light energy hits the solar cell, electrons are knocked loose from the atoms in the semiconductor material. When electrical conductors are connected to the positive and negative sides an electrical circuit is formed and electrons are captured in the form of an electric current that is, electricity. This electricity is used to power a load. A PV cell can either be circular or square in construction [10].

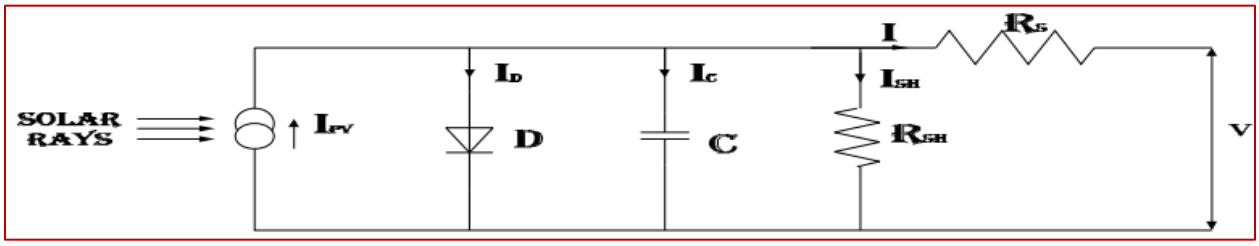

Figure 2.3 A solar cell electric circuit model *[11]*

In [10], the basic equation that represents the relationship between the solar cell current and voltage is given in (2.1), which implies the actual output current of a solar cell not only depends on sunlight, but also depends on output voltage and other factors. In (2.1), I_{pv} is the internal current generated by sunlight on solar cell, Io is the diode current, I_r is the leakage current through shunt resistor, and V_{pv} and I_{pv} are output voltage and current of the solar cell respectively. Some constant values used in the equations and have shown in Table 2.1. The diode saturation current

Io can be expressed by (2.2), where E_g is the band gap energy of semiconductor, T_n is the nominal temperature. I_{on} is the nominal saturation current and is described by (2.2), where I_{sc} and V_{ov} are the short circuit current and open circuit voltage of solar cell respectively, V_t is the thermal voltage, which is described by (2.4), where $N_s$the number of series is connected cells in an array. The internal current generated by sunlight of solar cell can be expressed by (2.3), where K_i the short circuit current/temperature coefficient, and G is the solar irradiation in W/m^2 and G_n is the nominal solar irradiation.

$$I = I_{PV} - I_O[\exp(\frac{q(V + IR_S)}{\alpha KT}) - 1] - I_r \tag{2.1}$$

$$I_o = I_{o,n}(\frac{T_n}{T})^3 \exp[\frac{qE_g}{\alpha K}(\frac{1}{T_n} - \frac{1}{T})] \tag{2.2}$$

$$I_{PV} = [I_{sc} + K_i(T - T_n)]\frac{G}{G_n} \tag{2.3}$$

$$V_t = \frac{KT}{q}\ln\left[1 - \frac{I - I_{PV}}{I_o}\right] \tag{2.4}$$

$$P = V \times I \tag{2.5}$$

Where, $K_t = \frac{N_s KT}{q}$ and $I_{o,n} = \frac{I_{SC}}{\exp(\frac{V_{oc}}{\alpha V_t}) - 1}$

Table 2.1 Parameters of solar cell constants

Quantity	Value
Q	1.6×10^{-19}C
K	1.38×10^{-23}J/K
α	1.5
E_g	1.2
K_i	1.141mA/K

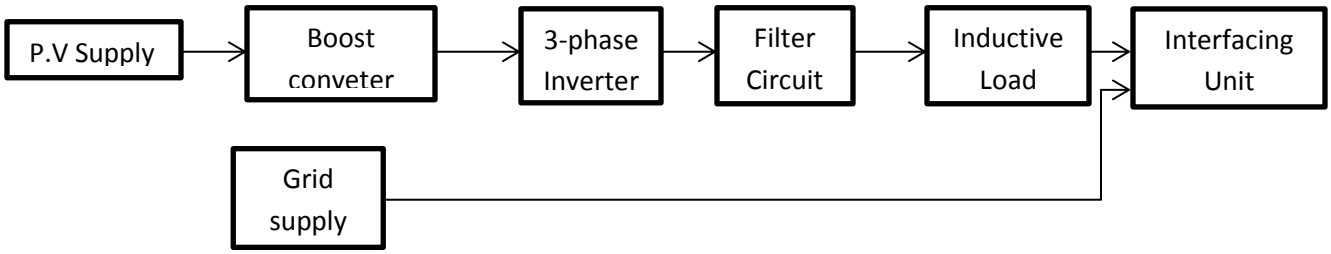

Figure 2.4 block diagram of PV –grid system

2.4 Fuel cell (FC)

Fuel cells work by the chemical reaction of combining hydrogen and oxygen to form electricity and water. Fuel cells have some advantages, namely, the potential for high efficiency (from 35% to 60%), low to zero emissions, quiet operation, and high reliability for the limited number of moving parts. There are several types of fuel cells currently available, including phosphoric acid fuel cell, molten carbonate fuel cell, solid oxide fuel cell (SOFC), and proton exchange membrane. Research and development of fuel cell system for various applications has been increased in past few years. Proton Exchange membrane Fuel cell (PEMFC) system is the most promising and accepting system in fuel cell technology. PEM fuel cells are environment friendly since they use hydrogen as fuel. Hydrogen can be obtained from Hydrocarbons, biomass, and nuclear energy or from cleaner sources such as water electrolysis. PEM fuel cells consists of a solid polymer electrolyte and operates low temperature (50^0-100^0C). They do not pollute the environment which is due to only by product is water. Electrical power output of a fuel cell is DC and this DC power is converted to AC power by an inverter to be compatible with the electric power system [12].

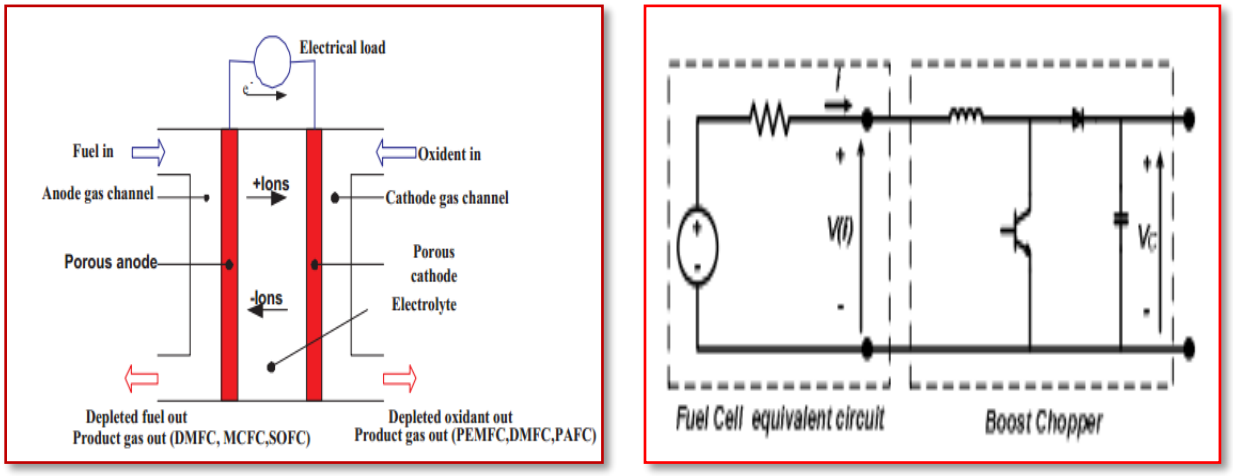

(a) (b)

Figure 2.5 (a) Operation principle, cathode reactions, and the mobile ion associated with most common fuel cell types and (b) Fuel cell equivalent circuit *[12]*

Electrochemical equivalent model: The electrochemical equivalent circuit shown in Figure 2.7 can be used for the analysis of the behavior of a PEM fuel cell. This mathematical model is described by a set of equations and corresponding parameters, which are essential for the analysis of the performance of the PEMFC [13].

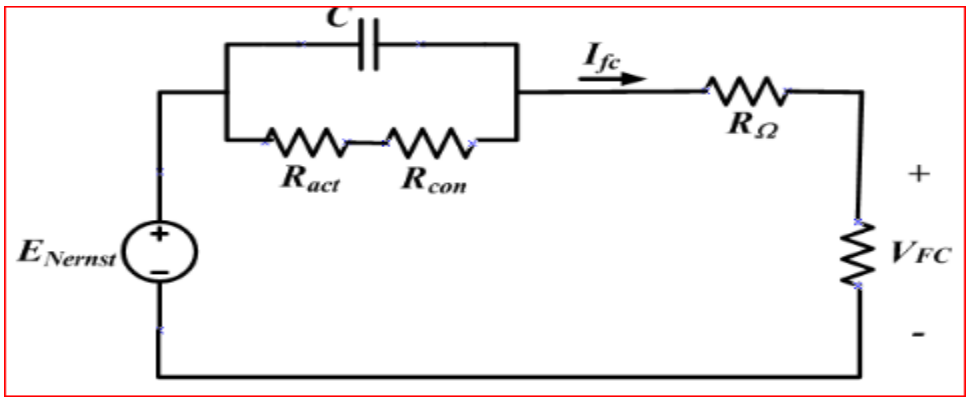

Figure 2.6 A simplified model of the PEM for only one cell

This model can be described as follows: The output voltage of a single cell can be calculated by the following expression, according to the Nernst's equation and Ohm's law:

$$V_{FC} = E_{Nernst} - V_{act} - V_{ohmic} - V_{con} \tag{2.6}$$

Where: E_{Nernst} is the thermodynamic potential of the cell in open circuit, which represents its reversible voltage. It is defined by:

$$E_{Nernst} = 1.229 - 0.85\times10^{-3}\times(T - 298.15) + 4.31\times10^{-5}\times T\times\left[\ln(P_{H_2} + \frac{1}{2}\ln(P_{O_2})\right] \quad (2.7)$$

P_{H2} and P_{O2} are the partial pressures (atm) of hydrogen and oxygen, respectively. T is the cell temperature in Kelvin. V_{act} is the voltage drop due to the activation of the anode and cathode (also known as activation over potential);

$$V_{act} = -\left[\xi 1 + \xi 2\times T + \xi 3\times T\times\ln(C_{O2})\right] \quad (2.8)$$

With C_{O2} the concentration of oxygen in the catalytic interface of the cathode (mol.cm-3) and the parametric coefficients for each cell model are represent by ξ1,2,3,4 and ψ.

$$C_{O2} = \frac{P_{O2}}{5.08\times10^{6}\times e^{-\left(\frac{498}{T}\right)}} \quad (2.9)$$

V_{ohmic} is the ohmic voltage drop (also known as ohmic over potential), a measure of the ohmic voltage drop resulting from the resistances of the conduction of protons through the solid electrolyte and the electrons through its path;

$$V_{ohmic} = i_{FC}(R_M + R_C) \quad (2.10)$$

R_M is the equivalent membrane resistance to proton conduction and R_C is the equivalent contact resistance to electron conduction.

$$R_M = \frac{\rho_M\times\lambda}{A} \quad (2.11)$$

V_{con} represents the voltage drop resulting from the reduction in concentration of the reactants gases or, alternatively, from the transport of mass of oxygen and hydrogen (also known as concentration over potential).

$$V_{con} = -B\times\ln\left(1 - \frac{J}{J_{\max}}\right) \quad (2.12)$$

Since a stack is as set of n cells connected in series, the output voltage V_s can be calculated by:

$$V_s = n \times V_{FC} \tag{2.13}$$

Therefore, based on the equations above, the parameters of the model that characterizes the system are; A-Area of the membrane (cm^2), λ-Thickness of the membrane (cm), R_C-Equivalent contact resistance (Ω), C –Equivalent capacitor (F), ξ's -Model coefficients, ψ-Empirical parameter and J_{max} -Maximum current density (A/cm^2) and the input variables are; partial hydrogen pressure PH_2(atm) , partial oxygen pressure PO2 (atm), temperature T(K). Once identified the set of equations and parameters of the model, which is based on analytical formulations of the electrochemical process, and because there is a lack of manufacturer data about the exact values of the parameters needed for a right model, a Second step is to get these values.

Working Principle of a fuel cell: A low-temperature, moderate-output fuel cell works as follows [14]:

1. A grooved porous holder plate at the entrance disperses H_2 uniformly.

2. A catalyst before the electrolyte breaks the H_2 into $H_2^+ + e^-$ electrons.

3. A proton energy membrane (PEM) is a polymer film that blocks passage of electrons but allows hydrogen protons to proceed through.

4. A porous graphite plate acts as an anode.

5. Electrons carried in from the external circuit to the anode react with H_2^+ protons and oxygen picked up from the air to form H_2O. Air is supplied externally at the anode. We have the following reactions:

At the cathode $H_2 \rightarrow H_2^+ + e^-$

At the anode $H_2^+ + ½O + e^- \rightarrow H_2O$

At the anode $H_2^+ + ½O + e \rightarrow H_2O$ without the e–, the chemical reaction of $H_2^+ + ½O$ cannot take place. Only when electrons flow through the external circuit is the reaction complete and water formed. A portion of energy is liberated as heat at the anode and must be carried away. This is the

portion that accounts for the losses in the fuel cell. Net system efficiency is defined as the electrical energy output/thermal energy or the heat energy in the raw fuel feed amount.

Table 2.2 Summary of chemical reactions in different types of fuel cell *[13]*

Fuel cell type	Anode reaction	Mobile Ion	Cathode Reaction
PEMFC and PAFC	$H_2 \rightarrow 2H^+ + 2e^-$	H^+	$1/2O_2 + 2H^+ + 2e^- \rightarrow H_2O$
AFC	$H_2 \rightarrow 2H^+ + 2e^-$	OH^-	$1/2O_2 + H_2O + 2e^- \rightarrow 2OH^-$
MCFC	$H_2O + CO_3^{2-} \rightarrow H_2O + CO_2 + 2e^-$	CO_3^{2-}	$1/2O_2 + CO_2 + 2e^- \rightarrow CO_3^{2-}$
SOFC	$H_2 + O^{2-} \rightarrow H_2O + 2e^-$	O^{2-}	$1/2O_2 + 2e^- \rightarrow O^{2-}$

2.4.1Characteristics of fuel cell types

There are four major fuel cell technologies with somewhat different characteristics. The main apparent difference is the electrolyte, which also has far reaching effects on the design and operating characteristics of the fuel cell. In Table 2.3, those four technologies are listed with some key characteristics.

Table 2.3 Fuel cell key characteristics *[13]*

	PEMFC (PEFC)	PAFC	MCFC	SOFC
Electrolyte	Proton exchange membrane	Phosphoric Acid	Molten Carbonate	Solid Oxide
Operating temperature (C^o)	80	200	650	800-1000
Electric efficiency based on natural gas (%)	30-35	35-40	45-55	45-55

All fuel cells generate a direct current, the voltage depending on cell voltage and the number of cells in series. Furthermore, the voltage varies with the load and also to some extent with time as

the fuel cell stack ages. To obtain AC current, the equipment should have power conditioning equipment to handle DC to AC conversion and current, voltage, and frequency control.

As fuel cells are in a development stage, it is difficult to make general statements about operating characteristics. Operating procedures tend to be on the cautionary side. Tentatively the following characteristics can be listed [14]:

1. Start-up time depends on type of fuel cell and type of fuel processing system. A low temperature fuel cell (PEMFC) with partial oxidation could probably be started in a couple of minutes while a high temperature fuel cell takes 3 to 4 hours due to the need of avoiding thermal stresses during warm up. Generally speaking, high temperature fuel cells are not suited for start-stop operation.

2. A fuel cell in itself can facilitate nearly instant load changes. However, a fuel cell system has a limiting factor in the fuel processing system which has a certain time lag (varying depending on the type) and a truly load following system would need a buffer. A typical turn down ratio of a fuel system is about 1:5 and high efficiencies are kept to at least 50% load.

3. Fuel cells have a potential for high reliability as the number of moving parts is low. It consists of auxiliary equipment such as fans and pumps.

2.4.2 Fuel Tank (Hydrogen tank)

Hydrogen is the simplest and most abundant element of the universe; it is clean and pollution free. It has a lot of interesting characteristics that prove it appropriate as an energy carrier: it is the lightest of all elements (molecular weight: 2.016 g /mol), its density is about to14 times less than air (0.08376 kg / m3 at standard conditions) and it has a very high diffusion rate. It is liquid at temperatures below 20.3 K at atmospheric pressure and the density in that case is about to 70.8 kg /m3. It contains the highest energy per unit mass of all fuels and because of its small molecular size leaks more easily through porous materials than other common gases at equivalent pressures (at the same holes or joints, it leaks 1.26 to 2.8 times faster than natural gas). It is generally non-corrosive and non-reactive with typical container materials, as well as non-toxic and non-poisonous. As a result of the above characteristics Hydrogen seems to be a promising energy carrier but with storage difficulties on the other hand [14].

2.4.2.1 Compressed Gaseous Hydrogen Storage

The most common and widely used method to store hydrogen is in compressed form. Special pressure tanks exist for this cause usually made of steel or aluminum; their shell is properly manufactured to be thick enough, so that few holes for hydrogen leakage exist. However, another approach of compressed hydrogen storage is in above ground earth caves; utilizing such cavities, great amounts of hydrogen may be stored at various pressures proportionally to geologic shape. The main advantage of the cave-storage is that the leak is almost zero, but there are a lot of parameters that have to be taken in so that storage can be possible. Among all storage technologies, the compressed gaseous hydrogen has the longest history and cheapest price. It is suitable for electrolyzers also, as most of them (bipolar cells) produce hydrogen at high pressures and no extra mechanism is needed so storage procedure to be completed.

2.4.2.2 Liquid Hydrogen Storage

Hydrogen is liquid at -253 °C (at atmospheric pressure), so an effective and energy efficient way of liquid Hydrogen storage requires complicated insulation techniques. At this natural state it has a volumetric energy density value of about 2760 kWh/m3 and that's why is used as a fuel in space technology for several years. The main advantage of this method is the reduced risks compared to compressed gas, a great amount of energy (approximately 20-30 % of the hydrogen's energy content) has to be used to accomplish liquefaction though. So it seems that it is not a cost-efficient approach for an energy storage system [14].

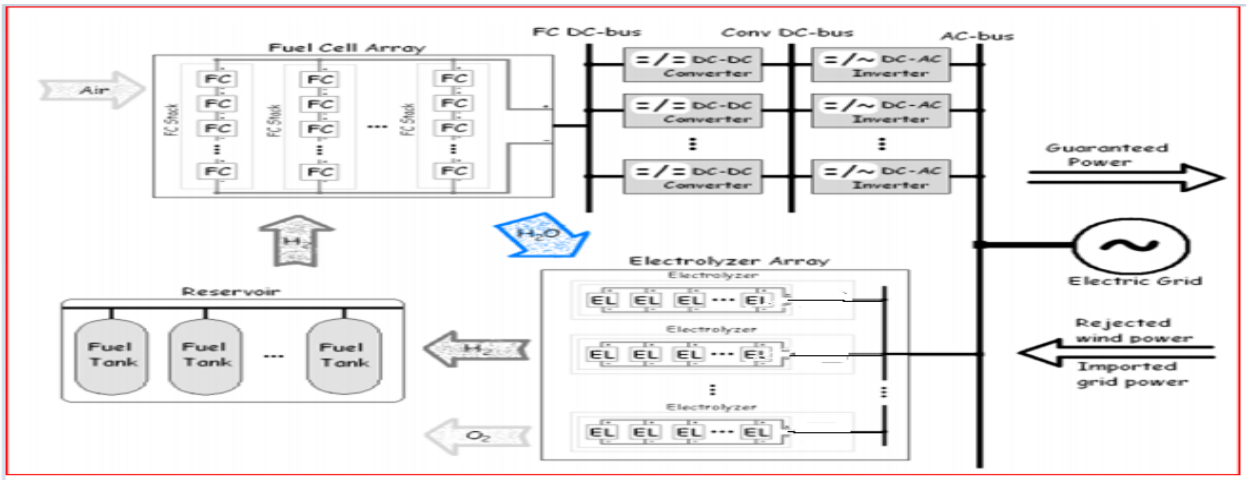

Figure 2.7 The FC energy storage system block diagram *[14]*

2.5 Wind Based Distributed Generation System

Wind turbines convert the kinetic energy of wind into electrical energy with three basic types of wind turbine technologies that are currently available for interconnecting with electric power systems [15]:

1) The wind turbine rotates the rotor shaft of an induction generator connected directly to the grid without any power electronic interface;

2) A double-fed induction generator (DFIG) requires a wound-rotor design;

3) Wind turbine design uses a conventional or permanent magnet synchronous generator to convert the wind turbine power to a variable voltage, variable frequency output that varies with wind speed. Then rectifiers and inverters are used to convert power to be compatible with the electric power system parameters

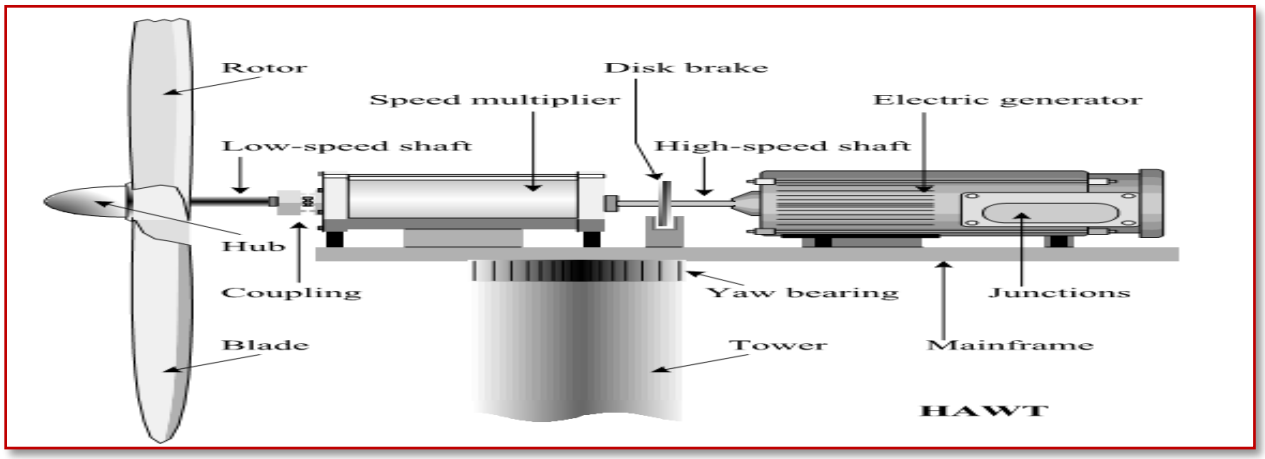

Figure 2.8 Block diagram of wind generator *[15]*

2.5.1 Wind Turbine

Wind turbines are packaged systems that include a rotor, a generator, turbine blades and a drive or a coupling device. As wind blows through the blades, the air exerts aerodynamic forces that cause the blades to turn the rotor. As the rotor turns, its speed is altered to match the operating speed of the generator. Most systems have a gearbox and a generator in a single unit behind the turbine blades. As with photovoltaic (PV) systems, the output of the generator is processed by an inverter that changes the electricity from DC to AC so that the electricity can be used.

The working principles of the wind turbine can be described in two processes that are carried out by its main components: the rotor which extracts kinetic energy from the wind passing it and converts it into mechanical torque and the generating system, the job of which is to convert this torque into electricity.

2.5.2 Squirrel Cage Induction Generator

It is the oldest and the simplest one, and it is illustrated in Figure 2.9, it consists of a conventional, direct grid coupled squirrel cage induction generator, which is coupled to the aerodynamic rotor through a speed increasing gearbox. The gearbox is used because the optimal rotor and generator speed ranges are different.

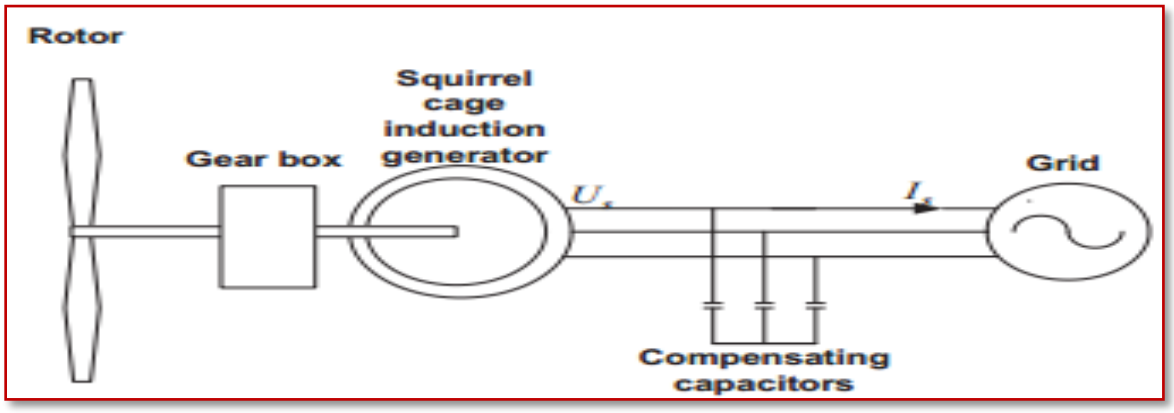

Figure 2.9 Squirrel cage induction generator is used in wind turbines as generating system *[15]*

The slip and the rotor speed of a squirrel cage induction generator vary with the generated power. These rotor speed variations are very small. Therefore, the turbine is normally considered to operate at constant speed. Because the squirrel cage induction generator consumes reactive power; capacitors are often added to generate magnetizing currents in the case of large wind turbines and/or weak grids, and improving the power factor of the system. The power extracted from the wind needs to be limited, because the generator could be overloaded or the pullout torque could be exceeded, leading to rotor speed instability.

In such case, this is often done by using the stall effect. This means that the rotor geometry is designed in such a way that its aerodynamic properties make the rotor efficiency decrease in high wind speeds, thus limiting the power extracted from the wind and preventing the generator from

being damaged and the rotor speed from becoming unstable. Thus, during normal operation of a stall regulated wind turbine no controllers are reactive.

2.5.3 Doubly Fed (Wound Rotor) Induction Generator and Direct Drive Synchronous Generator

Figure 2.10 shows the other two generating systems. They are used in variable speed turbines. With these it is possible to increase the energy captured by the aerodynamic rotor by maintaining the optimum power coefficient over a wide range of wind speeds [15]. However, it is then necessary to decouple the speed of the rotor from the frequency of the grid through some form of power electronic converters. In the doubly fed induction generator, a back-to-back voltage source converter feeds the three phase rotor winding. In this way, the mechanical and electrical rotor frequencies are decoupled and the electrical stator and rotor frequency can be matched, independently of the mechanical rotor speed. In the direct drive synchronous generator, the generator is completely decoupled from the grid by a power electronics converter. The grid side of this converter is a voltage source converter, i.e. an Insulated Gate Bipolar Transistor (IGBT) bridge. The generator side can either be a voltage source converter or a diode rectifier. The generator is excited using either an excitation winding or permanent magnets.

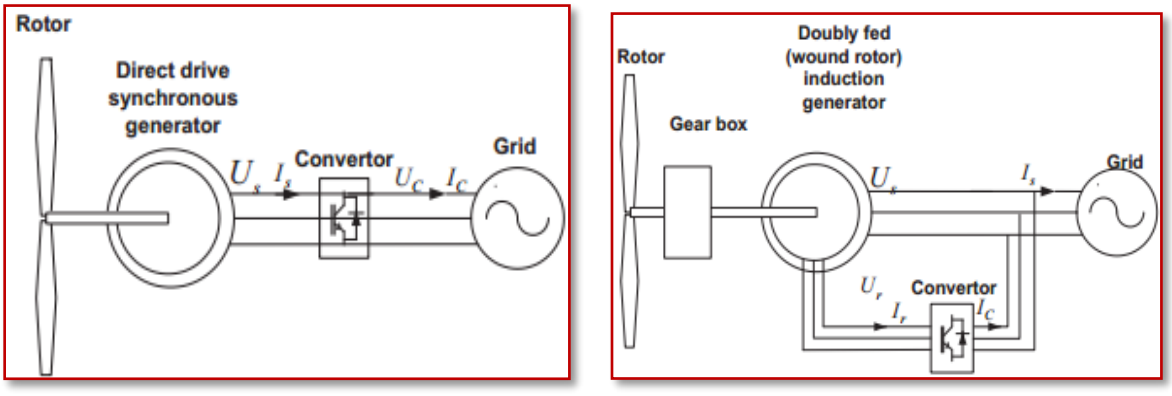

(a) (b)

Figure 2.10 Generating systems used in wind turbines (a) direct synchronous generator and (b) doubly fed (wound rotor) induction generator *[16]*

2.5.4 Wind Turbine Modeling Types

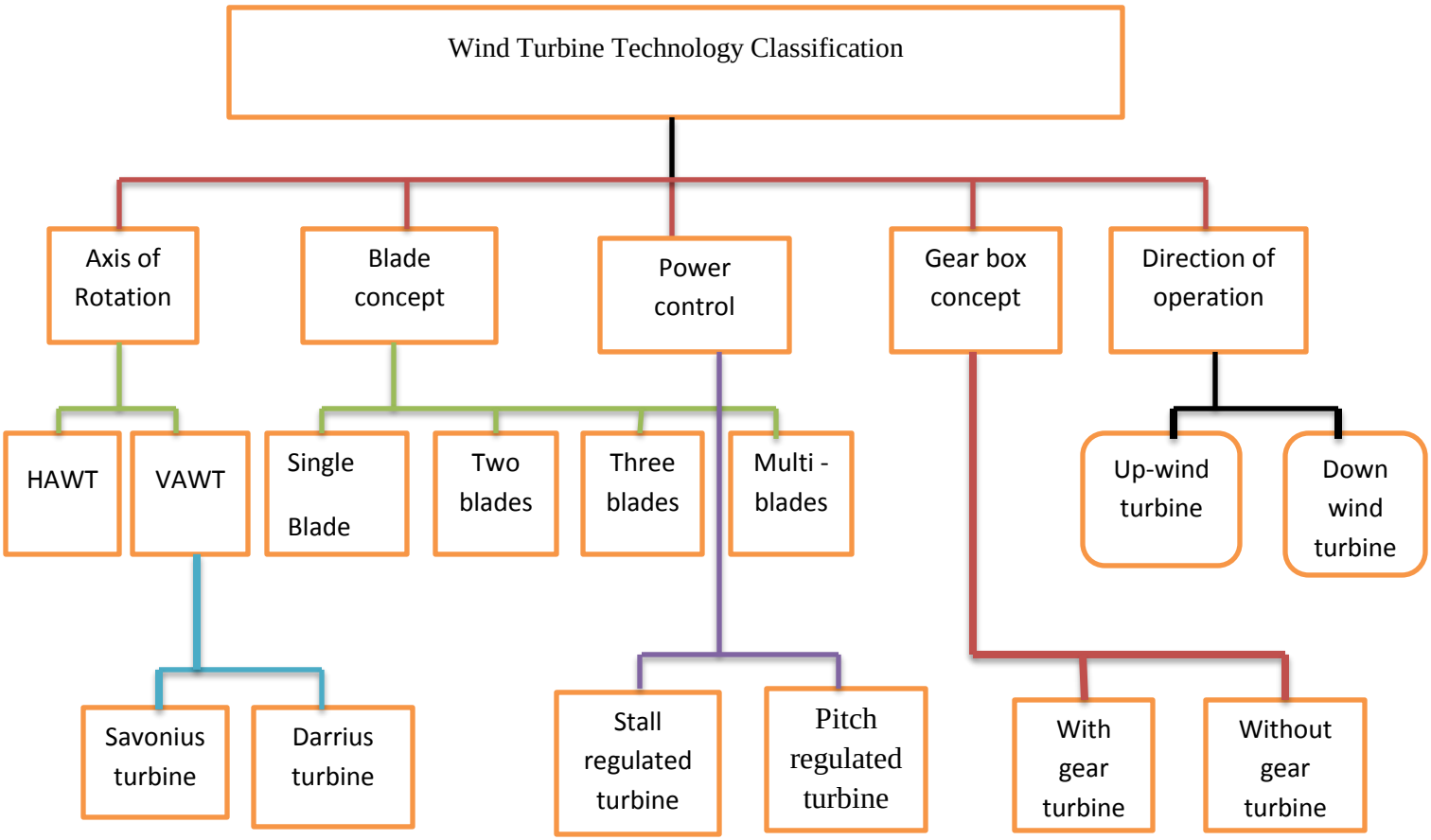

Figure 2.11 classification of turbine model

In *[16, 17]*, an overview of the developments in wind turbine modelling will be presented. The development of wind turbines (several hundreds of kWs to MWs) is addressed. The first wind turbines are based on a direct grid coupled synchronous generator with pitch controlled rotor blades to limit the mechanical power in high wind speeds. Therefore, the first modeling efforts are devoted to this wind turbine concept. The directly grid coupled synchronous generator is followed by the directly grid coupled asynchronous squirrel cage induction generator. This type of generator has a more favorable torque versus speed characteristic than the synchronous generator, thus reducing the mechanical loads and it is also cheaper. This concept is still applied nowadays by some manufacturers

2.5.5 Rotor Equation

A wind turbine operates by extracting kinetic energy from the wind passing through its rotor. The power developed by a wind turbine is given by (2.14). The model is based on the steady-state power characteristics of the turbine. The stiffness of the drive train is infinite and the friction factor and the inertia of the turbine must be combined with those of the generator coupled to the turbine. The output power of the turbine is given by the following equation.

$$P_m = c_p(\lambda, \beta)\frac{\rho A}{2}v^3{}_{wind} \tag{2.14}$$

Where: P_m is mechanical output power of the turbine (W); c_p is performance coefficient of the turbine; ρ air density(kg/m3); A is turbine swept area (m^2); V_{wind} is wind speed(m/s); λ tip speed ratio of the rotor blade tip speed to wind speed; β blade pitch angle (deg).

The Simulink model of the turbine is illustrated in Figure 2.12. The three inputs are the generator speed (ωr_pu) in Pu of the nominal speed of the generator, the pitch angle in degrees and the wind speed in m/s. The tip speed ratio λ in Pu of λ_nom is obtained by the division of the rational speed in Pu of the base rotational speed and the wind speed in Pu of the base wind speed. The output is the torque applied to the generator shaft.

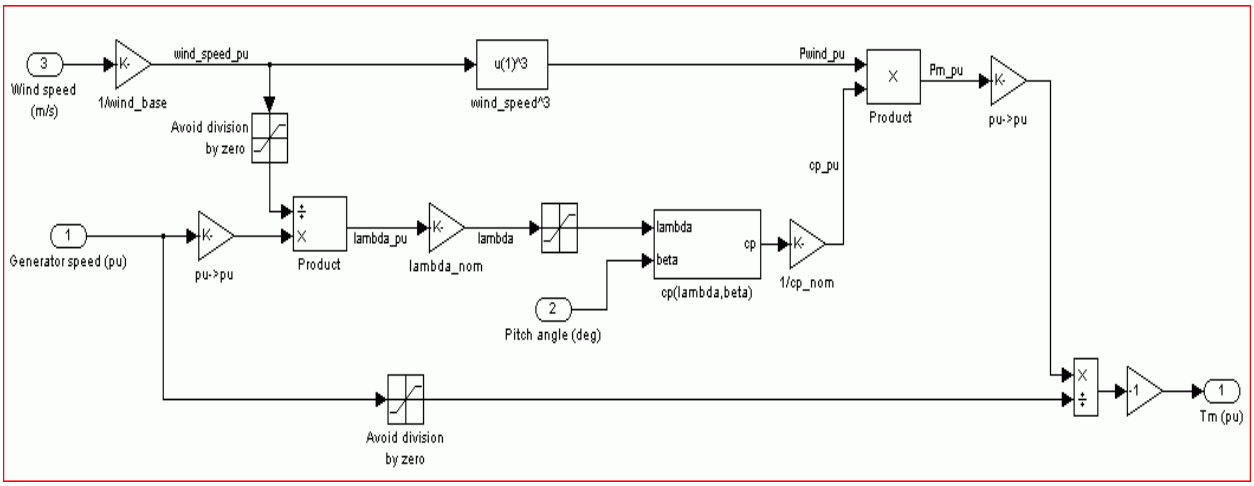

Figure 2.12 Wind turbine model [18]

The force extracted on the rotor is proportional to the cubic of the wind speed and so the wind turbine must be designed to withstand large forces during storms. Most of modern designs are three-bladed horizontal-axis rotors as this gives good value of peak C_p together with an

aesthetically pleasing design. The power coefficient $C_p$is a measure of how much of energy in the wind is extracted by the turbine. It varies with rotor design and the relative speed of the rotor and wind (known as the tip speed ratio to give a maximum practical value of approximately 0.4 [19]. The power coefficient C_p is a function of the tip speed ratio, λ and the pitch angle, β which will be investigated further. The calculation of the performance coefficient requires the use of blade element theory [16]. As this requires knowledge of aerodynamics and the computations are rather complicated, numerical approximations have been developed. Here the following function will be used:

$$C_p(\lambda,\beta) = 0.5176\left(\frac{116}{\lambda_i} - 0.4\beta - 5\right)e^{\frac{-21}{\lambda_i}} + 0.0068\lambda \tag{2.15}$$

With

$$\frac{1}{\lambda_i} = \frac{1}{\lambda + 0.08\beta} - \frac{0.035}{\beta^3 + 1} \tag{2.16}$$

Figure 2.13 shows the $C_p(\lambda,\theta)$ versus λ characteristics for various values of β ,Using the actual values of the wind and rotor speed, which determine, β and the pitch angle, the mechanical power extracted from the wind can be calculated from equations (2.21) to (2.23). The maximum value of C_p (C_{pmax}=0.48) is achieved for β = 2 and for λ = 8.1. This particular value of λ is defined as the nominal value (λ nom).

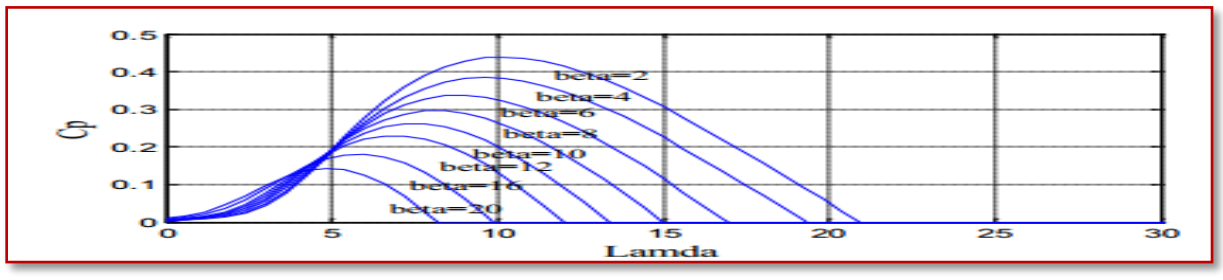

Figure 2.13 Performance coefficient C_p as a function of the tip speed ratio lambda, with pitch angle beta, β as a parameter *[15]*

2.5.6 Generator Equation

Generator is the device converting mechanical energy into electricity, so it is important to the whole system. When modeling the doubly fed induction generator, the generator convention will

be used, which means that the currents are outputs instead of inputs and the real power and reactive power have positive signs when they are fed into the grid. By using the generator convention, the following set of equations is obtained [20]:

$$v_{ds} = -R_s i_{ds} - \omega_s \psi_{qs} + \frac{d\psi_{ds}}{dt} \tag{2.17}$$

$$v_{qs} = -R_s i_{qs} + \omega_s \psi_{ds} + \frac{d\psi_{qs}}{dt} \tag{2.18}$$

$$v_{dr} = -R_r i_{dr} - s\omega_s \psi_{qr} + \frac{d\psi_{dr}}{dt} \tag{2.19}$$

$$v_{qr} = -R_r i_{qr} + s\omega_s \psi_{dr} + \frac{d\psi_{qr}}{dt} \tag{2.20}$$

Where: V is the voltage in [V], i is the current in [A], R is the resistance in [Ω], ω_s is the stator electrical frequency in [rad/s], ψ is the flux linkage in [Vs] and s is the rotor slip. Subscripts d and q are direct and quadrature axis components respectively; subscripts s and r indicate the stator and the rotor quantities. All the quantities in equation (2.17-2.20) are functions of time. The d-q reference frame is rotating at synchronous speed with the q- axis 90^0 ahead of the d-axis. The position of the d-axis coincides with the maximum of the stator flux, which means that V_{qs} equals the terminal voltage and V_{ds} equals to zero [20].

. The rotor slip is defined as

$$s = \frac{\omega_s - \frac{p}{2}\omega_m}{\omega_s} \tag{2.21}$$

Where P is the number of poles and ω m is the mechanical frequency of the generator in [rad/s].

We can rewrite the voltage-current relationships of the doubly fed induction generator in (2.17-2.20) into the following equation [20] .

$$vds = -R_s i_{ds} + \omega_s((L_s + L_m)i_{qs} + L_m i_{dr}) \tag{2.22}$$

$$vqs = -R_s i_{qs} - \omega_s((L_s + L_m)i_{ds} + L_m i_{dr}) \tag{2.23}$$

$$vdr = -R_r i_{dr} + s\omega_s((L_r + L_m)i_{qr} + L_m i_{qs}) \tag{2.24}$$

$$vqr = -R_r i_{qr} + s\omega_s((L_r + L_m)i_{dr} + L_m i_{ds}) \tag{2.25}$$

The active power, P and reactive power, Q generated by the generator can be written as:

$$P = v_{ds} i_{ds} + v_{qs} i_{qs} + v_{dr} i_{dr} + v_{qr} i_{qr} \tag{2.26}$$

$$Q = v_{ds} i_{ds} - v_{qs} i_{qs} + v_{dr} i_{dr} - v_{qr} i_{qr} \tag{2.27}$$

From this equation, it can once more be concluded that the reactive power Q is not necessarily equal to the generated reactive power fed into the grid. Equations (2.17-2.20) and (2.22, 2.27) describe the electrical part the generator. However, also the mechanical part must be taken into account in a dynamic model. The following expression gives the electromechanical torque developed by the generator:

$$T_e = \psi_{dr} i_{qr} - \psi_{qr} i_{dr} \tag{2.28}$$

2.6 Micro-grid distributed generation control systems

A typical DG system based on micro-source depicted that the micro-source generation involves all the generation, storage, interfacing and control technologies. A most distinguishing feature of the micro-gird is its power electronics interfaces. Voltage source inverters (VSI) are now widely used in many grid applications to interface distributed generation (DG) systems to the utility system. When the inverter operates in standalone mode, the micro-grid inverter performs like a voltage source to provide required voltage to the local load. A traditional average voltage feedback control could maintain a desirable steady-state rms output voltage, but their response to load step change is noticeably slow, and nonlinear loads could greatly distort the output waveform. Instantaneous voltage feedback control can have faster transient response, lower total harmonic

distortion and better disturbance rejection capability because of the lower output impedance. There are many instantaneous controllers been presented recently [21]:

- State feedback controllers show good performance but the duty cycle has to be calculated on a pulse-by-pulse basis.
- The hysteresis-type controllers have variable and relatively high switching frequencies and the control variable error is twice of the hysteresis band.
- Dead-beat control can make the capacitor voltage exactly tracks the reference voltage with the accurate knowledge of the filter parameters.
- A discrete-time sliding mode control technique has also been used in inverter control due to its robustness and overshoot-free fast tracking capability.
- A predictive controller can enhance the system stability limits but its performance is also subject to the accuracy of the plant model and the accuracy of the reference current prediction.
- A H∞ control strategy can improve the robust stability under model uncertainty and load disturbance. However, the control performance under nonlinear load is not satisfactory.
- The rotating synchronous frame PI controller for current control is used widely to obtain a zero steady state error. However, significant computation arises from the need of multiple reference frames for harmonic current attenuations.

Generally, the control system of the DGs work in both standalone and grid connected mode of operations have their own good and bad side as mentioned above. Therefore, the multi-loop control system can alleviate these constraints.

2.6.1 Standalone Operation Mode Control System

The presence of DG can provide a supply to customers in a network where the utility connection is unavailable due to unplanned or planned islanding. In [22], a typical inverter-interfaced distributed generator unit and its control structure for islanded-mode operation are shown in Figure 2.14. The primary source produces DC power which is stored in the DC bus and then convert to AC power by the inverter. The control of a single inverter operating in islanded mode is focused on regulating output voltage magnitude and frequency. The multi-loop control structure in Figure 2.14 is popular because it provides good dynamic performance and disturbance rejection and the presence of an explicit current reference facilitates inclusion of a current limit. The inverter is interfaced to the network through a low pass filter (L_f and C_f) and a coupling inductance (Lcc). The inner loop regulates the inductor current i_L and is usually designed to have a high bandwidth. The outer loop regulates the output voltage v_o across the filter capacitor by setting a current demand for the inner loop and is designed with a slower bandwidth.

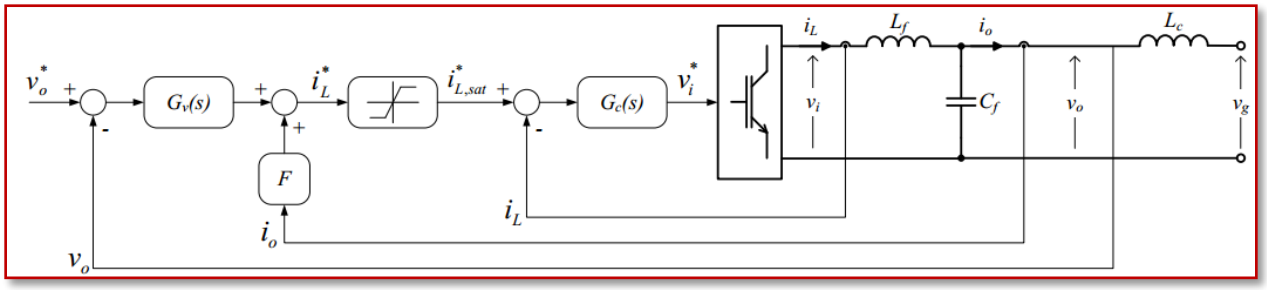

Figure 2.14 Multi-loop control of a stand-alone inverter *[22]*

The corresponding standard for standalone operation is IEEE Standard 446-1995 (IEEE Recommended Practice for Emergency and Standby Power Systems for Industrial and Commercial Applications). The main points are [21]:

Security: This is the basic requirement for the grid-connected inverter as a back-up supply to the load. The ground connection is an important factor, which is described in IEEE Std 142-1991

(ANSI) IEEE Recommended Practice for Grounding of Industrial and Commercial Power Systems.

Power quality: This includes the voltage amplitude, waveform quality, frequency and dynamic response, and so on. The basic topologies of the interface between distributed generation and grid-connected inverter plays the role of the interface between the renewable energy source and other distributed generation source and the grid, in order to best utilize the power and converter the voltage to the requirement voltage. Many topologies are proposed for this application. According to the structure, there are single stage, double stage and multi-stage. According to the isolation, it can be divided into isolated and non-isolated. According to the source, it can be classified into voltage source inverter and current source inverter, single-phase or three-phase.

2.6.2 Grid Connected Operation Mode System Analysis

In the grid connected mode, the steady state system frequency is fixed to the utility frequency. It is assumed that the distributed generators supply their rated power at rated frequency. When the load requirement is less than the total rated power of the DGs, the excess power flows from DGs go to the grid. Therefore the PCC voltage should not deviate much from its nominal value and the VSCs must supply the change in the power demand as quickly as possible. Therefore, the control is changed to a state feedback control which uses the feedback of DG output voltage; output current and the current through the filter capacitor. The reference voltage magnitude and angle are calculated from the droop similar to the islanded mode. However the steady state frequency is fixed to the grid frequency and the power output of the DGs are equal to their rated power. The active and reactive power requirements for an individual DG are calculated based on their rating. The output current reference is calculated from the power and voltage reference. The reference for the filter capacitor current is calculated from the voltage reference [21].

As the development of micro-grid, many distributed generations are connected to the grid. IEEE STD 1547-2003 (IEEE Standard for Interconnecting Distributed Resources with Electric Power Systems) is the first standard of grid connected inverter with fuel cell, photovoltaic, energy storage as the front stage. This standard includes response to the grid fault, power quality, islanding, protection, testing and so on. Several important standards will be explained as follows:

The response to the grid voltage abnormity: when the inverter operates in grid-connected mode, the normal range of grid voltage is within 88% and 110% of the standard voltage. When the grid voltage exceeds this limit, the inverter system should detect this fault and disconnects with the grid in a required short time.

Table 2.4 The response time to the abnormal voltage

Voltage range	**Response time (utility cycle)**
Vrms<50%	6
50%<Vrms<88%	120
88%<Vrms<110%	Normal operation
110%<Vrms<120%	120
Vrms>120%	6

Response to the grid frequency abnormity: In IEEE Std 1547-2003, the normal range of frequency is within 49.3~50.5 Hz. This range also changes with the power rating. The details of response time to different power rating is shown in the Table 2.5

Table 2.5 The response time to grid frequency abnormity

Capacity of the Distributed Generation (KW)	Frequency range (Hz)	Response time (s)
<30	<49.3	0.16
	>50.5	0.16
>30	<47.0	0.16
	<(47.0-49.8)	0.16-3.00
	>50.5	0.16

2.6.3Voltage Source Converter (VSC) Circuit Analysis

Inverter-based distributed energy resource can be simply regarded as constant dc voltage sources connected to three-phase inverters. The schematic connection of a voltage source inverter (VSI) is shown in Figure 2.15, which consists of six IGBT switches driven by PWM gate circuits. The VSI converts dc voltage into three phase ac voltage. To analyze the dynamic performance of the inverter-based DER, the average three-phase DC-AC VSC model including the ac link inductor

dynamics and the dc-link capacitor dynamics is first developed in the instantaneous abc frame applying KCL and KVL [23]:

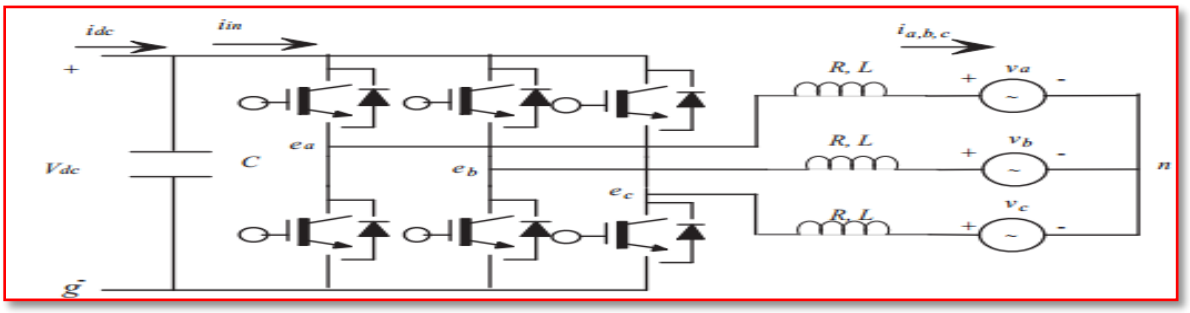

Figure 2.15 Gird connected distributed energy resource circuit *[23]*

$$
\begin{aligned}
L\frac{di_a}{dt} &= -Ri_a - v_{an} + e_{an} \\
L\frac{di_b}{dt} &= -Ri_b - v_{bn} + e_{bn} \\
L\frac{di_c}{dt} &= -Ri_c - v_{cn} + e_{cn} \\
C\frac{dV_{dc}}{dt} &= i_{in} - i_{dc}
\end{aligned}
\tag{2.29}
$$

Where i_{in},i_{dc},$i_{a,b,cn}$, $v_{a,b,cn}$ and $e_{a,b,cn}$, are all labeled in Figure 2.15. To relate the model in (2.29) to the duty cycle of the PWM switching of the converter, the exporting dc current i_{in} and the output voltages of the inverter,$e_{a,b,cn}$, will be re-examined. Neglecting the switching loss of the inverter, the instantaneous power coming to the inverter from the dc side (P_{dc}) should equal to the power transferring to the ac side (P_{ac}).

The following equations are given:

$$
\begin{aligned}
P_{ac} &= P_{dc} \\
P_{ac} &= v_a i_a + v_b i_b + v_c i_c \\
P_{dc} &= V_{dc} i_{in}
\end{aligned}
\tag{2.30}
$$

Hence the expression of the dc side current i_{in} can be expressed as:

$$
i_{in} = \frac{v_a i_a + v_b i_b + v_c i_c}{V_{dc}} = \sum_{i=a,b,c} i_i d_i \tag{2.31}
$$

Where, $d_{a,b,c}$ are the duty cycles of the PWM and $d_i = \frac{v_i}{V_{dc}}, i = a,b,c$

The three-phase voltages from the VSC can be expressed as: considering a three-wire connected balanced AC system, where the summation of the three-phase voltages is zero. $v_{an} + v_{bn} + v_{cn} = 0$, then the neutral to ground voltage v_{ng} can be expressed as follows

$$v_{ng} = \frac{e_{ag} + e_{bg} + e_{cg}}{3} = \sum_{i=a,b,c} d_i \frac{V_{dc}}{3} \tag{2.32}$$

Hence the model in (2.29) can be expressed as:

$$\begin{aligned}
L\frac{di_a}{dt} &= -Ri_a - v_{an} + V_{dc}(d_a - \frac{\sum_{i=a,b,c} d_i}{3}) \\
L\frac{di_b}{dt} &= -Ri_b - v_{bn} + V_{dc}(d_b - \frac{\sum_{i=a,b,c} d_i}{3}) \\
L\frac{di_c}{dt} &= -Ri_c - v_{cn} + V_{dc}(d_c - \frac{\sum_{i=a,b,c} d_i}{3}) \\
C\frac{dV_{dc}}{dt} &= \sum_{i=a,b,c} i_i d_i - i_{dc}
\end{aligned} \tag{2.33}$$

The q-d reference frame where d-axis leads the q-axis by 90^0 is widely used in modeling inverter based circuits. Therefore, the model in (2.33) will eventually be transformed into a qd reference frame. All three-phase variables (voltages, currents, switch functions) can be transformed to a qd reference frame by the qd/abc relationship

$$\begin{bmatrix} f_q \\ -f_d \\ f_o \end{bmatrix} = K_s \begin{bmatrix} fa \\ fb \\ fc \end{bmatrix} \tag{2.34}$$

Where

$$Ks = \frac{2}{3}\begin{bmatrix} \cos\theta & \cos(\theta - \frac{2\pi}{3}) & \cos(\theta + \frac{2\pi}{3}) \\ \sin\theta & \sin(\theta - \frac{2\pi}{3}) & \sin(\theta + \frac{2\pi}{3}) \\ \frac{1}{2} & \frac{1}{2} & \frac{1}{2} \end{bmatrix} \tag{2.35}$$

$$\theta = \int \omega_s dt \tag{2.36}$$

Where θ is an arbitrary angle. If the synchronous frame is angular frequency, then the qd reference frame is a synchronous reference frame. The model in (2.34) in a synchronous reference frame is given as:

$$\begin{aligned} L\frac{di_q}{dt} &= -Ri_q + \omega L i_d + v_q - V_{dc}d_q \\ L\frac{di_d}{dt} &= -Ri_d + \omega L i_q + v_d - V_{dc}d_d \\ C\frac{dVdc}{dt} &= \frac{3}{2}(d_q i_q + d_d i_d) - i_{dc} \end{aligned} \tag{2.37}$$

Since the inverter-based DERs are integrated into an ac micro-grid, per unit system is preferred. The RL circuit model at the ac side in (2.37) can be expressed in state-space and in per unit system as listed

$$\frac{d}{dt}\begin{bmatrix} i_q \\ i_d \end{bmatrix} = \omega\begin{bmatrix} -\frac{R}{X} & 1 \\ -1 & -\frac{R}{X} \end{bmatrix}\begin{bmatrix} i_q \\ i_d \end{bmatrix} + \frac{\omega}{X}\begin{bmatrix} v_q - V_{dc}d_q \\ v_d - V_{dc}d_d \end{bmatrix} \tag{2.38}$$

Where all currents, voltages and impedances are per unit values and ω = 377 rad/s. Inner current control loop vector control is popularly used in converter control where the q-axis is aligned to the output voltage vector. Hence, V_q =V, and V_d= 0. Thus (2.38) can be expressed as:

$$V = -L\frac{di_q}{dt} - Ri_q + \omega L i_d - V_{dc}d_d$$
$$0 = -L\frac{di_d}{dt} - Ri_d - \omega L i_q - V_{dc}d_d \quad (2.39)$$

The cross coupling terms in (2.40) can be treated as disturbance and new variables are defined to have the following relationship

$$v'_q = Ri_q + L\frac{di_q}{dt}$$
$$v'_d = Ri_d + L\frac{di_d}{dt} \quad (2.40)$$

Equation (2.40) describes the control law of the inverter's inner current loop outer power loop. The alignment of the voltage vector to the dq-axis also simplifies active power and reactive power expression. The active power will be proportional to i_q while the reactive power will be proportional to i_d. The overall control diagram of inverters is shown in Figure 2.16 to provide load following service.

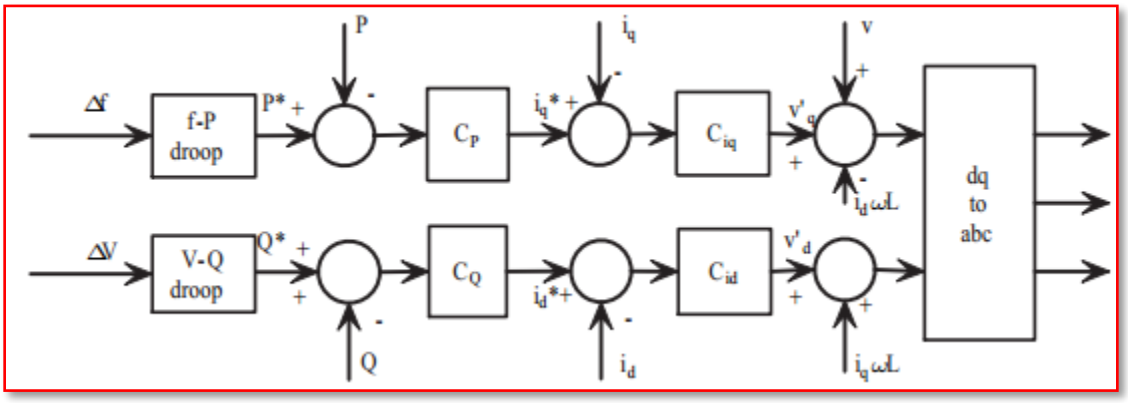

Figure 2.16 Control diagram of an inverter loops and outer slow power control loops *[23]*

The reference active/reactive powers are obtained through the f − P droop characteristic which is shown in Figure 2.16. Proportional and integral (PI) controllers are used in the inverter controls. The outer power control loops generate reference currents i^*_q and i^*_d. The inner current controls

which are PI controls will force the measurements i_q and i_d to follow the reference values.

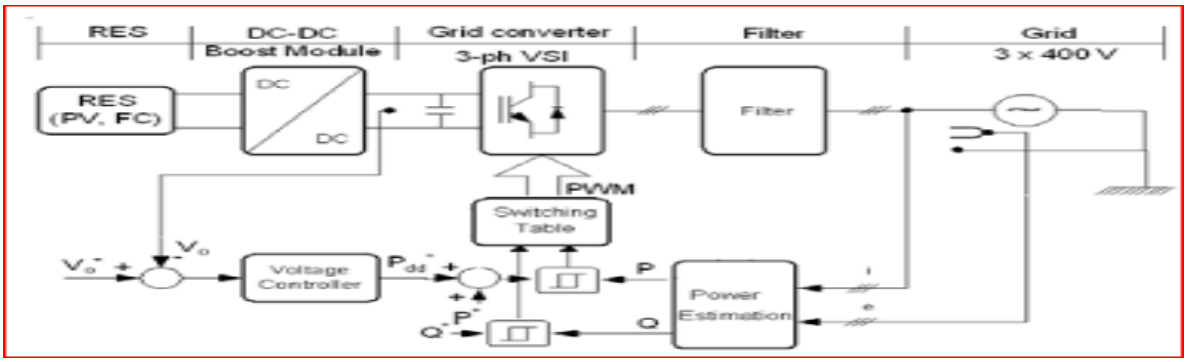

Figure 2.17 Power Control based on the active and reactive power reference *[19]*

2.7 Literature Review

In this section previous works which are directly or indirectly related to the idea of this thesis work are examined. Works reviewed in this section are generally categorized in to three: a published journal papers, M.Sc. thesis and Ph.D. dissertation and international conference report.

T. Suman published "Modelling and Simulation of Micro Grid Equipped Based on Photo Voltaic /Fuel Cell Equipped with Power Electronic Interfaces" in International Journal of Research Studies in Science [24]. The simulation results showed that the detection algorithm can distinguish between islanding events and changes in the loads and can apply the load-shading algorithms when needed. The re-closure algorithm causes the DG to resynchronize itself with the grid. In addition, it is shown that the response of the proposed control schemes is capable of maintaining the voltages and currents within permissible levels during grid connected and islanding operation modes. The simulation results showed that the proposed control schemes are capable of maintaining the voltages within the standard permissible levels during grid-connected and islanding operation modes.

A work entitled as "Technical Challenges on Micro grids" has been developed by a group of A. A. Salam, A. Mohamed and M. A. Hannan [25]. Development of micro-grid concept and technologies requires more effort to resolve numerous economic, commercial and technical challenges by close cooperation and exchange of information among researcher on these activities has highly beneficial for the advancement of the micro-grid research.

The paper indicated in [26] entitled as "Robust Repetitive Feedback Control Of A Three-Phase Grid Connected Inverter", has been published by M. Jamil, S. M. Sharkh, M. Abusara, R. J. Boltryk in University of Southampton. Simulations results show repetitive control can significantly improve the Total Harmonic Distortion (THD) quality of the output current. The RC parameters need to be selected carefully to ensure stability despite uncertainty in grid impedance, while achieving a fast response and a small steady state error. The proposed controller was demonstrated to be robust to changes in grid impedance. The author recommends to the other researchers, further work is needed to improve the steady state error.

The work indicated in [27] entitled as **"**Active and Reactive Power Control and Quality Management In DG-grid Interfaced Systems", has been contributed by R. D. Patidar and S. P. Singh. This paper discusses the application of active power filters as an interface between distributed generation and grid. The proposed active power filter (APF) system is capable for injecting DG power to electric grid while compensating load power factor, harmonics and load balancing. The utility currents are sinusoidal and in-phase with their respective voltages (forwarded mode) and sinusoidal and 1800 out of phase in (reverse mode).The proposed controller is also suitable under unbalanced and distorted Grid voltages. Apart from these the proposed control Strategy is suitable for islanding mode of operation. The computation of reference source (grid) currents in natural reference frame rather than transformation reduces the computational burdens.

K.Jaganmohangoud, et al. [28]. The article proposes a cascaded current voltage control strategy has been proposed for inverters in micro grids. It consists of an inner voltage loop and an outer current loop and offers excellent performance in terms of total harmonic distortion (THD) for both the inverter local load voltage and the grid current. In particular, when nonlinear and/or unbalanced loads are connected to the inverter in the grid-connected mode, the proposed strategy significantly improves the THD of the inverter local load voltage and the grid current at the same time. The controllers are designed using the H∞ repetitive current control and fuzzy based voltage control in this paper. The proposed strategy also achieves seamless transfer between the standalone and the grid-connected modes. The strategy can be used for single-phase systems or three-phase systems. As a result, the nonlinear harmonic currents and unbalanced

local load currents are all contained locally and do not affect the grid. Simulation results under various scenarios have demonstrated the excellent performance of the proposed strategy [28].

Tomas, et al, [29]. In this paper, the H∞ repetitive control strategy has been applied to the current controller for grid-connected Voltage source inverters (VSI). The proposed controller is compared with the traditional proportional resonance (PR), proportional integrator (PI), and predictive data base (DB) controllers, all implemented in the natural frame with the main focus on harmonics distortion and tracking performance. The H∞ repetitive controller offers significant improvement over the conventional PI, PR, and DB controllers and leads to very low THD for the output current, even in the presence of nonlinear/unbalanced loads and/or grid-voltage distortion. The price paid for this is its relatively slow dynamics (the slightly more complex calculation and design are no longer a main issue because of the advances in digital signal processing and controller design.

"Adaptive Droop Control Applied to Voltage-Source Inverters Operating in Grid-Connected and Islanded Modes" has been developed by Juan C. Vasquez, Josep M. Guerrero [30]. This paper has presented a novel control for Voltage source inverters (VSI) that is able to operate in islanding mode, as well as in grid-connected mode. In this last case, the inverter is able to inject the desired active and reactive power to the grid. The control has two main structures. The first one is the grid parameter estimation, which calculates the amplitude and frequency of the grid, as well as the magnitude and phase of the grid impedance. The second one is a droop-control scheme, which uses these parameters to inject independently active and reactive power to the grid. The proposed droop control uses such parameters to close the loop, achieving a tight P and Q regulation. Owing to the feedback variables of the estimator, the system dynamics is well decoupled from the grid parameters. The results point out the applicability of the proposed control scheme to DG VSIs for micro-grid applications [30].

Daniele Menniti, et.al [31]. This paper simulation results by using grid-connected inverter, the DG systems have been able to influence the power flows of the Micro-grid very quickly and in significant manner. However, the good characteristics of the control strategy used, such fast performances have been achieved without generating perturbations and instability problems on the Micro-grids. In fact, the numerical simulations show that the DG systems effectively provide services as reactive power compensation and load balancing without influence each other.

Ashna Mohan, et.al. [32]. In this paper, stable control strategies were designed for a single PWM inverter addressing the issues of both stand-alone and grid connected power supply modes. An adaptive total sliding mode controller was used for voltage and current control of the single phase inverter in stand-alone and grid connected power supply mode respectively. This lead to the minimization of THD in the output voltage and the improvement of power factor of the output current of the inverter. Hence, the PWM inverter has been used to provide high power quality ac output through the proposed control technique. Robust control performance, high standalone power supply quality, high grid connected power supply quality and automatic transformation between the standalone and grid connected power supply modes are the advantages of the DG inverter with the ATSMC scheme. The simulation results obtained using the Matlab/Simulink software environment were incorporated to verify the effectiveness of the proposed system [32].

Generally, the description of the literature reviews show that the mitigation technique of the gird connected distributed generation units are different with this study. This alleviation of the problem is done by using capacitor voltage differential feedback controlling method. The Proposes a multi-loop controller with voltage differential feedback, and with output voltage decoupling and output current decoupling by using the output voltage feedback. The output voltage differential feedback loop actively damps the output LC filter resonance thus increases the system stability margin. The decoupling of output voltage and current makes the inner loop equivalent to a first order system thus improve the system dynamic response to load disturbance. In addition to this, this study begins from modeling of the distributed generations models to the controlling technique when there are interfacing in gird for synchronizing.

CHAPTER THREE

3. FEASIBILITY STUDY OF DISTRIBUTED GENERATION SYSTEM

3.1 Source Overview

The proposed energy system should be met the critical load demand of the community. The main sources of energy considered in this thesis are solar, fuel cell and wind. Fuel cell systems are employed in the energy system due to the intermittent nature of the other two renewable sources. Some of the input values into the software are expressed in size and in quantity. Wind turbines is the power system components which vary in quantity, and solar PV and converter are other components that vary in size. This chapter is to illustrate the input variables that help for optimization of modeling of the system and to show some resulted value related to the inputs. Detail of the components of the power system would be explained in the next chapters. Figure 3.1 presents the schematic representation of HOMER simulation model of the hybrid system architecture considered in this thesis.

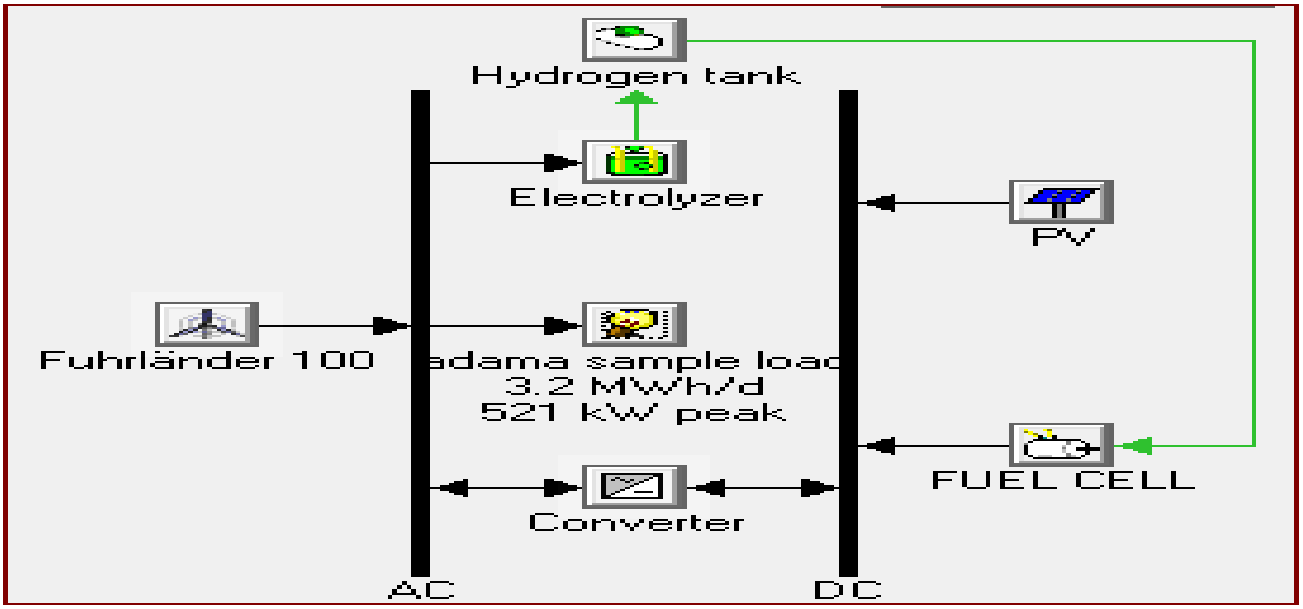

Figure 3.1 Architecture of the Selected Technologies of the DG system produced by HOME

3.2 Load Estimation

The electricity load determination is the first to be considered in any modeling tool. The primary load input, which is taken as a sample, is estimated for modeling and analysis of hybrid system. In this thesis, the proposed energy system should meet the load demand of the community but two hundred households loads are taken for sample modeling. The load analysis is supported by HOMER software. The loads have entered on hourly basis (24 hours data) and thereafter the software modeled the peak load. Moreover, it also synthesized the monthly load from the 24 hour input data. Serving loads is the reason for the existence of power systems, so the modeling of power system begins with the modeling of the load or loads. The daily power demand and energy need for the community of two households are estimated by considering basic domestic appliances listed in the Table 3.1.

Table 3.1 Power and energy consumption of a house appliances assumption

No	Appliances per house	Rating (W)	Hourly used per day	Number of units	Consumption per day (kWh/day)	Assumed usage time interval (hr)
1	Stove	1500	3	1	4.500	7-8,19-20,11-12
2	Electric Mitad	2500	1	1	2.500	6-7
3	CFL	11	6	4	0.264	18-24
4	LED light bulbs	9	6	4	0.216	18-24
5	Washing machine	500	1	1	0.500	9-10
6	Electric Iron	400	2	1	0.800	21-23
7	Laptop	50	3	1	0.150	19-20,7-8,13-14
8	Toaster	600	1	1	0.600	22-23
9	Coffee maker	600	1	1	0.600	12-13
10	Refrigerator	105	24	1	2.520	1-24
11	Mobile charger	3	3	1	0.009	19-20,7-8,12-13
12	Internet modem	10	24	1	0.240	1-24
13	Air conditioner	400	6	1	2.400	11-17
14	Television	150	5	1	0.750	19-22,7-8,13-14

From the Table 3.1 the total power and energy consumption can be calculated. The total maximum load of an assumed house is 6,916Watt and energy consumption is 16.049 kwh/day. If the assumption is taken for 200 households of the town, the power demand and the energy consumed are 1.3832MW and 3.2098MWh/day respectively.

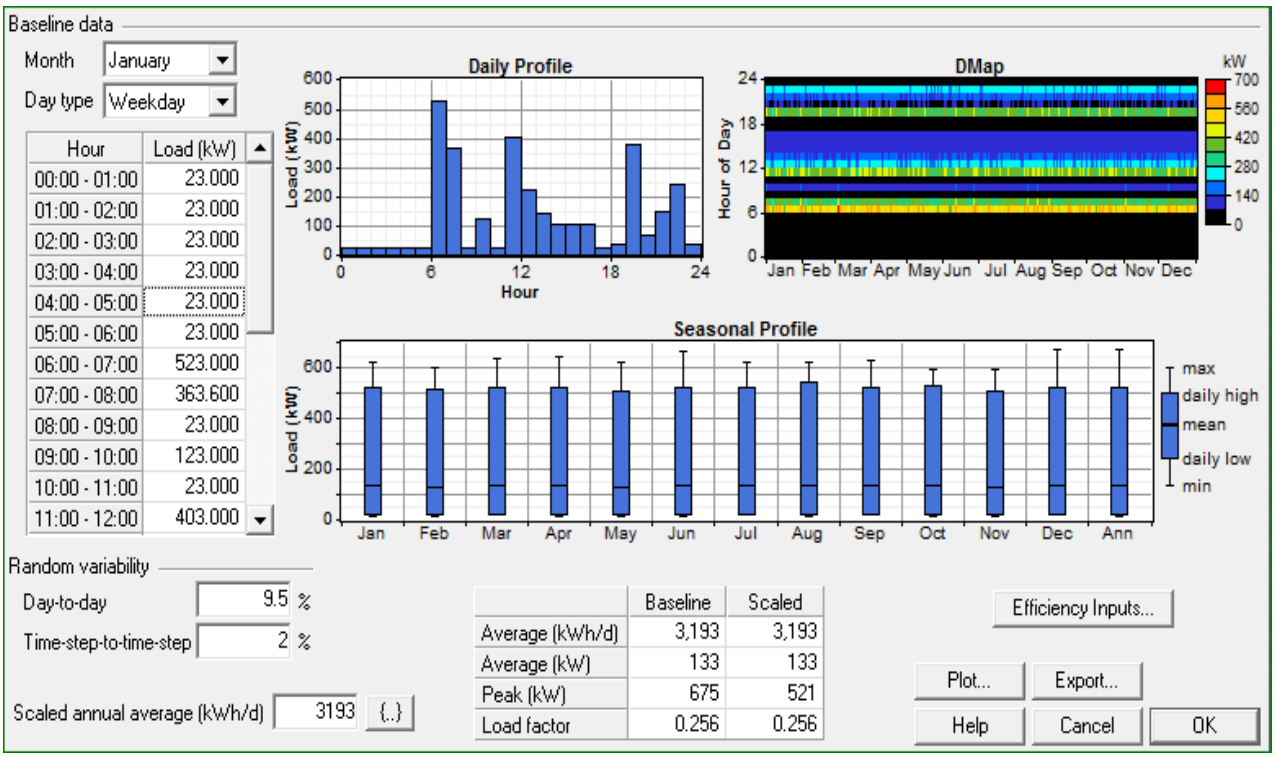

Figure 3.2 Diurnal Variation of Primary Load Profile

Most of the appliances employed in residential and service areas operate with alternating current voltages and hence AC loads are suggested.

3.3 Solar and Wind Energy Sources

3.3.1 Monthly average solar radiation and wind speed from NASA website

The solar resource raw data inputting to the software is the average global horizontal radiation obtained from NASA website over 22 years' experience average data. On top of the solar resources data the latitude and longitude of this area would also be used as an input. The time zone is another parameter to be set. The place is located at latitude: 8º33'35"N - 8º36'46" N, longitude: 39º11'57" E – 39º21'15" E, and with time zone of GMT +3:00. In order to get how much power is generated by the solar PV, it requires inputting solar resources data in units of kW/m^2 into HOMER software.

Table 3.2 Monthly Radiation, Wind and temperature data of the study area

Months	Solar radiation [NASA]			Wind speed (m/s) [NASA]			Air temp. (^oC) [NASA]	
	$kWh/m^2/day$	Cl.Index	kW/m^2	10m	50m	100m	Max	Min
January	6.08	0.670	0.81	3.42	4.33	4.80	37.1	12.3
February	6.57	0.677	0.86	3.14	3.97	4.40	40.2	13.1
March	6.52	0.634	0.86	3.01	3.81	4.22	41.5	12.6
April	6.31	0.601	0.84	3.06	3.87	4.29	39.6	11.3
May	6.36	0.616	0.83	2.86	3.62	4.01	37.6	10.4
June	5.77	0.569	0.78	2.89	3.66	4.06	31.1	7.80
July	5.23	0.491	0.70	2.53	3.20	3.55	27.5	6.52
August	5.36	0.517	0.74	2.29	3.91	3.22	27.4	6.68
September	5.84	0.567	0.80	2.31	2.93	3.25	30.1	8.09
October	6.31	0.642	0.83	2.84	3.60	3.99	33.0	10.1
November	6.27	0.642	0.84	3.24	4.09	4.54	34.4	11.2
December	6.08	0.688	0.82	3.37	4.26	4.72	34.8	11.5
Average	6.05	0.610	0.81	2.91	3.77	4.09	34.53	10.13

3.3.2 Monthly Averaged Wind Speed from Data Recording Software

The anemometer masts are accompanied with the wind vanes for the sake of recording the wind speed. These data have been recorded using the SymphoniePLUS3 data logger of Adama wind farm II .The wind speed with height variation is also presented in Table 3.3 using the monthly average wind speed. The anemometer greater than 50 m height is selected due to the fact that the influences of the terrain around the mast are less as compared to the anemometer at 10 m and 30m.

Table 3.3 Monthly Averaged Wind Speed form data recording software of Adama wind II

Months	Wind Speed(m/s)			
	10meter	30meter	50 meter	70meter
January	6.83	9.08	10.34	10.74
February	6.71	8.87	9.85	10.63
March	6.54	8.75	9.65	9.81
April	4.45	5.58	6.43	6.63
May	5.13	6.67	7.28	7.82
June	5.54	6.91	7.13	7.14
July	5.73	7.10	7.56	7.62
August	4.52	5.67	6.39	6.43
September	3.61	4.55	5.17	5.49
October	5.93	7.81	8.78	9.51
November	6.14	8.63	9.29	10.23
December	6.43	8.94	9.84	10.57
Average	5.52	7.38	8.14	8.55

Similar to the solar sources data the wind speed was taken from Adama wind II recorded of anemometer of the site. Wind speed was taken at 10meter, 30meter, 50meter and 70 meter height wind mast but the data used in this thesis take only the 50 meter height data put under Table 1.2.

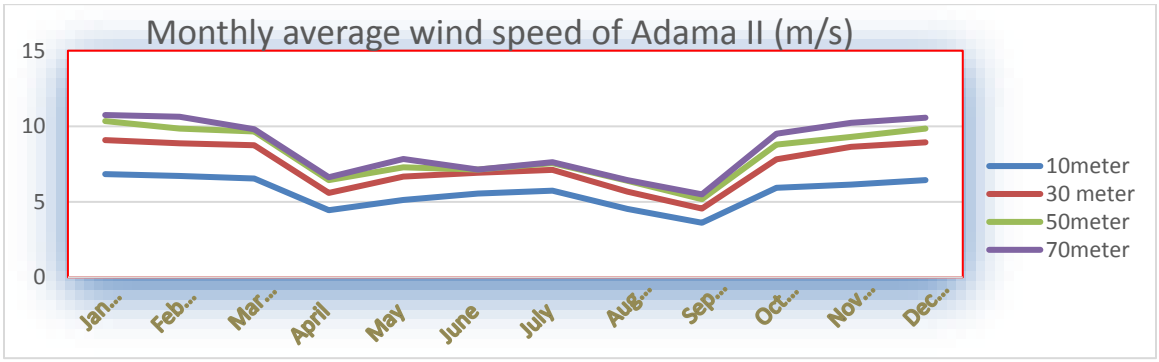

Figure 3.3 Graphical representation of Adama wind II monthly average wind speed

Share of electricity generated by wind turbine is calculated by the software, thus average wind speed data is inputting into HOMER for the determination of energy production from wind

sources. In addition to the wind speed resources the altitude above sea level, the anemometer height are the required inputs too.

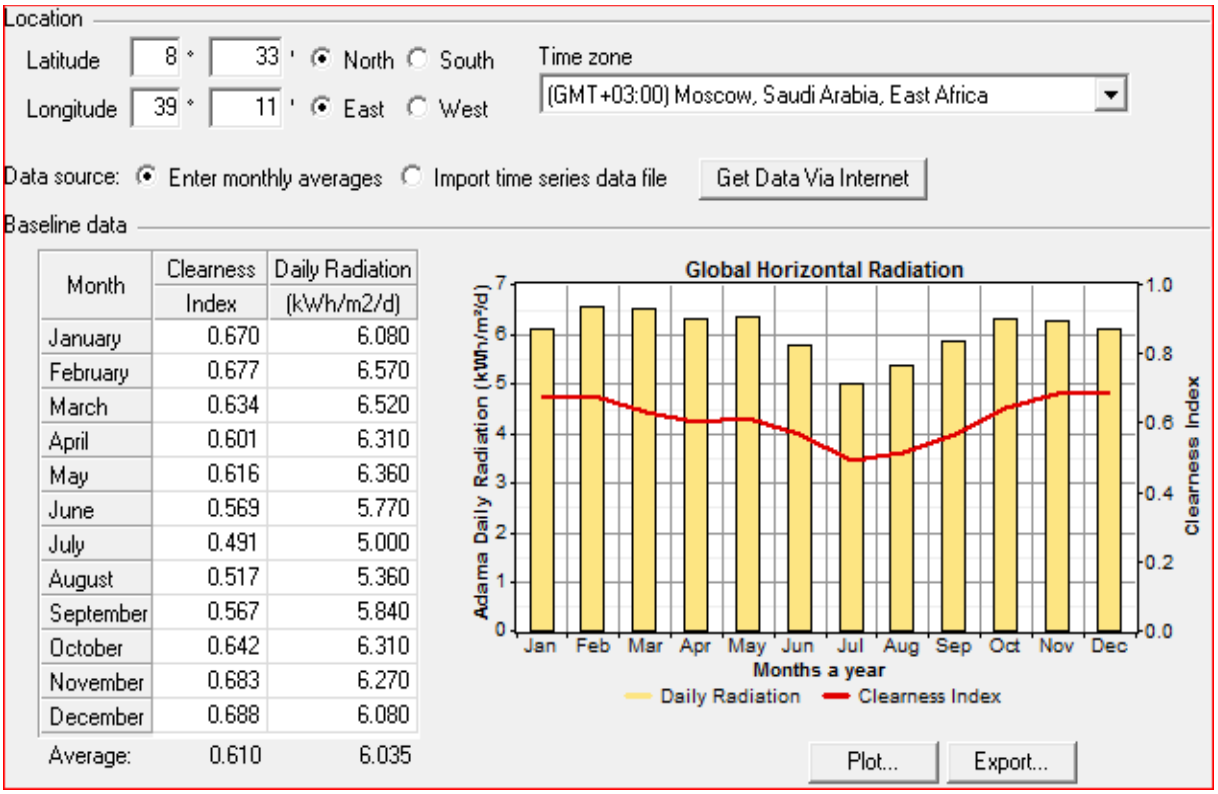

Figure 3.4 Monthly Variation of Global Horizontal Solar Radiation Source

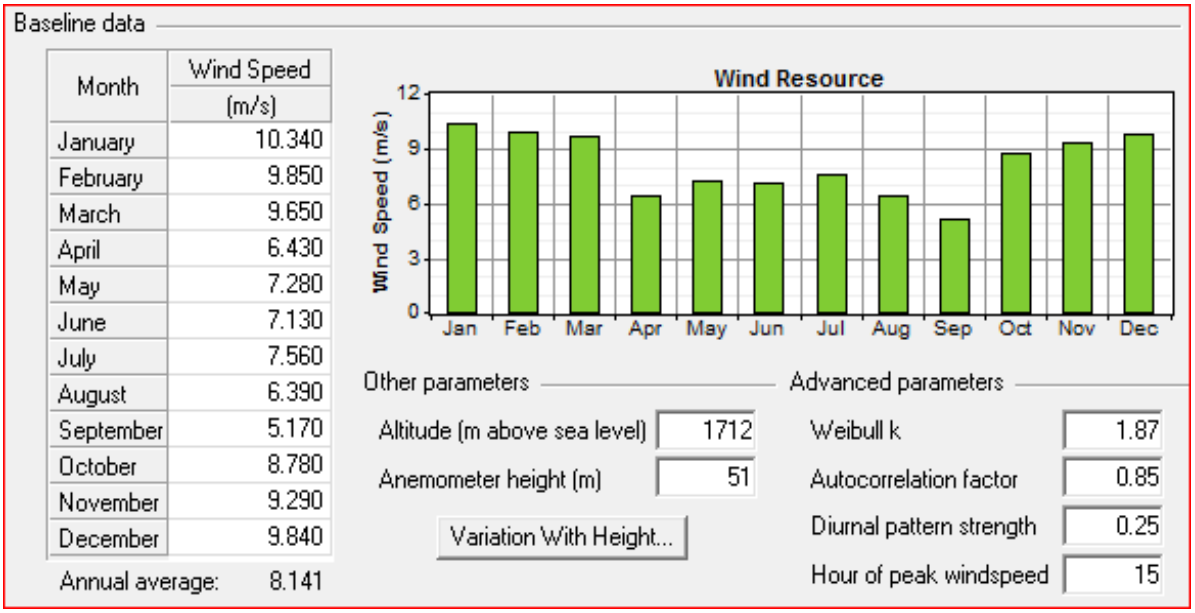

Figure 3.5 Monthly Variation of Wind speed for each month

3.4 Cost Data and Size Specifications of Each Component

The basic criterion related to the selection of the power system components in this thesis work is the cost of components, as the main purpose of the work is searching the optimum power system configuration that would meet the demand with minimum net present cost (NPC) and cost of energy (COE). The estimation of the components cost is made based on the current cost available in market.

Initial capital cost of components: It is the total installed cost deployed to purchase and install the component at the commencement of the project.

Replacement cost: This is the cost required to replace wear out components at the end of its life cycle. This cost is different from initial cost of the component, due to the following reasons. At the end of its life cycle not all of the spares of the component need to replace, Costs from donors may eliminate or can reduce initial cost, however replacement cost may not account travel costs but initial costs do.

Operation and maintenance (O&M) cost: It is the cost accounted for maintenance and operation of the system. The entire scheme components considered in this thesis has different operation and maintenance costs. Miscellaneous O&M costs considered by HOMER are like emission penalties, capacity shortage penalty and fixed operation and maintenance costs.

3.5 Solar PV Size and Cost

After surveying different products focusing on the cost provided the following panel is chosen. The reason for choosing the product from the stated company is due to its low cost delivered as long as efficiency is not a big concern here. The solar panel considered is a 1kW, which is with 4 number of solar module having 250 W capacities from a schott Mono-250Watt solar panel company. The selected panel is mono-crystalline silicon solar cell and manufactured by USA which is known as Item-1202401 model with an efficiency of 14.9% [appendix]. In this paper the operation and maintenance cost would be 1% per year.

Table 3.4 PV input costs, sizes and lifespan of *[33]*

PV Size (Kw)	Capital cost ($)	O&M cost ($/year)	PV Life (year)	Size considered (kW)
1	1000	10	25	0,1000,2000,3000 ,4200,4300,4500

Derating factor is a term accounted for both PV systems efficiency and charge controller efficiency since charge controller is not being designed by HOMER. This factor is to be subsidized for dust, high temperature, shading, wiring losses, and so on. The size of the PV panels input in to HOMER is in kW, not in m^2, thus its efficiency is not taken into account as an input. The azimuth angle or orientation and angle of inclination of the PV panel are the two important factors that should be considered during solar system design. For sufficient amount of electricity generation the ideal orientation of solar PV is due south, but however it is also possible to face south-east or south-west, there will actually small loss due to the shift of west or east of south. The following parameters are considered for modeling of the power system like; the derating factor is taken as 75%, ground reflectance is also considered as 20%, slope 8.5 (latitude of the location) and azimuth 0 (south orientation).

3.6 Wind Turbine Size and Cost

Depending on the wind speed sources the turbine has to generate large amount of energy to contribute significant renewable fraction and this can be performed using single large wind turbine or number of smaller turbines. Quantities of turbines, service time, hub height, Cost of the component, type of electricity generated, cut-in wind speed are the restrictive values to select wind turbine. The selected turbines can generate AC type electricity to satisfy the need of AC load consumer appliances. The wind turbine taken for this thesis work is fifteen fuhrlander 100kW AC power rating type to produce 1.5MW power output. The wind turbine is manufactured by the D-56477 Waigandshain, Germany. The total installed capital cost is averaged from $1377/kW to $2867/kW in U.S and Germany [33]. In this thesis mean installed cost is taken about $1377/kW. Replacement cost and operation and maintenance cost of the wind turbine is considered about 65% and 2% of capital cost respectively.

Table 3.5 The Wind Turbine Parametric Inputs into HOMER *[33]*

Capacity (Kw)	Capital cost ($)	Replacement cost($)	O&M cost ($/year)	Life (years)	Tower height(m)	Quantity
1	1377	895	27.54	33	50	0,10.15

3.7 Fuel cell size and cost

The cost of fuel cell varies greatly depending on type of technology, reformer, auxiliary equipment and power converters. At present, fuel cell costs varies from $3,000 to $6,000/5kW. Considering these factors, the capital, replacement and operational costs are taken as $3000, $2500 and $0.080/hr for a 5 kW system, respectively. The cost of fuel cell is one of the most significant issues in commercializing a hybrid energy system with hydrogen storage, a sensitivity analysis with varying cost is necessary. Here, a set of cost multiplying factors for fuel cell is taken into account [34].

3.7.1 Electrolyzer

An electrolyzer consumes electricity to generate hydrogen via the electrolysis of water. In HOMER, the user specifies the size of the electrolyzer, which is a decision variable, in terms of its maximum electrical input. The user also indicates whether the electrolyzer consumes ac or dc power, and the efficiency with which it converts that power to hydrogen. HOMER defines the electrolyzer efficiency as the energy content (based on higher heating value) of the produced hydrogen is divided by the amount of electricity consumed. The final physical property of the electrolyzer is its minimum load ratio, which is the minimum power input at which it can operate, expressed as a percentage of its maximum power input. The economic properties of the electrolyzer are its capital and replacement cost in dollars, its annual O&M cost in dollars per year, and its expected lifetime in years. Current production cost of electrolyzer is $1,000–$3,000/5kW [34]. With improvements in polymer technology, control systems and power electronics it is expected that costs would reduce much. In this analysis, a 5 kW system is associated with $1000 capital, $100 replacement and $10 maintenance cost [34].

3.7.2 Hydrogen tank

In HOMER, the hydrogen tank stores hydrogen produced by the electrolyzer for later use in a hydrogen-fueled generator. The user specifies the size of the hydrogen tank, which is a decision

variable, in terms of the mass of hydrogen it can contain. HOMER assumes that the process of adding hydrogen to the tank requires no electricity, and that the tank experiences no leakage. The user can specify the initial amount of hydrogen in the tank either as a percentage of the tank size or as an absolute amount in kilograms. It is also possible to require that the year-end tank level must equal or exceed the initial tank level. If the user chooses to apply this constraint, HOMER will consider infeasible any system configuration whose hydrogen tank contains less hydrogen at the end of the simulation than it did at the beginning of the simulation. This ensures that the system is self-sufficient in terms of hydrogen. The economic properties of the hydrogen tank are its capital and replacement cost in dollars, its annual O&M cost in dollars per year, and its expected lifetime in years. Hydrogen produced at 30 bar from the electrolyzer will be stored in conventional hydrogen storage tanks. The lifetime is also considered 20 years [35]. The selected hydrogen tank the purchase and replacement costs of the hydrogen tank are estimated to be about 19,500$ and 752.5$ per kW, respectively. The maintenance cost of hydrogen tank is taken to be $10 per kW [36, 34].

3.8 Power Converter Size and Cost

A converter needs to maintain flow of energy between AC and DC power system components. The rated power of the inverter should be equal to or larger than the peak load but since the load will supply both from the renewable and non-renewable, even below the peak would be installed. There is no estimated operating and maintenance cost for this case. The considered Converter sizes are: 0,200,300,500 and 1000kW; Capital cost of converter is taken as $2,000, replacement cost is about $1400 which is 70% of the capital cost, efficiency of converter is around 90% and the lifetime of the converter will end for 15 years. Generally, the cost effective system in the form of categorized simulation result is displayed in Table 3.6. [33, 34].

Table 3.6 Simulation Result

PV (kW)	FL100	FC (kW)	Conv. (kW)	Elec. (kW)	H2 Tank (kg)	Disp. Strgy	Efficiency Measures	Initial Capital	Operating Cost ($/yr)	Total NPC	COE ($/kWh)	Ren. Frac.	Capacity Shortage	FC (hrs)
1000	15	500	500	3400	955000	CC	No	$ 4,203,000	90,269	$ 6,942,790	0.196	1.00	0.00	1,780
1000	15	500	500	3400	955000	LF	No	$ 4,203,000	90,269	$ 6,942,790	0.196	1.00	0.00	1,780
1000	15	500	500	3400	955000	CC	Yes	$ 4,203,000	90,269	$ 6,942,790	0.196	1.00	0.00	1,780
1000	15	500	500	3400	955000	LF	Yes	$ 4,203,000	90,269	$ 6,942,790	0.196	1.00	0.00	1,780
1000	15	500	500	3400	955500	CC	No	$ 4,203,250	90,272	$ 6,943,131	0.196	1.00	0.00	1,780
1000	15	500	500	3400	955500	LF	No	$ 4,203,250	90,272	$ 6,943,131	0.196	1.00	0.00	1,780
1000	15	500	500	3400	955500	CC	Yes	$ 4,203,250	90,272	$ 6,943,131	0.196	1.00	0.00	1,780
1000	15	500	500	3400	955500	LF	Yes	$ 4,203,250	90,272	$ 6,943,131	0.196	1.00	0.00	1,780
1000	15	500	500	3400	955600	CC	No	$ 4,203,300	90,272	$ 6,943,198	0.196	1.00	0.00	1,780
1000	15	500	500	3400	955600	LF	No	$ 4,203,300	90,272	$ 6,943,198	0.196	1.00	0.00	1,780
1000	15	500	500	3400	955600	CC	Yes	$ 4,203,300	90,272	$ 6,943,198	0.196	1.00	0.00	1,780
1000	15	500	500	3400	955600	LF	Yes	$ 4,203,300	90,272	$ 6,943,198	0.196	1.00	0.00	1,780
1000	15	500	500	3400	956000	CC	No	$ 4,203,500	90,275	$ 6,943,472	0.196	1.00	0.00	1,780
1000	15	500	500	3400	956000	LF	No	$ 4,203,500	90,275	$ 6,943,472	0.196	1.00	0.00	1,780
1000	15	500	500	3400	956000	CC	Yes	$ 4,203,500	90,275	$ 6,943,472	0.196	1.00	0.00	1,780
1000	15	500	500	3400	956000	LF	Yes	$ 4,203,500	90,275	$ 6,943,472	0.196	1.00	0.00	1,780
1000	15	500	500	3500	955000	CC	No	$ 4,213,000	90,405	$ 6,956,935	0.197	1.00	0.00	1,780
1000	15	500	500	3500	955000	LF	No	$ 4,213,000	90,405	$ 6,956,935	0.197	1.00	0.00	1,780
1000	15	500	500	3500	955000	CC	Yes	$ 4,213,000	90,405	$ 6,956,935	0.197	1.00	0.00	1,780
1000	15	500	500	3500	955000	LF	Yes	$ 4,213,000	90,405	$ 6,956,935	0.197	1.00	0.00	1,780
1000	15	500	500	3500	955500	CC	No	$ 4,213,250	90,408	$ 6,957,276	0.197	1.00	0.00	1,780
1000	15	500	500	3500	955500	LF	No	$ 4,213,250	90,408	$ 6,957,276	0.197	1.00	0.00	1,780
1000	15	500	500	3500	955500	CC	Yes	$ 4,213,250	90,408	$ 6,957,276	0.197	1.00	0.00	1,780
1000	15	500	500	3500	955500	LF	Yes	$ 4,213,250	90,408	$ 6,957,276	0.197	1.00	0.00	1,780
1000	15	500	500	3500	955600	CC	No	$ 4,213,300	90,409	$ 6,957,344	0.197	1.00	0.00	1,780

The best energy system is selected with less net present cost (NPC), less cost of energy (COE), less capacity shortage, less excess electricity and less fuel consumption. The maximum annual capacity shortage and minimum renewable fraction are the worst constraints case. Based on the selection, the electricity generation from optimum system of each source has been put in Figure 3.6.

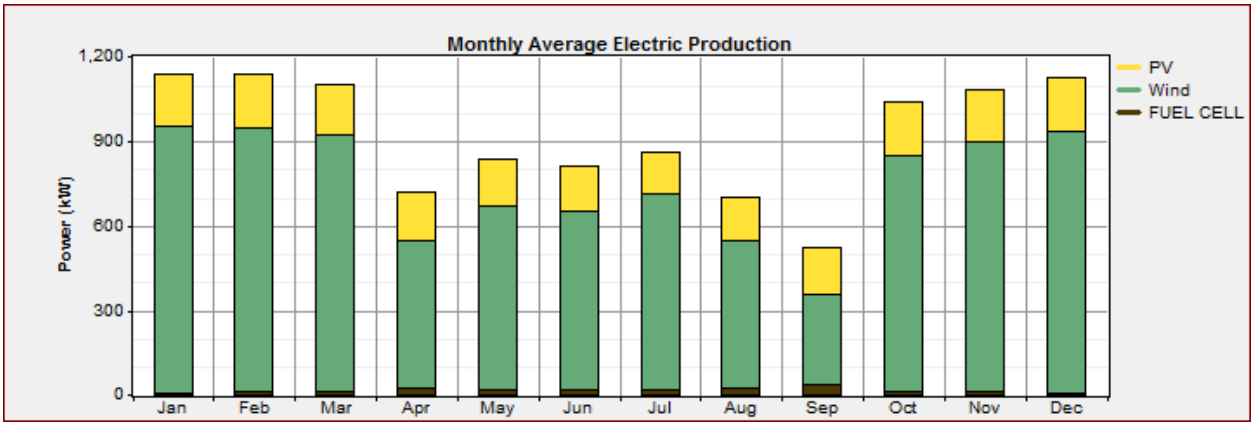

Figure 3.6 Share of Electricity Generation from the Optimum System

3.9 Cost Summary

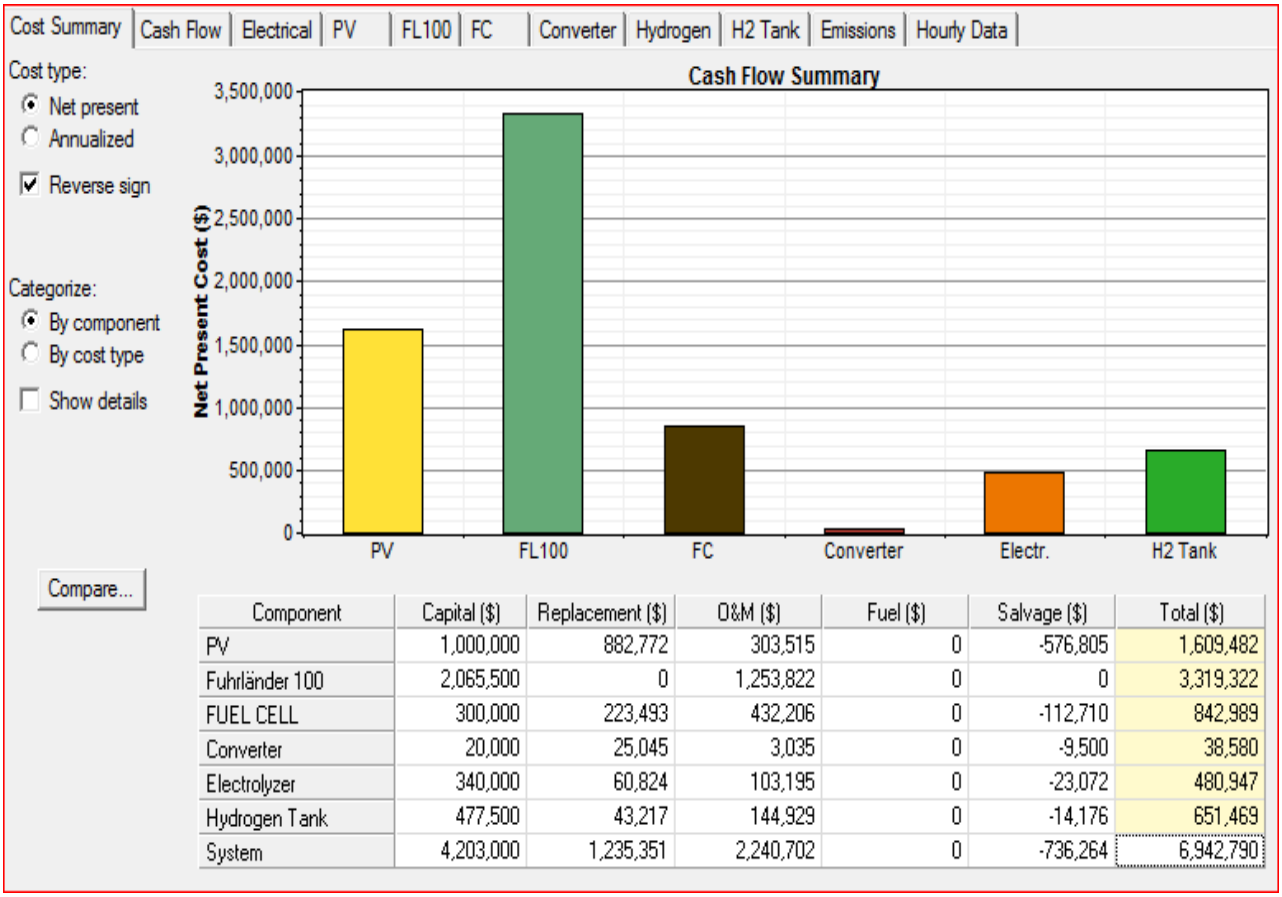

Component	Capital ($)	Replacement ($)	O&M ($)	Fuel ($)	Salvage ($)	Total ($)
PV	1,000,000	882,772	303,515	0	-576,805	1,609,482
Fuhrländer 100	2,065,500	0	1,253,822	0	0	3,319,322
FUEL CELL	300,000	223,493	432,206	0	-112,710	842,989
Converter	20,000	25,045	3,035	0	-9,500	38,580
Electrolyzer	340,000	60,824	103,195	0	-23,072	480,947
Hydrogen Tank	477,500	43,217	144,929	0	-14,176	651,469
System	4,203,000	1,235,351	2,240,702	0	-736,264	6,942,790

Figure 3.7 Cash Flow Summary in terms of NPC by Component Type

Generally, the cost sharing of each components of the system has been shown in Figure 3.7. The system cost of wind generator has incurred high cost to purchase which is about 47.8% of the total NPC cost, however due to its renewable nature and existence of the availability of the study area, it is loaded to install within the area. Solar PV (23.18%) and fuel cell stack (28.45%) is the second and third of the net present cost respectively. The last 0.5% is for the converter system. Therefore, total NPC is $ 6,942,790 .Wind generators take the first highest total NPC which is around $ 3,319,322. The second is fuel cell stack $ 1,975,405. Fuel cell stack cost is the summation of generator, electrolyzer and hydrogen tank because of the nature of the generator and PV is the third placed scheme with cost of $1,609,482. Therefore, the FC, electrolyzer and hydrogen tank costs are $ 842,989, $ 480,947 and $ 651,469 respectively. The power system capital cost, Net present cost and the levelized COE are $ 4,203,000, $ 6,942,790 and $0.196/kWh, respectively.

CHAPTER FOUR

4. DISTRIBUTED GENERATION SYSTEMS MATLAB MODELING

4.1 General Simulink Model of the Hybrid System

The distributed generation power systems are combination of wind generator, solar PV and fuel cell technologies to produce power as model in chapter three. This chapter deals with the detail modeling of each component of sub-system models using matlab/Simulink. The wind turbine produces AC type voltage as they are alternating in nature, whereas the PV panels and fuel cell output are DC types. Therefore, all type of sources must convert in the same AC type to analysis and synchronize with grid system. However, the AC sources first convert into DC in order to design the control system when they are working with grid connected and standalone system. Bidirectional converter is fitted in this configuration which is basically used to convert the AC to DC or DC to AC source depend on the load type. Most of loads required by consumers are AC type. The general Matlab/Simulink model of the optimum hybrid power system is given in Figure 4.1. The detailed models of subsystems are presented in the coming subsequent sections.

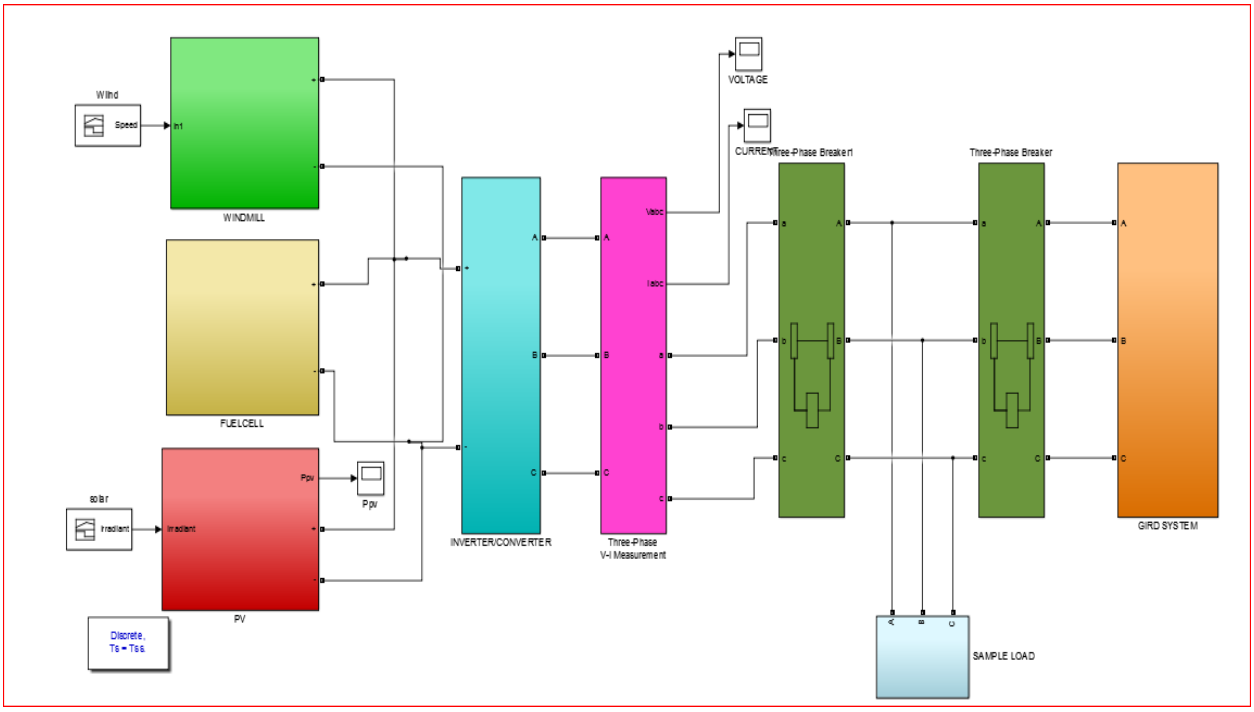

Figure 4.1 General MATLAB/Simulink model of hybrid system

4.2 Solar Energy Conversion System

The photovoltaic system is one of the way that can generate direct current electricity without environmental impact when is exposed to sunlight. This study focus on modeling of the PV system using matlab/Simulink of the study area based on the data available. The basic building block of PV arrays is the solar cell, which is basically a p-n junction that directly converts light energy into electricity. Therefore, this detail matlab/Simulink model of PV has been shown how the PV system works using solar energy. This model is done based of the data obtained from NASA freely accessible data table to determine the solar radiation energy of the area. The Table 3.2 put at chapter three and the analysis of the design was done with the market available solar panel which indicated in appendix of this thesis in the last pages.

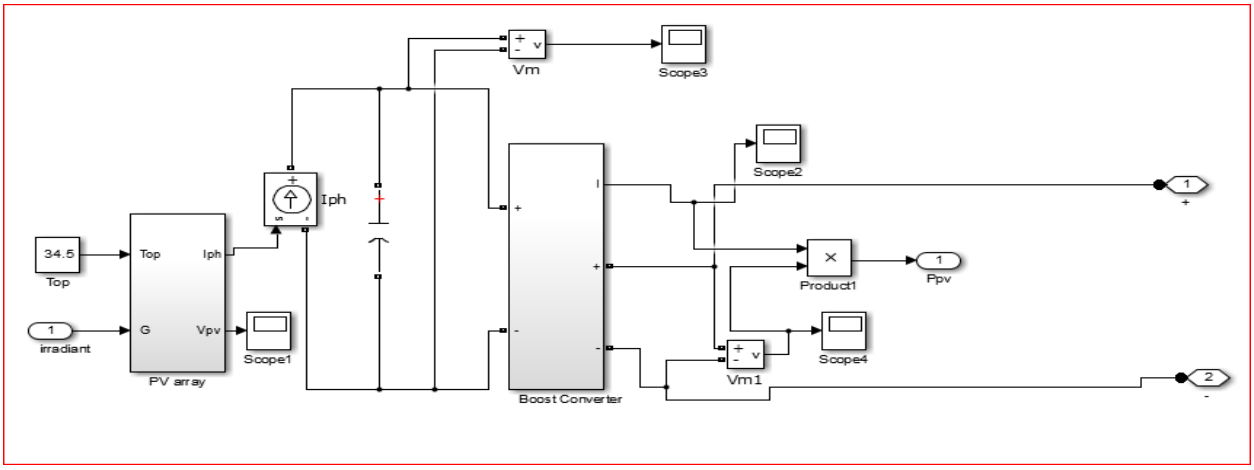

Figure 4.2 Expanded view of photovoltaic model

The output characteristic of PV module depends on the cell temperature, solar irradiation, and output voltage of the module [16].

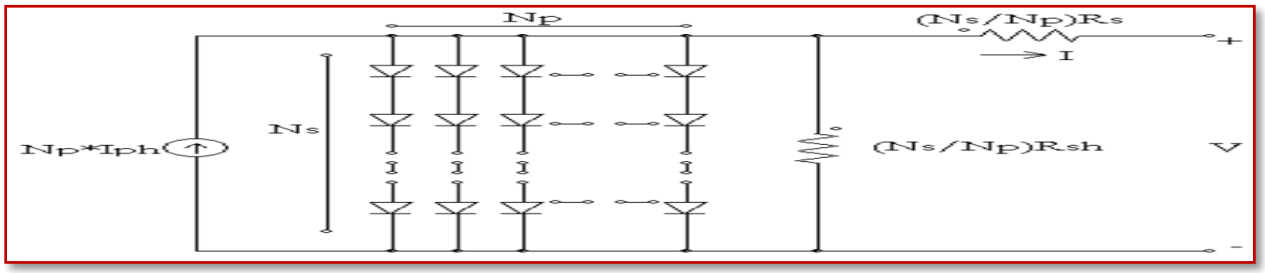

Figure 4.3 Circuit model of a generalized PV array [37]

The Figure 4.3 shows the equivalent circuit of a PV array with a load. Usually the equivalent circuit of a general PV model consists of a photo-current, a diode, a parallel resistor, R_{sh} which expresses a leakage current, and a series resistor (R_s) which describes an internal resistance to the current flow. The voltage current characteristic equation of a solar cell is given as,

$$I = N_p I_{ph} - N_p I_o \left[\exp\left(\frac{q(V_{pv} + I_{pv} R_s)}{N_s AKT} \right) - 1 \right] - \frac{V + IR_s}{R_{sh}} \tag{4.1}$$

The photocurrent mainly depends on the cell's working temperature and solar irradiation, which is explained as,

$$I_{ph} = [I_{sc} + K_i (T_c - T_{ref})](\frac{G}{1000}) \tag{4.2}$$

The saturation current of the cell varies with the cell temperature, which is represented as,

$$I_s = I_{rs} \left(\frac{T_c}{T_{ref}} \right)^3 \left[\exp\left(\frac{qE_g \left(\frac{1}{T_{ref}} - \frac{1}{T_c} \right)}{KA} \right) \right] \tag{4.3}$$

The shunt resistance R_p of the cell is inversely related with shunt leakage current to the ground. Usually efficiency of PV array is insensitive to variation in R_p and the shunt-leakage resistance can be assumed to approach infinity without leakage current to ground.

$$I_{pv} = I_{ph} - I_s [\exp(q(V_{pv} + I_{pv} R_s) / KT_c A) - 1] \tag{4.4}$$

Therefore, the Matlab mathematical modeling of the equation described above are the following.

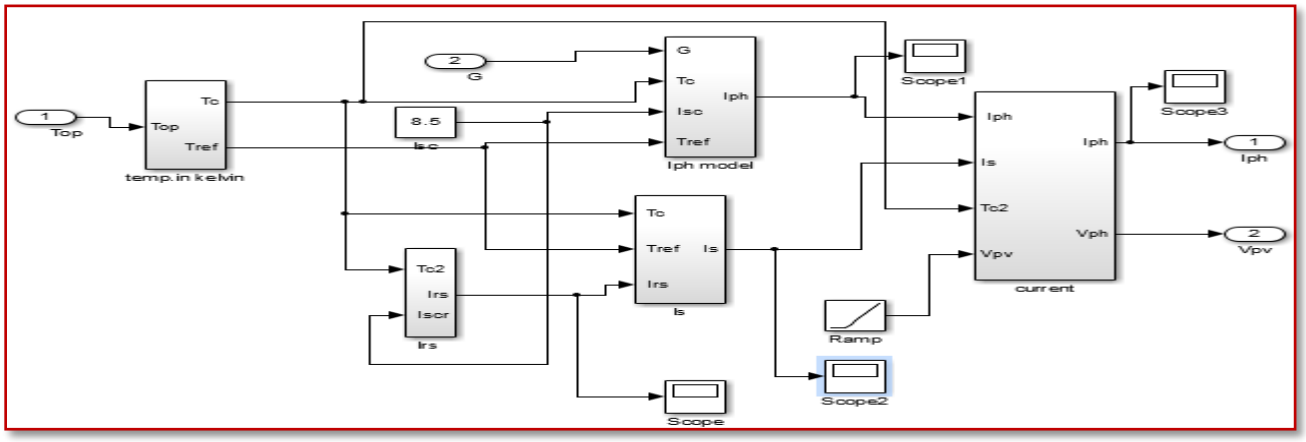

Figure 4.4 Expanded view of the array subsystem

There is no series loss and no leakage to ground for an ideal PV cell, i.e., R_s = 0.002 and R_P=100,000. So equation (4.1) can be rewritten as:

$$I_{PV} = I_{ph} - I_S[\exp(qV_{PV}/kT_CA) - 1] \tag{4.5}$$

The open-circuit voltage, V_{oc} and short-circuit current, I_{sc} are the two most important parameters used which describes the cell electrical performance. The above mentioned equations are implicit and nonlinear; hence, it is not easy to arrive at an analytical solution for the specific temperature and irradiance. Normally $I_{ph} \gg I_S$, so by neglecting the small diode and ground-leakage currents under zero-terminal voltage, the short-circuit current is approximately equal to the photocurrent, i.e. $I_{PH}=I_{SC.}$

The open-circuit voltage parameter is obtained by assuming the zero output current. With the given open-circuit voltage at reference temperature and ignoring the shunt-leakage current, the reverse saturation current can be acquired as,

$$I_{rs} = \frac{I_{scr}}{\left[\exp\left(\frac{qV_{oc}}{N_sKAT}\right) - 1\right]} \tag{4.6}$$

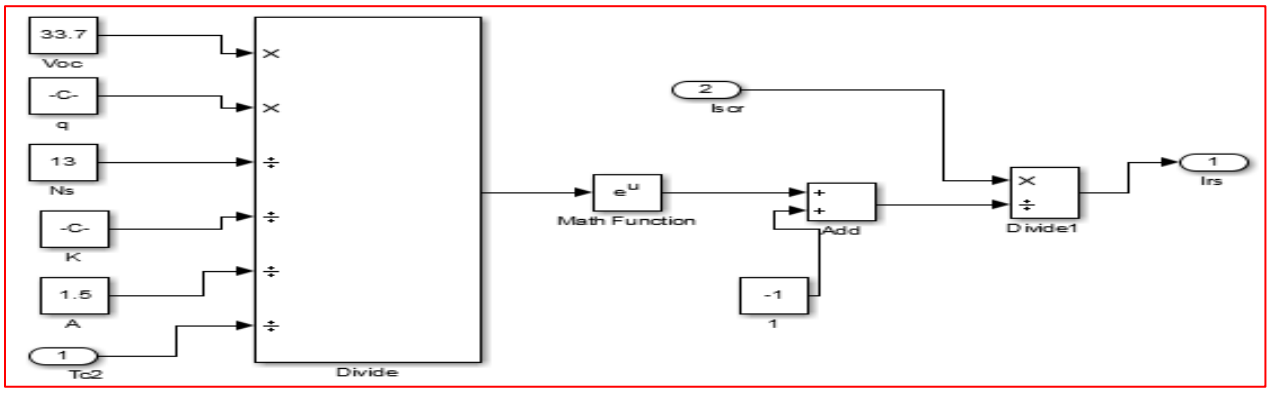

Figure 4.5 Expanded view of reverse saturation current model

The detail of the array subsystem model in the Simulink is given in the Figure 4.5. A PV array is a group of several PV modules which are electrically connected in series and parallel circuits to generate the required current and voltage. So the current and voltage equation of the array with N_p parallel and N_s series cells can be calculated in the following ways.

A solar PV system design can be done in four steps: load estimation, estimation of number of PV panels and cost estimation of the system. The study considered to supply 1MW power load satisfied from the photovoltaic power source for 6 hrs a day and the type of panel specification put at [appendix].

Total watt-hours rating of the system=Total connected load (watts) ×Operating hours

$$=1MW\times6hrs=6MWh.$$

Actual power output of a PV module = Peak power rating × operating factor

$$= 250 \times 0.85 = 212.5 \text{ watt.}$$

The power used at the end use is less (due to lower combined efficiency of the system)

$$=\text{Actual power output of a module} \times \text{combined efficiency}$$

$$=212.5 \times 0.81 = 172.13 \text{ watts (VA)} = 172.13 \text{ watts}$$

Energy produced by one 250Wp module in a day = Actual power output × 8 hours/day (peak equivalent) =172.13×8=1377.04watts-hour

Number of solar modules required to satisfy given estimated daily load

= (Total watt-hour rating daily load)/ (Daily energy produced by a panel)

= (6×10^6)/1377.04 =4357.17.

Therefore, the number of modules required is equal to 4357(round figure).

In order to know the values of Np and Ns, in 1202401 solar module

- Module in series (N_s) = DC bus voltage/Nominal voltage of the module = 400/31.7 = 13.
- Strings in parallel (N_p) = Total no of modules/Modules in series = 4357/13 = 335.

The required area coverage of the PV array can be calculated. From module specification of listed in the appendix, one PV panel size is 66.34 inches by 39.09 inches or 16730.487cm^2. Therefore, the total area required to install 1MW PV system=4357×16730.487 cm^2

=72,894,729.85 cm^2

=7,289.473m^2

The area coverage is not large. So, the PV modules can be installed between the existing Adama wind II since the distance between the tours of the wind farm is far apart each other.

Figure 4.6 Adama wind farm II

Therefore, the output power of the matlab/Simulink PV model of the above could be approximately 1MW.

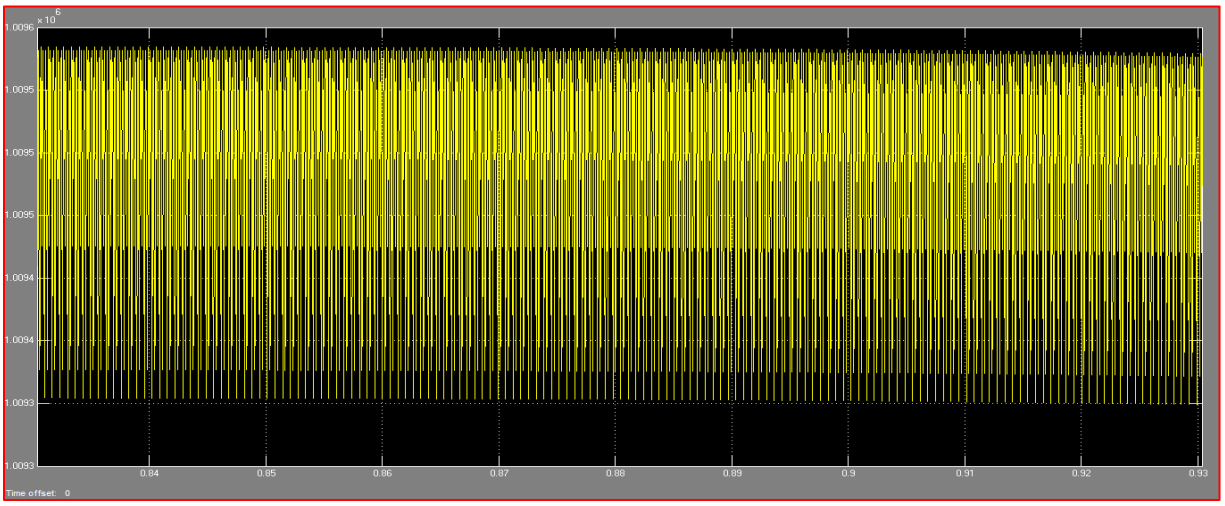

Figure 4.7 SCHOTT panel Item_1202401 PV model I-V characteristics curve with 800w/m^2 solar radiation

Table 4.1 the parameters used for the modeling of photovoltaic panel specification

Symbols	**Value**	**Symbol Descriptions**
V_{oc}	33.7V	Open circuit cell voltage
Q	1.602×10^{-19}C	Electron charge
K	1.38×10^{-23} K	Boltzmann constant
A	1.50	Ideality factor
I_{SC}	8.5A	Short circuit current
K_i	1.7×10^{-3}	Short circuit temperature coefficient
T_{Ref}	298K	Reference temperature
I_{rs}	2.0793×10^{-6}A	Reverse saturation current
T_C	307K	Operating temperature
G	800W/m^2	Module illumination (when G is constant)
N_P	335	Number of cell connected in parallel
N_S	13	Number of cell connected in series
E_g	1.2eV	Band gap of silicon

4.3 Wind energy conversion system Model

A wind turbine can be modeled at various detail levels depending on the model application in chapter three. The turbine models range from simplified model, used for simulations to study the effects of integrating wind farms to a national grid, to highly accurate and detailed finite element models to study the behavior of a single component within the turbine. The parts of the wind turbine of interest for this thesis are mainly the electrical components, namely the generator, the back-to-back converter, and the grid connection. This section presents dynamic models of the sub-systems of a full power converter wind turbine with an asynchronous machine, which can be used to study of the interaction between the sub-systems during operation. The mathematical equation and analysis is explained in chapter two for modeling the windmill below.

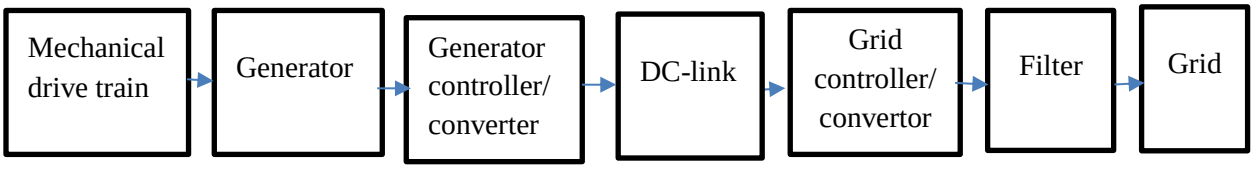

Figure 4.8 Illustrate a system overview representation of the wind model using block diagram

In wind energy conversion system the energy from wind is used to cause a rotation motion in turbine. This motion will make the generator produces electrical energy which can be regulated and controlled by the power interface. The mechanical power produced by a wind turbine can be represented by (2.14). Based on the data obtained from Ethiopia electric power corporation and from NASA international accessible data table mentioned in chapter two, the average wind speed of the site could be from 3m/s-12m/s with different height and elevation. The air density (ρ) of the study area is taken as 0.98 kg/m^3. The rotor area of Fuhrlander wind turbine is 346.36m^2. Cp is taken as 59% = 0.59. The hub heights of Fuhrlander wind turbine are 50m freestanding tubular. Gear and generator efficiency of 95 % is also considered (hence, cumulative efficiency of gear-generator = 0.95×0.95 = 90.25 %). With this details, the wind turbine in MATLAB/Simulink is given below in Figure 4.9.Therefore, the wind speed model is made by using these data [18]. The turbine model is done using lookup.

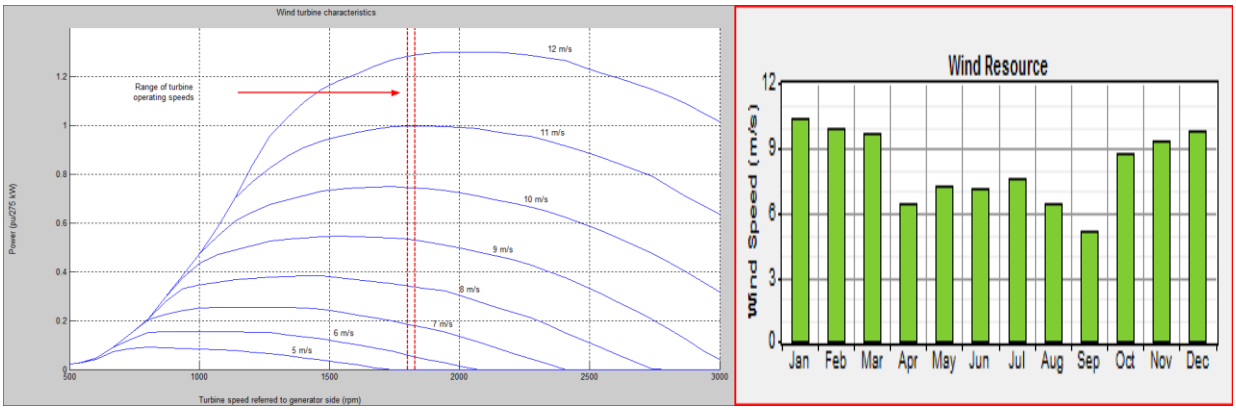

(a) (b)

Figure 4.9 (a) Wind turbine model speed –power characteristics (b) wind resource

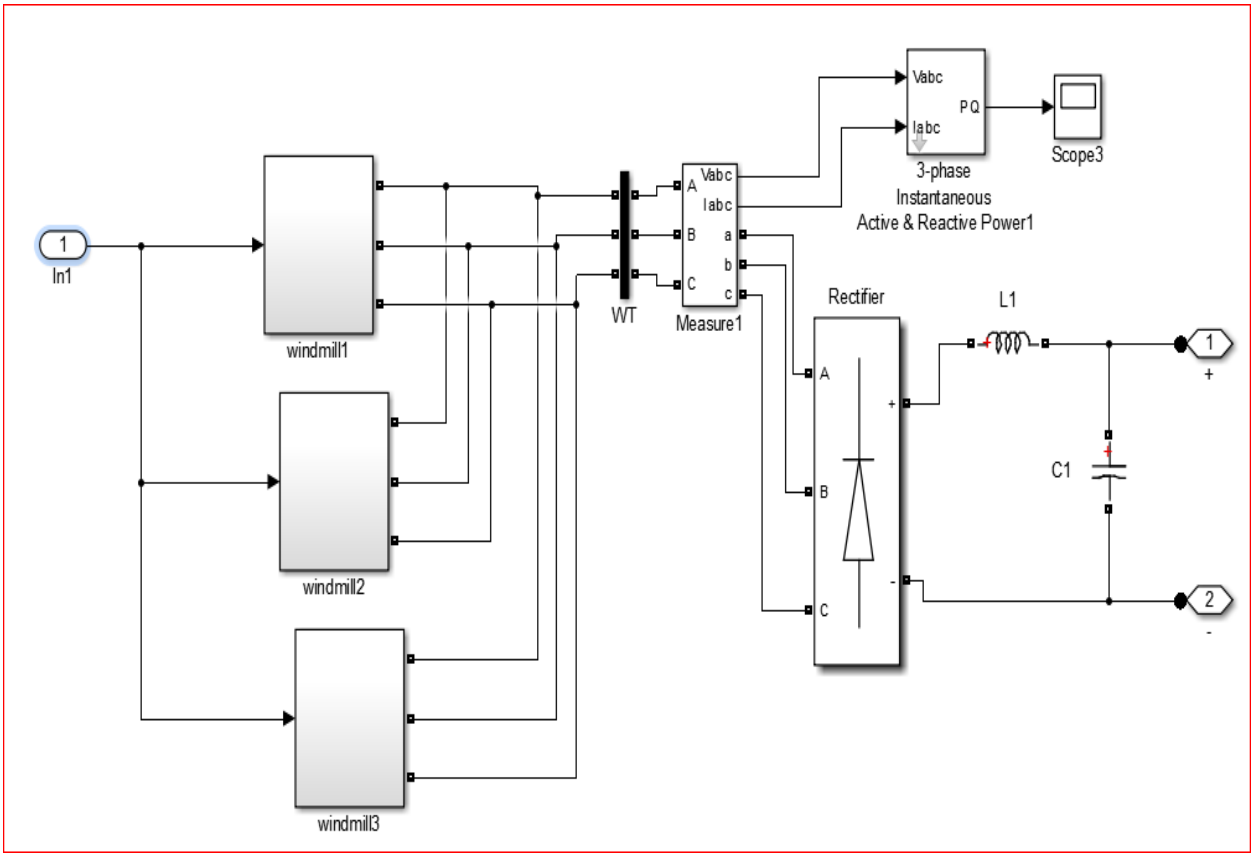

Figure 4.10 Expanded view of the windmill model

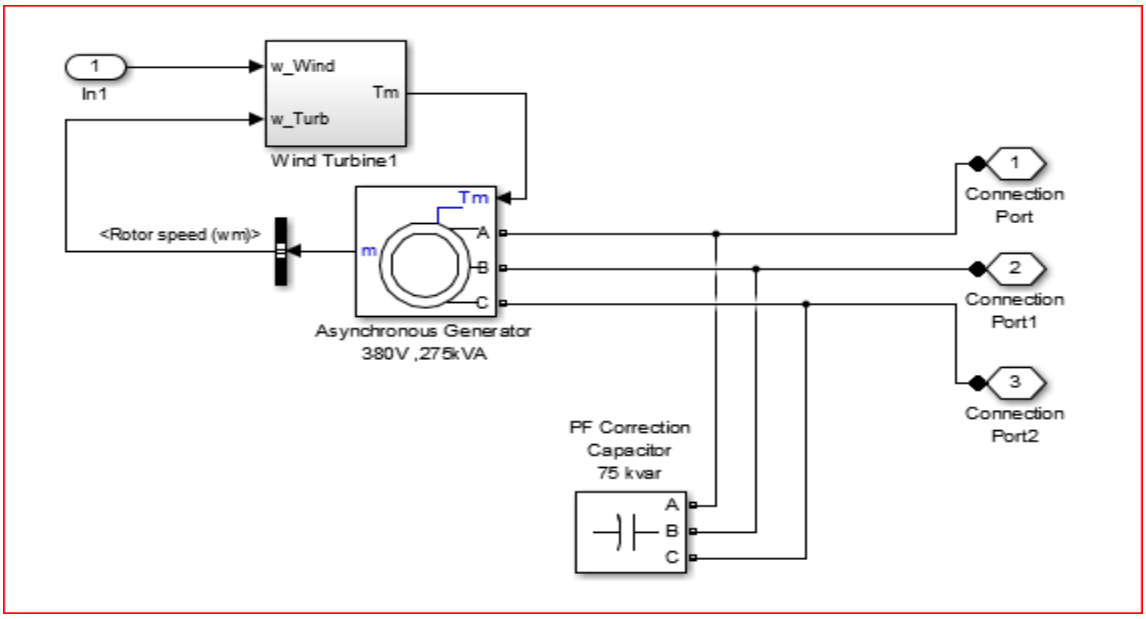

Figure 4.11 Expanded view of the wind turbine and generator model

As the asynchronous machine operates in generator mode, its speed is slightly above the synchronous speed (1.011 pu). According to turbine characteristics, for a 10 m/s wind speed, the turbine output power is 0.75 pu (206 kW). Because of the asynchronous machine losses, the wind turbine produces 200 kW. Voltage stays at 1 p.u and no flicker is observed.

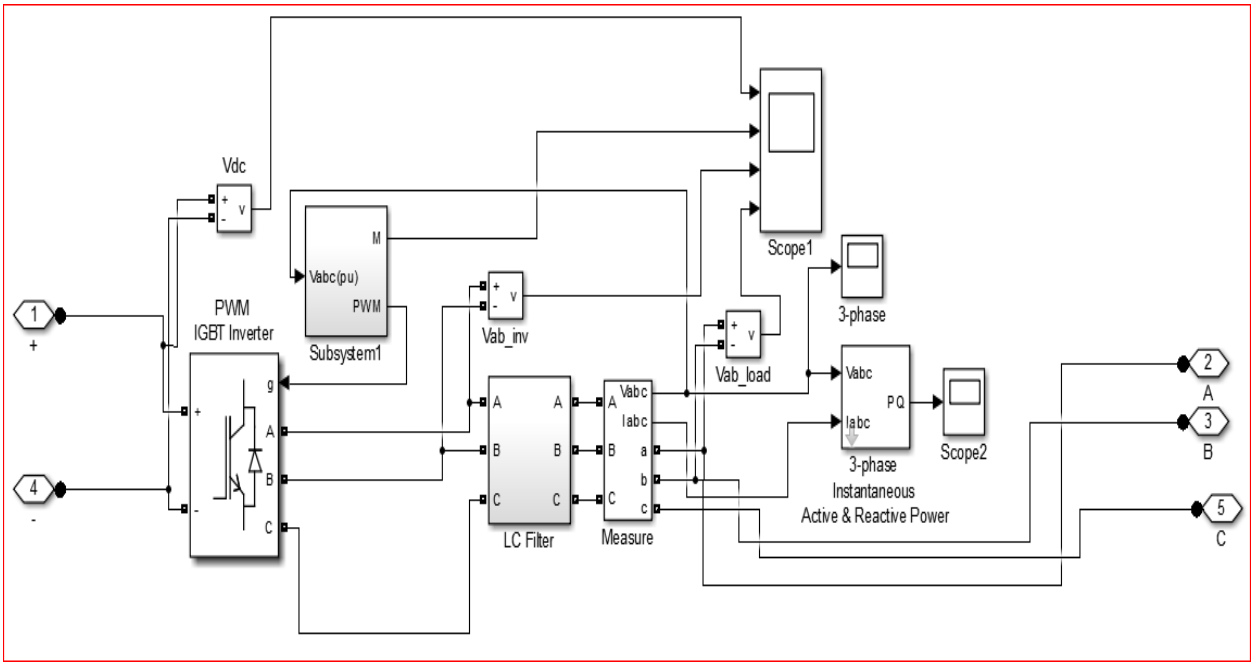

Figure 4.12 Detail circuit model of the back -to-back converter and filter

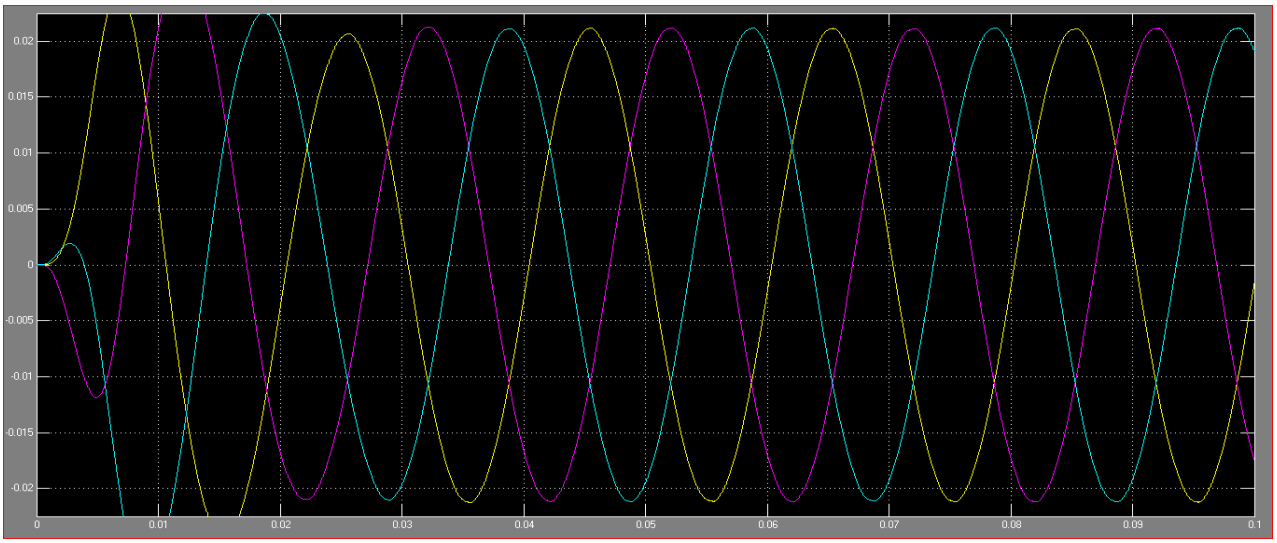

Figure 4.13 windmill model 3-phase Output voltage in per unit

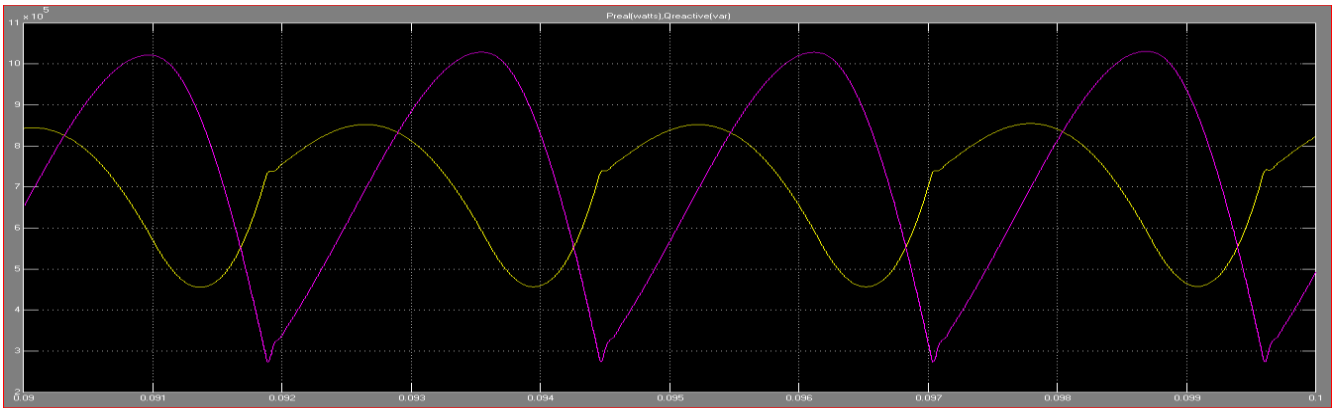

(a)

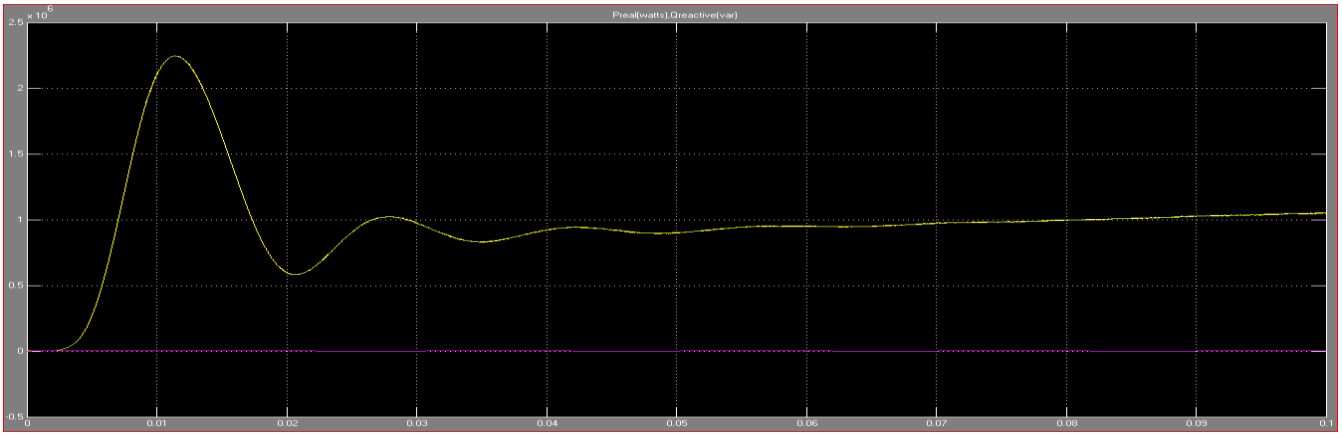

(b)

Figure 4.14 (a) Output Power of wind model before inverter (b) Output Power of wind model after inverter and filter

4.4 Fuel Cell Stack Power Generation Modelling

4.4.1 Mathematical Model of PEM Fuel Cell

E-Nernst is the electrochemical thermodynamic potential of the cell and it represents its reversible voltage, which is an ideal output voltage. E-Nernst can be calculated by a modified version of the equation of Nernst, with an extra term to take into account changes in the temperature with respect to the standard reference temperature 25^0C. Using the standard pressure and temperature (SPT) values, we can get a simplified equation. When we get the water production in the form of steam, 1.229 should be replaced by 1.18. Usually, the fuel stack will be controlled by changing the oxygen pressure PO_2, so we can assume that hydrogen pressure is constant. When we compare the two parameters T and PO_2 ,we can find $-0.85\times10^{-3}T$ changes "faster" than $4.31\times10\text{-}5T\ln(PO_2)$, because with the parameter x the function f(x)=ln(x) is always smaller than f(x)=x. So, T will mainly determine the E-Nernst value. The E-Nernst equation gives the open circuit cell potential (E) as a function of cell temperature (T) and the reactant partial pressures [12];

$$E = E_O - 0.85\times10^{-3}(T - 298.15) + \frac{RT}{2F} IN\left(\frac{PH_2 PO_2^{0.5}}{PH_2OP^{0.5}}\right)V \tag{4.7}$$

E_0 represents the reference potential at unity activity, R is the universal gas constant and P is the total pressure inside the stack.

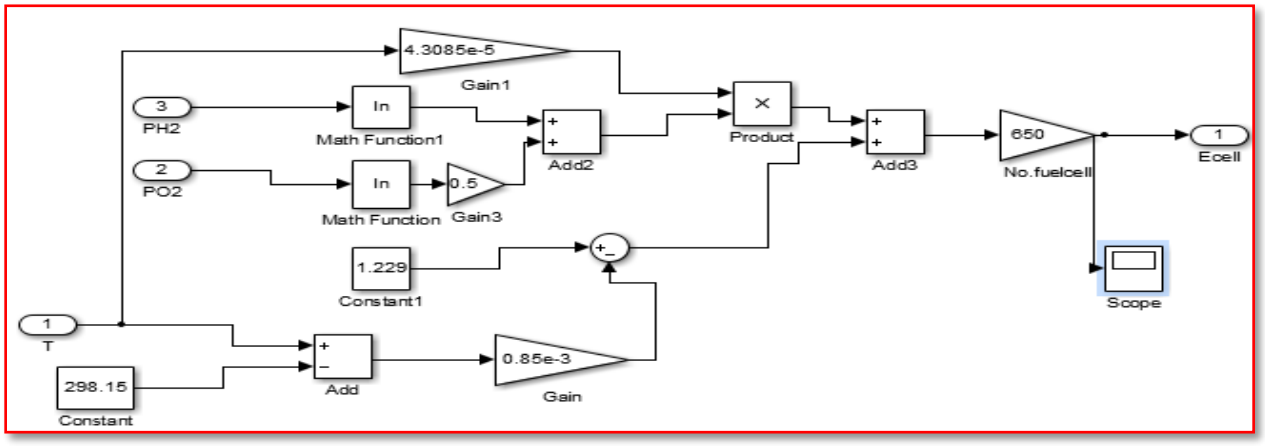

Figure 4.15 Nernst model of fuel cell

4.4.2 Inverter Triggering

Inverters that take DC and produce a constant amplitude sinusoidal output have been studied and designed. Significant research and development in the area of pulse width modulation (PWM) has been done in attempt to reduce the passive filter size and create a better sinusoidal output, thus reducing harmonics. Here we take the inverter input dc voltage from fuel cell output. Voltage regulator is taken for comparing and controlling the inverter triggering pulse with the given reference voltage. The input of the voltage regulator is taken from the output of the inverter (V_{abc} line voltage). After that a reference signal which is passes through a discrete PWM generator and get the pulses for inverter triggering. That is inverter triggering is controlled by the line voltage [12].

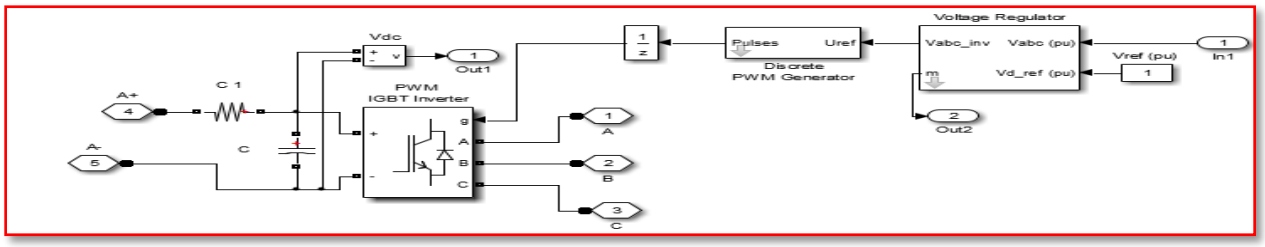

Figure 4.16 DC-AC inverter control

4.4.3 Fuel Cell and Fuel Cell Outputs

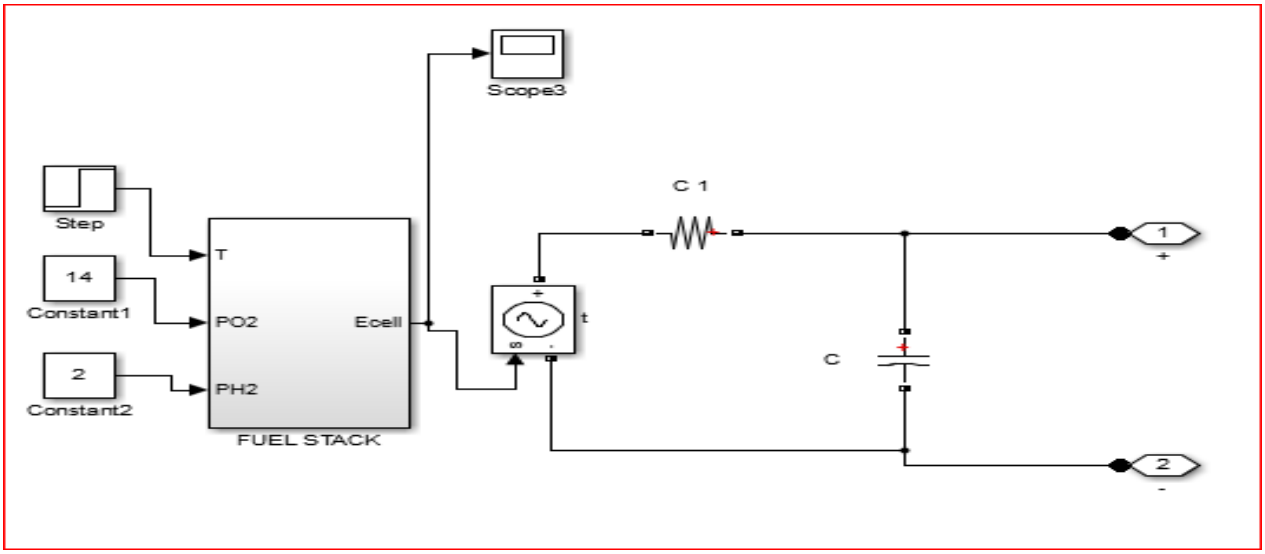

Figure 4.17 Overall model fuel cell model

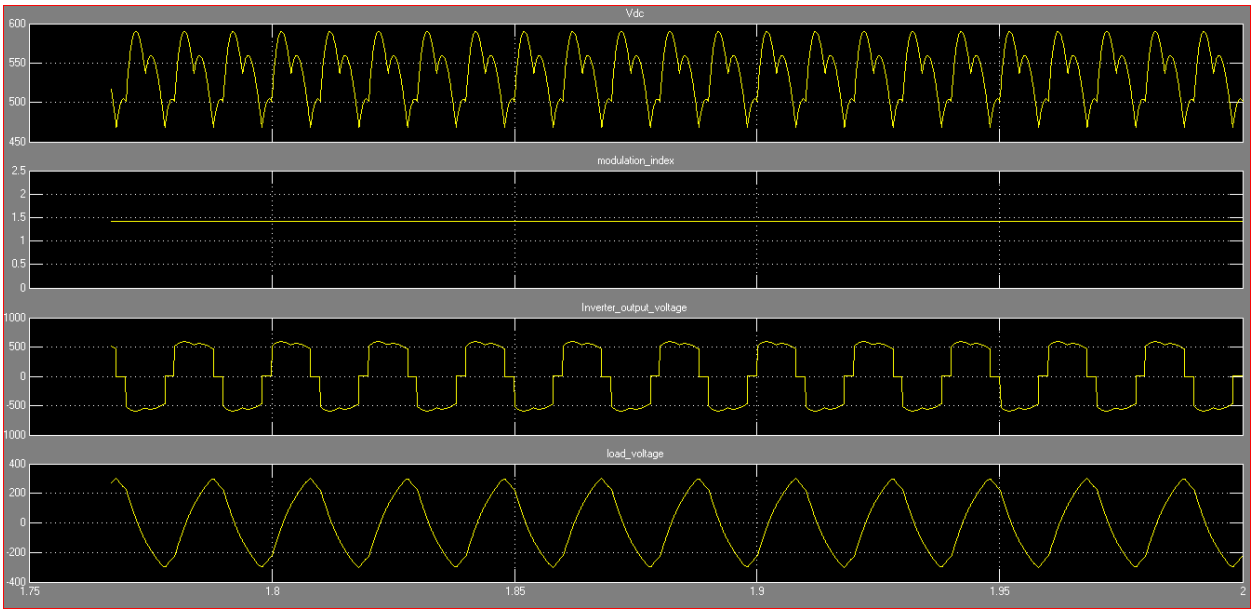

Figure 4.18 Fuel cell model DC voltage, modulation index, inverter output voltage, and load terminal voltage after filter respectively

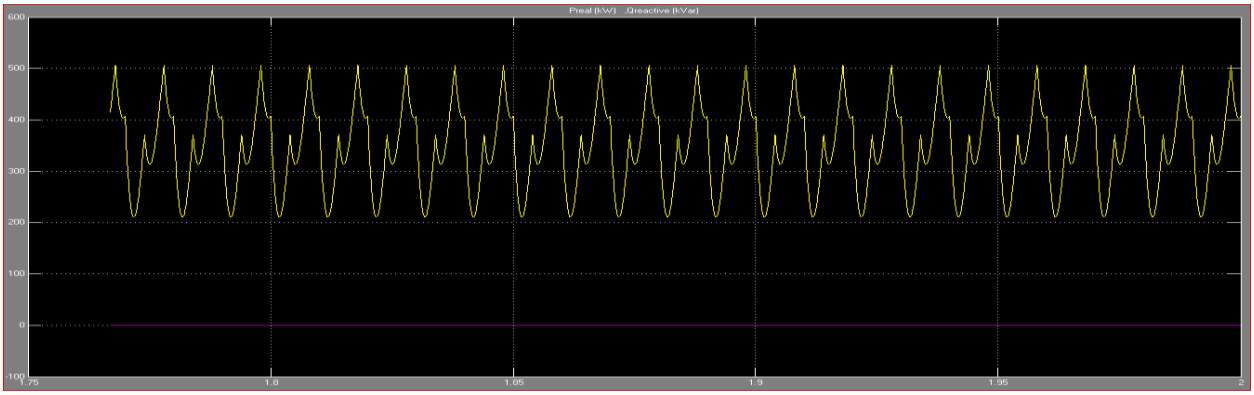

Figure 4.19 Simulation of Fuel stack model power output result

4.4.4 Modeling of an electrolyzer system

One of the contemporary decisions uses fuel cells based on PEM (a proton exchange membrane) technology which provide electrochemical water partition to hydrogen and oxygen. Thus all redundant energy is transformed and stored as hydrogen. This method has some advantages in respect to classic electrolysis. It ensures the production of a higher electric current density and a lower waste of power due to parasite capacitances.

4.4.4.1 Principles of PEM Operation

The fundamental principal of PEM electrolysis is shown in Figure 4.20. It consists of two electrodes – an anode and a cathode powered by constant voltage. The water is passed to the anode, where a chemical reaction proceeds. The latter involves electrons withdrawal from the water molecule resulting in hydrogen ions and oxygen gas formation. The hydrogen ions pass through the PEM membrane to the cathode, where they receiving electrons form hydrogen molecules. The chemical reactions describing the anodic and the cathodic processes are shown below [38]:

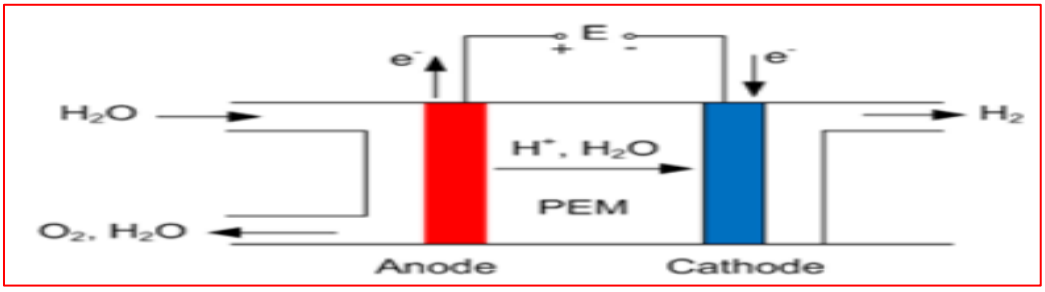

Figure 4.20 Electrolyzer *[12]*

$$H_2O - 2e^- = 2H^- + \frac{1}{2}O_2$$
$$2H^+ + 2e^- = H_2 \tag{4.8}$$

The equation describing the electrolyzer`s work is as,

$${}^{n}H_2 = \frac{{}^{n}F.{}^{n}C.i_e}{2F} \tag{4.9}$$

Where ${}^{n}H_2$ is the amount of hydrogen produced [mol s^{-1}], ${}^{n}F$ is the Faraday effectiveness, ${}^{n}C$ is the number of the elelctrolyzer's cells connected in series, i_e is the electrolysis current [A], while F stands for the Faraday constant (F = 9, 648.5×10^4 C mol^{-1}). If electrolyzer work temperature is chosen and set to be -40°C, based on the Faraday effectiveness can be calculated using the following equation:

$$^{n}F = 96.5\exp\left(\frac{0.09}{i_e} - \frac{75.5}{i^2{}_e}\right) \tag{4.10}$$

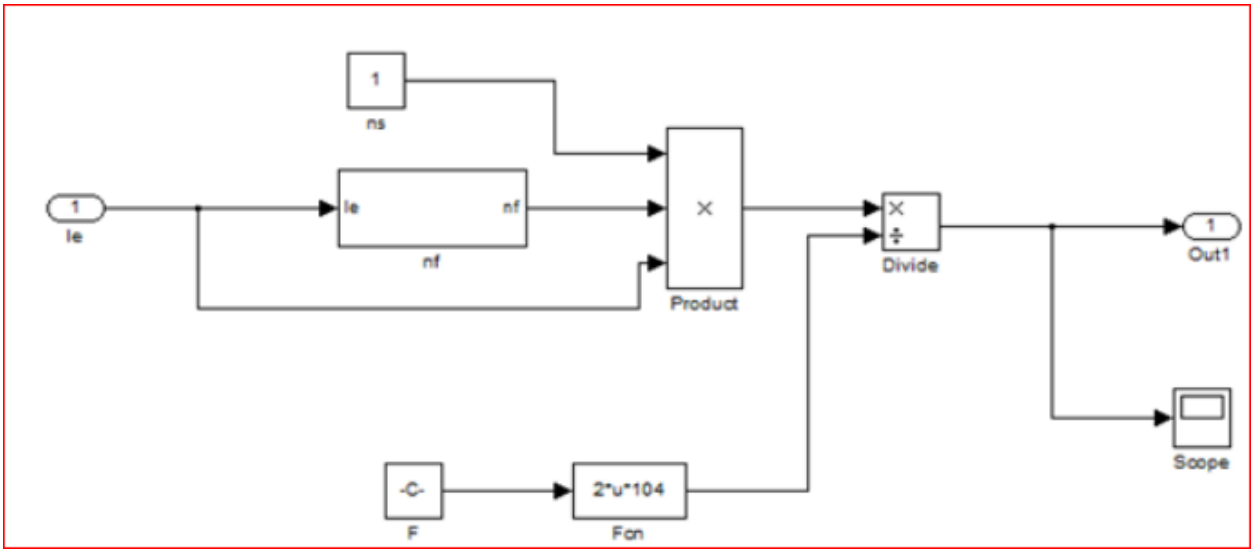

Figure 4.21 General simulation model of electrolyzer

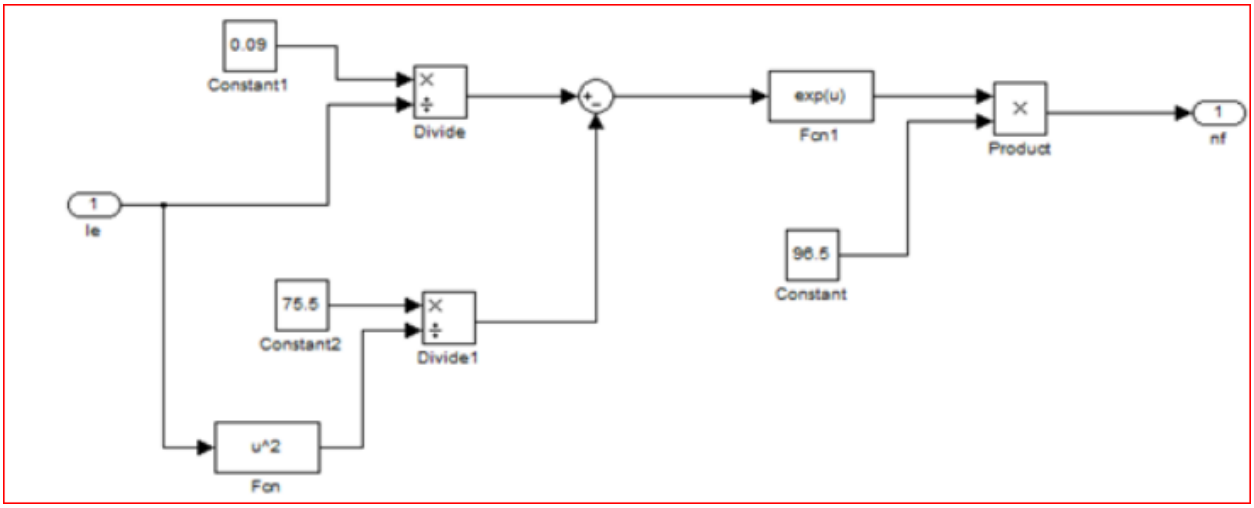

Figure 4.22 Electrolyzer model subsystem for Faraday effectiveness determination

A simulation model of a PEM electrolyzer is developed using Matlab/SIMULINK. It is based on (4.9) and (4.10). It is illustrated in Figure 4.21 and Figure 4.22. An electric current generated from wind power is used as an input signal changing in time.

Table 4.2 Parameters specification of fuel cell model

No of cell series	650
Eo represents the reference potential at unity activity	1.229
Reference temperature	298K
Inductance of filter	2mH
Proportional gain	0.4
V_{rms} of load	380V
Maximum Active power	500kW
Maximum temperature	360K
Capacitive reactive power of load	0W

4.5 Model Summary

In this chapter, the detail of the models of the windmill system, PV system and fuel cell which are compatible to the modelling of chapter three output, are modelled using MATLAB/Simulink environment. This is done by creating a subsystem and masked block sets of the major dynamic component models and then cascading in to a single aggregate model. The output of simulation model for the proposed hybrid power system, 1MW photovoltaic, 1.5MW windmill and 0.5MW fuel cell power output are modelled. The chapter deals also about modeling of the system and the converter system without controlling mechanism. Therefore, the chapter shows the detail components of each model with proper analysis and the means of connection clearly. In addition, Matlab and HOMER outputs comparison is done. Therefore, the result of matlab/ Simulink modeling are almost similar with Homer output.

CHAPTER FIVE

5. MULTI-LOOP CONTROL SCHEME FOR DGs-GRID INVERTER INTERFACED SYSTEM

5.1 Inverter Interfaced Distributed Generations

There are two basic classes of distributed energy resources (DERs). One is a DC resources such as fuel cells and photovoltaic cells; and the other is high frequency AC resources such as wind which needs to be rectified. In both cases, the resultant DC voltage is converted to an acceptable AC source using an inverter. Therefore, a power electronic interface is necessary to convert DC to AC or AC to DC. These types of DERs which are connected to grid by means of inverter are named inverter interfaced distributed generations (IIDGs). The general schematic of an IIDG is shown in Figure 5.1. In [39], an IIDG is composed of hybrid system, DC interface and DC to AC converter. The hybrid system consists of fuel cell, a photovoltaic cell or a rectified output of other high frequency DERs. The most important advantage of IIDGs are their quick response to change in the output. If a change happens in the grid, the IIDGs can quickly compensate it. During an event, the IIDG response basically depends on the inverter control structure. To prevent damaging of switching devices used in the inverters, IIDGs are usually equipped by instantaneous over-current shutdown protection.

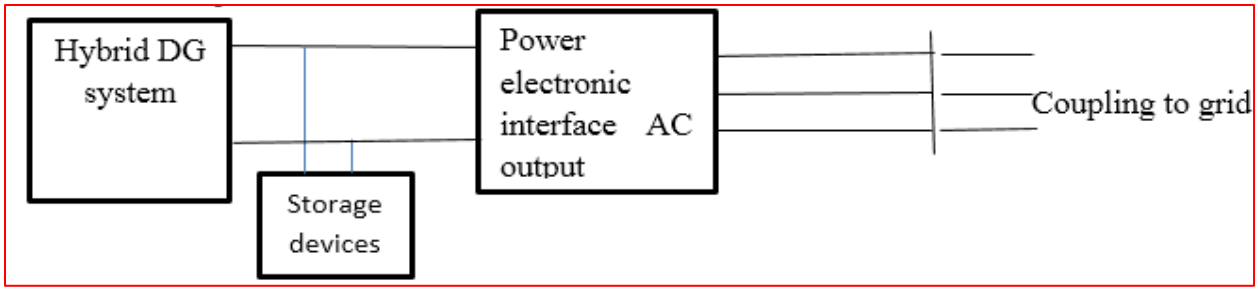

Figure 5.1 Basic Parts of an IIDG

5.2 Adama Distribution Substation System

The network topology for Adama town is a radial grid system. The primary distribution system takes 132 kV from the transmission line and step down to 15 kV by using two parallel connected transformers as shown in Figure 5.2.

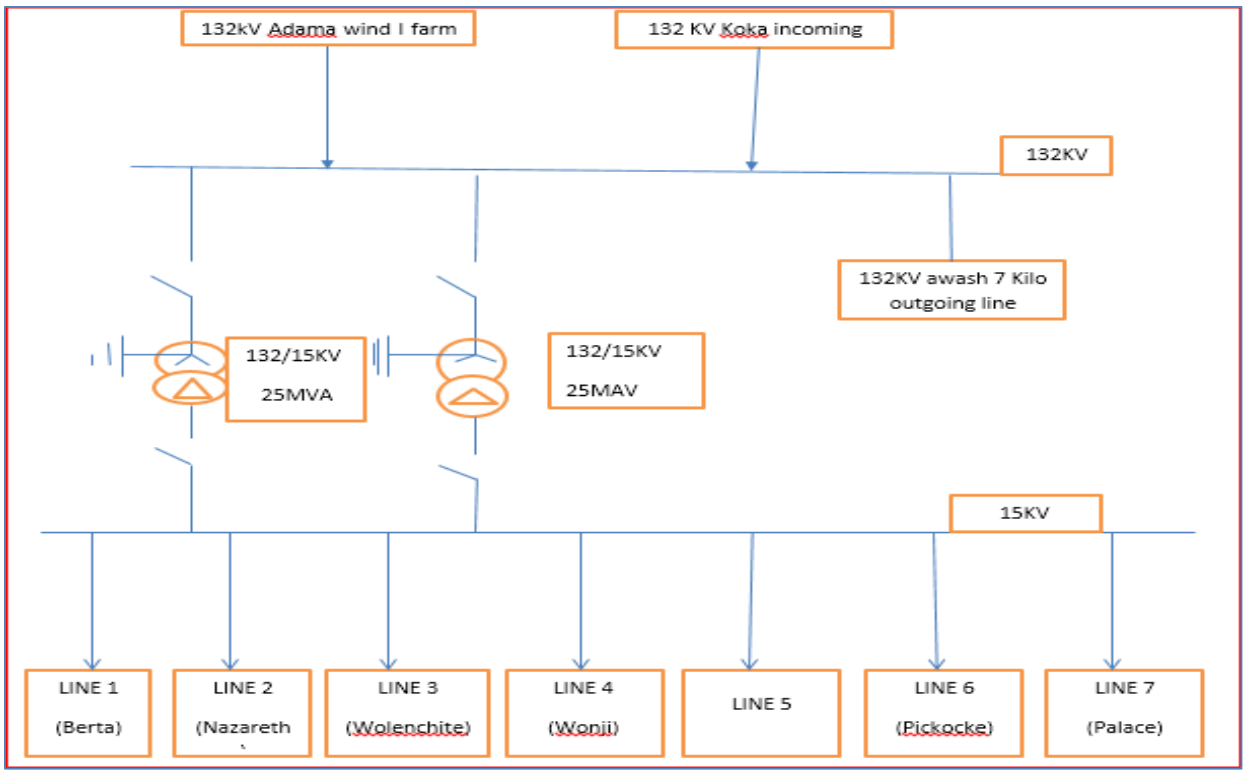

Figure 5.2 Single-line diagram for the power distribution system at Adama town

Almost all lines are loaded to carry their maximum capability since the supply and the demand are not fitted. In [1], 70% up to 80% of the faults are estimated to be originally temporary faults and become permanent faults, as the protection system of the distribution system is deficient to clear the temporary faults timely. Therefore, this frequent interruption will be solved by installing new additional plants and by better controlling modes.

5.3 System Configuration and Prototype Picture

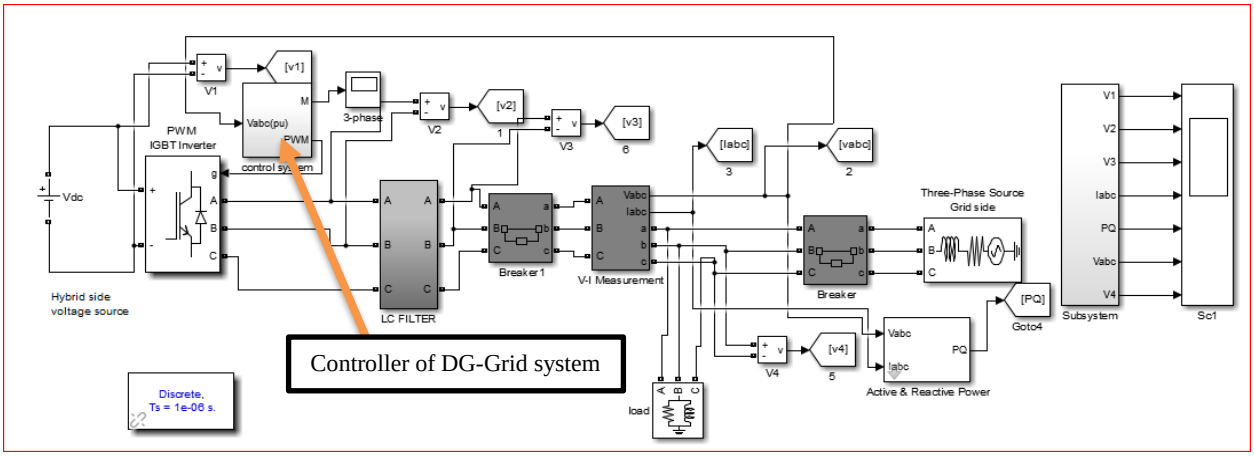

Figure 5.3 Configuration of three-phase grid-connected VSI with LC filters and local load

Figure 5.3 shows the configuration of three-phase grid-connected VSI with LC filters and local load. It will operate in grid-connected or standalone mode by controlling the switch devices. This concentrates on the control strategy for both grid connected and standalone modes. To select proper inverter-side inductor, several factors need to be considered: inverter output current ripple, system cost, size and efficiency. Larger L_f can reduce the output current ripple which enables the controller to have a high gain to achieve smaller steady state error and faster dynamic response. The maximum current ripple is calculated as, $\Delta I_{\max} = V_{dc} T_s / 4L$. So inductor is selected here to make the maximum ripple current within 30% of the rated current. For the capacitor design, the goal is to keep the resonant frequency of LC filter be smaller than 1/10 of the switching frequency to get enough attenuation at high frequency. A bigger capacitor can reduce the inductor value, but would also increase the reactive power it produces hence increase the current stress on the switches and inductors. So the capacitor is selected to provide 2% reactive power of the rating power [21].

5.4 Power Electronics Interface

In order to realize a hybrid system, the output voltage and frequency of each component should be maintained at a predetermined level so that the interconnection between the different components of the hybrid system can be achieved. This is made possible by employing power electronics interface which has the ability to control the system output variables such as voltage, frequency, active and reactive power to keep or bring them to match their reference values after a disturbance. The power electronics interface comprises of a rectifier and voltage source inverter. A pulse width

modulation (PWM) controller is used to control the inverter in order to satisfy the voltage regulation as well as to achieve real and reactive power control. The power electronics interface used has the ability to control the real and reactive power by controlling the inverter output voltage, angle and frequency [40]. This is realized by converting AC power output from the generator in to DC and then in to AC. A 3-phase uncontrolled rectifier made up of six bridge connected diodes has been used to rectify the generator output from AC to DC. A voltage source inverter (VSI) is then employed to convert the DC output from the rectifier to AC. Control of voltage source inverter is achieved by means of two control loops namely, the inner current control and the outer voltage regulator loop. The overall system along with its control strategies is shown in Figure 5.4.

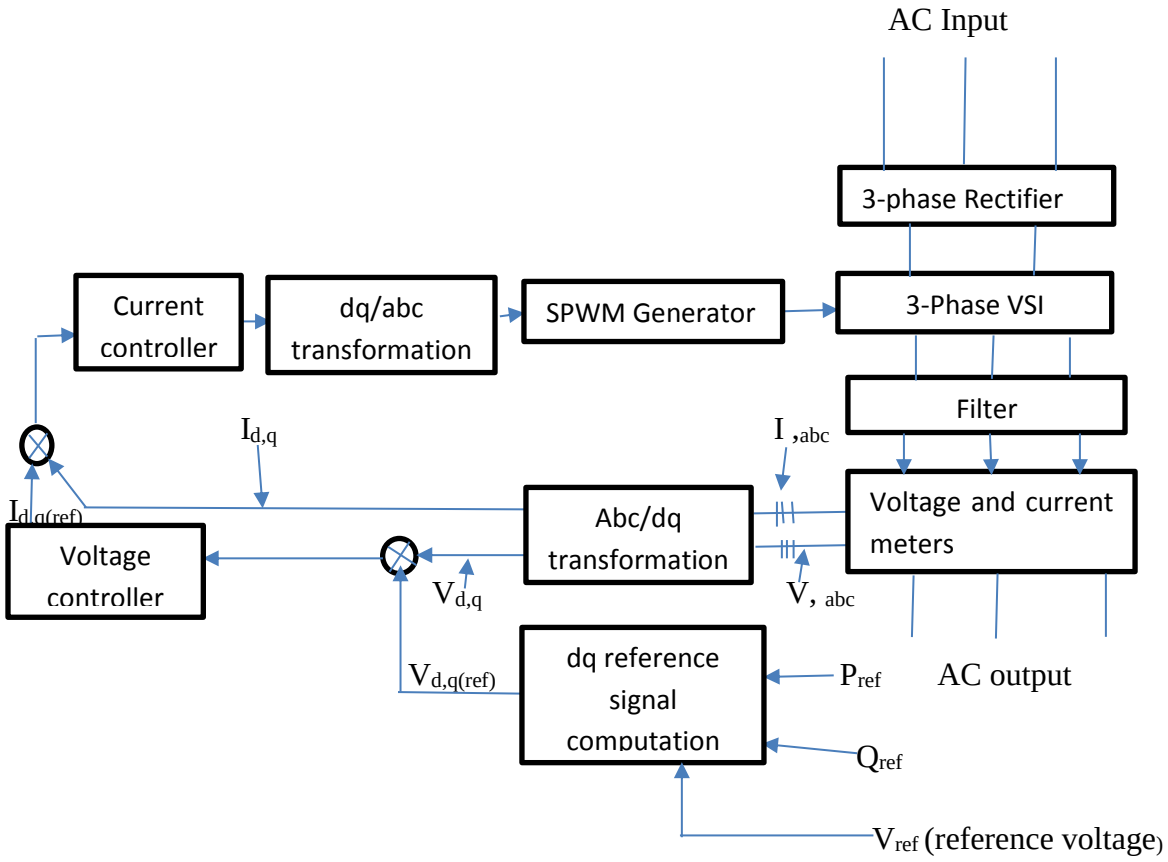

Figure 5.4 Block diagram of the power electronics interfacing

The "abc/dq Transformation" block takes the time varying currents and voltages (in abc coordinates) from the voltage and current measurement devices and converts them into dq (time-invariant) values. The voltage controller takes the error signals between the actual output in dq frame ($V_{d,q}$) and the reference voltage ($V_{d,q(ref)}$) and generates the current reference signals ($I_{d,q(ref)}$)

for the current controller loop. The current controller produces the d-q control signals, which are converted back to the control signals in abc coordinates through the “dq/abc Transformation” block. These control signals are used to generate the gating pulses for the inverter to control its output voltage, using sinusoidal pulse-width modulation (SPWM) generator. In the following paragraphs the control principle of the power electronics interfacing along with the control loops are presented [40].

5.5 Multi-loop controller with capacitor voltage differential feedback

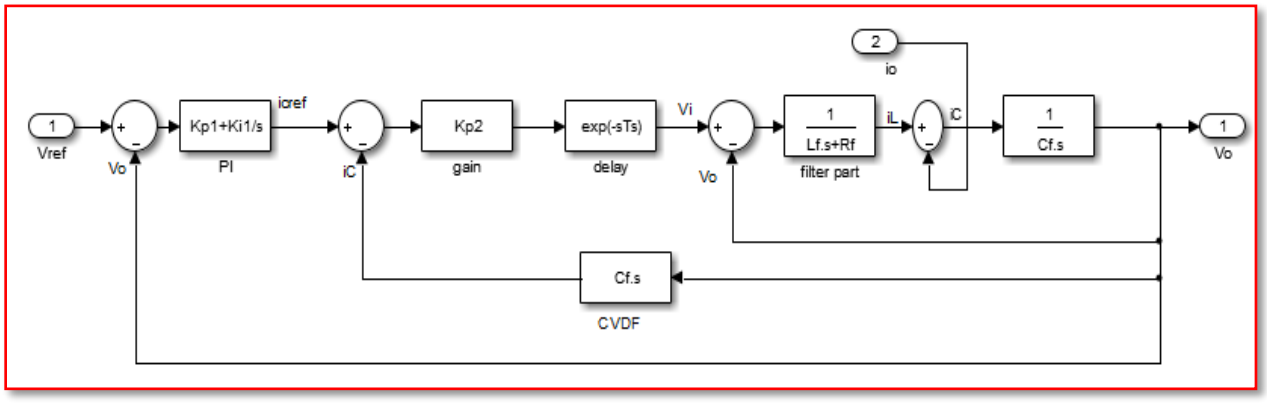

Figure 5.5 Bode diagrams of capacitor voltage differential feedback

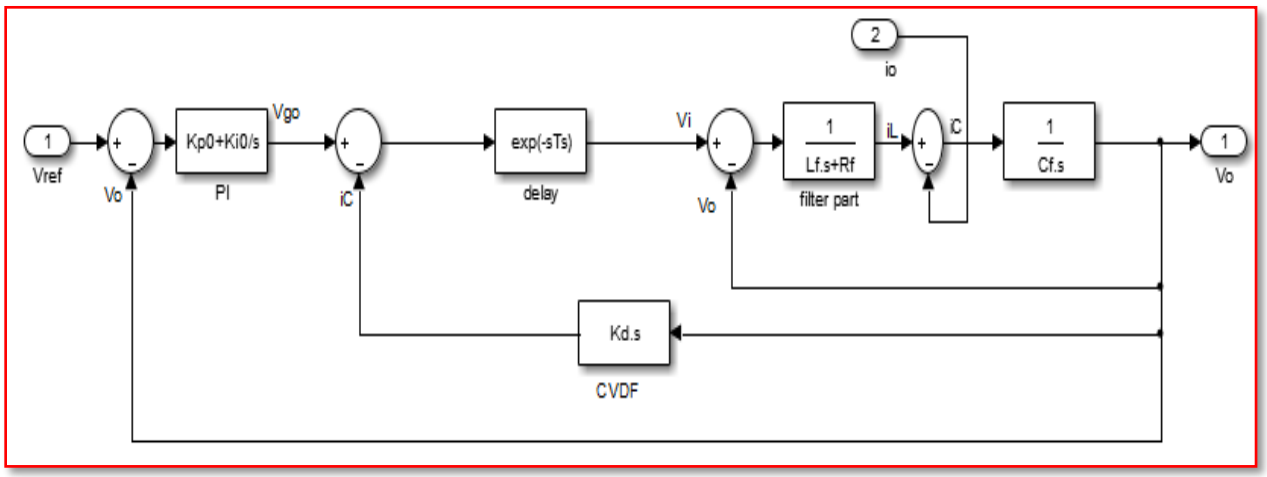

Figure 5.6 . Simplified diagrams of capacitor voltage differential feedback

5.5.1 Control block diagram

The control block diagrams of this chapter use the matlab/Simulink tools. This Simulink block is not run directly. It is implemented by using Matlab /M-file to show the characteristic graph of the control system of capacitor voltage differential feedback in inner loop and all decoupling techniques.

5.5.1.1 Capacitor voltage differential feedback

A capacitor voltage differential feedback loop is used with the outer voltage regulation loop in order to damp the LC filter resonance thus increases the system stability margin as shown in Figure 5.5. The reason will be described as follows.

To prevent the pollution of the utility by high-frequency current ripple, an LC filter is used at the output of the inverter. The capacitor is used to provide a low-impedance path for the high frequency components. But the LC filter is virtually un-damped (especially at no load) and thus its resonance can severally affect the quality of V_o and the overall stability of the controller. Controllers with the inductor current feedback as inner loop can be used to actively damp the resonance, while capacitor current feedback can also be utilized since it has better disturbance rejection capability than that of inductor current feedback. In capacitor current feedback control, a highly accurate current sensor is needed because the capacitor current is in small scale. It also requires the sensor which has fast dynamic response. Since capacitor current can be calculated from the voltage, capacitor voltage differential feedback can be used to replace capacitor current feedback so that the current sensor can be saved. Like the capacitor current feedback, the capacitor voltage differential feedback can also eliminate the resonant peak of L-C filter.

Also we can see this from another point of view. The control block diagram can be simplified into the form in Figure 5.6. The inner loop is simplified a single capacitor voltage differential feedback loop with feedback coefficient. The closed-loop transfer function of the inner loop (without consideration the control delay) is

$$G_{VO-Vgo}(s)=\frac{Vo}{V_{go}}=\frac{1}{L_fC_fs^2+R_1C_fs+K_{ds}+1}=\frac{\omega^2{}_n}{s^2+2\varepsilon\omega_ns+\omega^2{}_n} \tag{5.1}$$

Where, $K_d = C_{fs}.K_{p2}$ which is the differential feedback coefficient. The damping ratio can be derived as

$$\xi = \frac{R_f C_f + K_d}{2\sqrt{L_f C_f}} \tag{5.2}$$

From (5.1) and (5.2), the LC filter transfer function has a high-resonant peak because the damping ratio ξ is close to zero; after introducing the output voltage differential feedback, the control plant from the traditional LC filter has become to an improved control plant. The damping ratio ξ changes from zero to a variable value, which can be adjusted by the differential coefficient K_d. When K_d is equal to the designed value, the damping ratio is about 0.67, which is very close to the technical optimum (TO) value 0.707. Thus this control method is consistent with the capacitor current feedback [41].

5.5.1.2. Low pass filter in the feedback loop

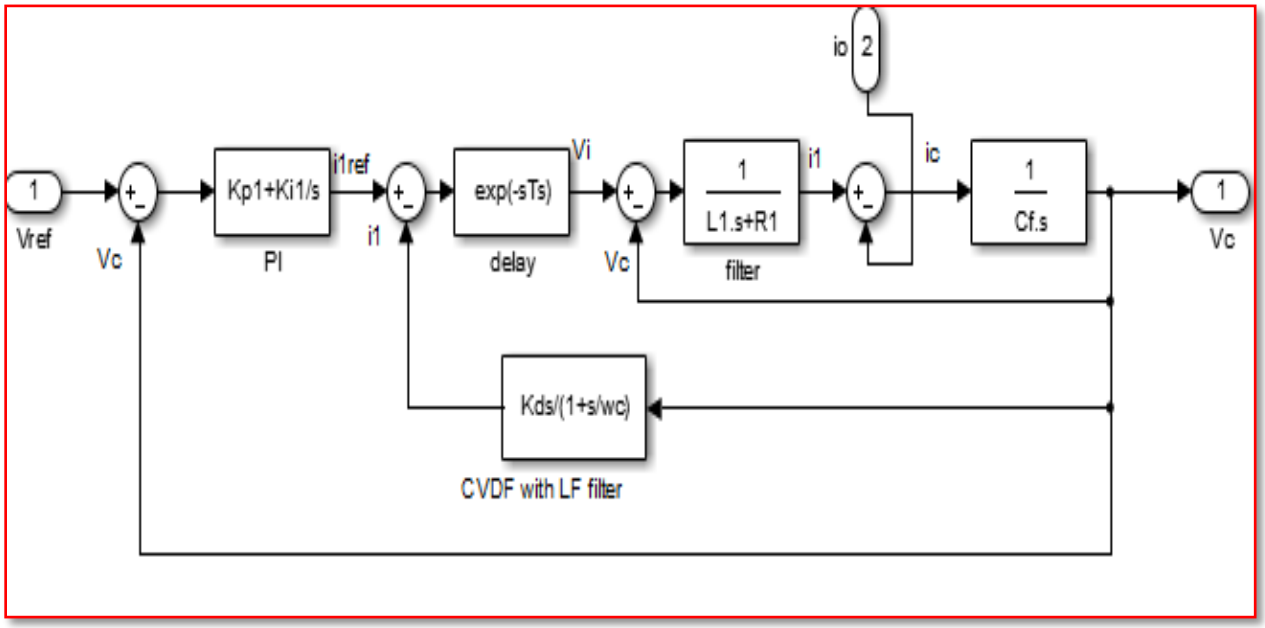

Figure 5.7 Bode diagrams of capacitor voltage differential feedback with low pass filter

$$G_{vo\_Vgo}(s) = \frac{V_O}{V_{go}} = \frac{1}{L_1 C_f s^2 + R_1 C_f s + K_{ds}/(1+\frac{s}{\omega_c}) + 1} = \frac{\omega^2{}_n}{s^2 + 2\varepsilon\omega_n s + \omega^2{}_n} \tag{5.3}$$

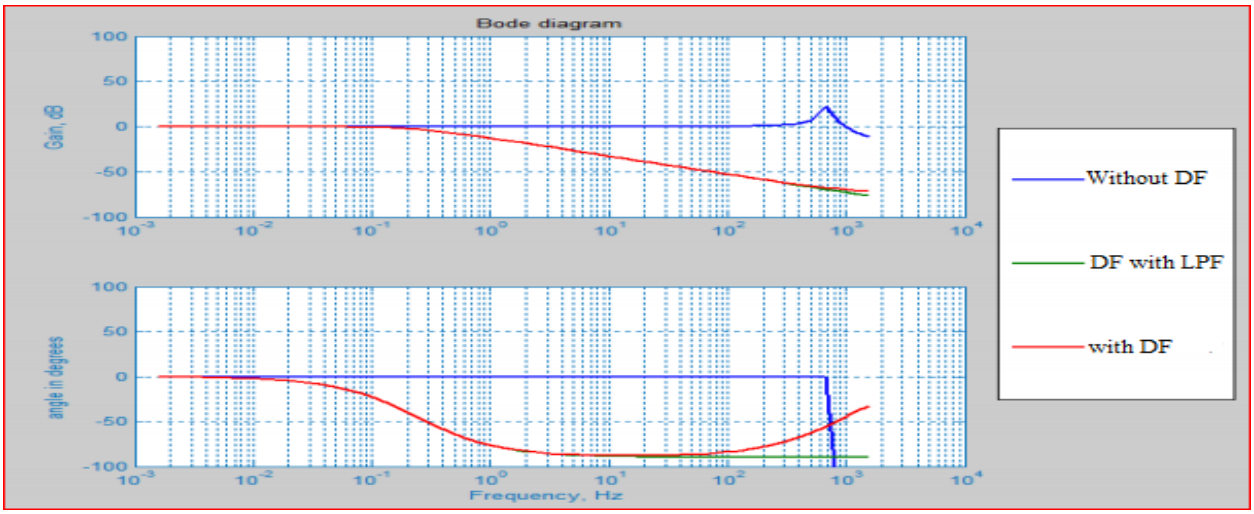

Figure 5.8 Bode diagrams of inner open loop transfer function

However, the differential function will enlarge some small disturbance in the output voltage, especially in the high frequency range so as to cause stability problem. Hence a low pass filter (LPF) is introduced to use with differential feedback to eliminate the high frequency disturbance, as shown in Figure 5.8. Figure 5.9 shows the bode diagrams of inner current loop transfer function without considering the control delay and voltage differential feedback (DF),with voltage DF and with voltage DF and low pass filter (LPF). As indicated, the voltage differential feedback eliminates the high resonant peak of output L-C filter. Moreover, using low pass filter increases the phase margin at crossover frequency hence improves the system stability.

5.5.1.3 Voltage reference feed-forward in the outer loop

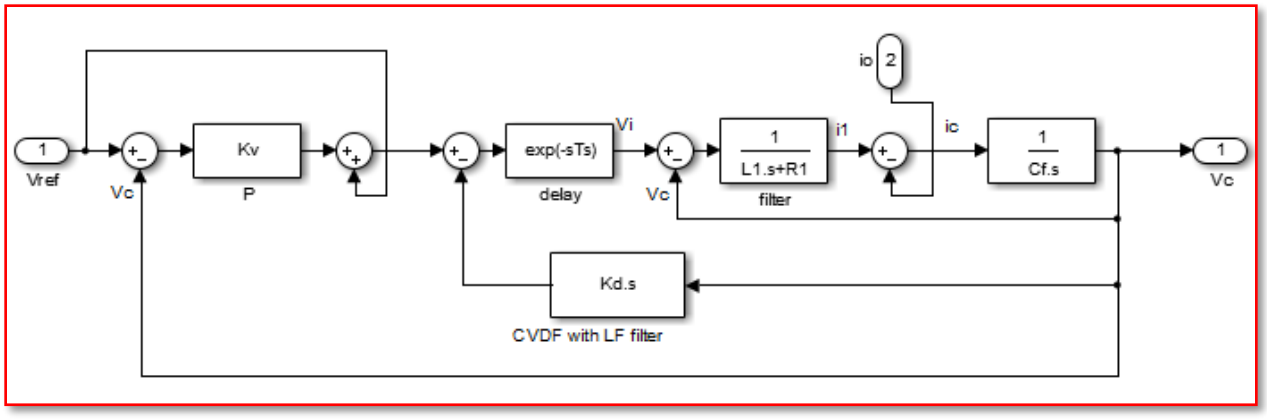

Figure 5.9 Proportional compensator plus feed-forward control strategy

Considering the transient performance when the inverter changes from grid-connected operation mode to standalone mode, with proposed outer voltage PI controller, the initial output voltage is zero which causes the voltage fall to zero immediately after the mode switching. So the voltage waveform becomes discontinuous in transition. In order to overcome this disadvantage, a voltage reference feed-forward path is added to the outer loop, which is shown in Figure 5.9. The reference voltage is generated by multiplication of voltage amplitude and phase angle which is synchronized with grid voltage in grid-connected operation mode. So the initial output voltage of this system which is equal to the feed forward reference voltage is in phase with grid voltage at the moment of control mode switching. Hence it maintains the continuity of voltage waveform.

In addition, the feedforward path can also improve the steady-state performance. Without feedforward path, the outer loop gain needs to be designed to be a large value to obtain small steady-state error which will make the system face stability problem. Moreover, feedforward path can enhance the dynamic response which is beneficial in transition process or nonlinear load case. Also, a single proportional controller is used instead of PI controller to reduce the harmonics in the waveform which is analyzed as follows. With considering the control delay, the output voltage-to-reference voltage and output voltage-to-load current transfer function can be expressed as follows:

$$V_O(s) = G'_{vo\_vref}(s).V_{ref} - G'_{vo\_io}(s).i_O$$

$$= \frac{(1+K_v)e^{-sTs}}{L_f C_f s^2 + (R_f C_f + K_d e^{-sTs})s + K_v e^{-sTs} + 1} v_{ref} - \frac{L_f s + R_f}{L_f C_f s^2 + (R_f C_f + K_d e^{-sTs})s + K_v e^{-sTs} + 1} io \quad (5.4)$$

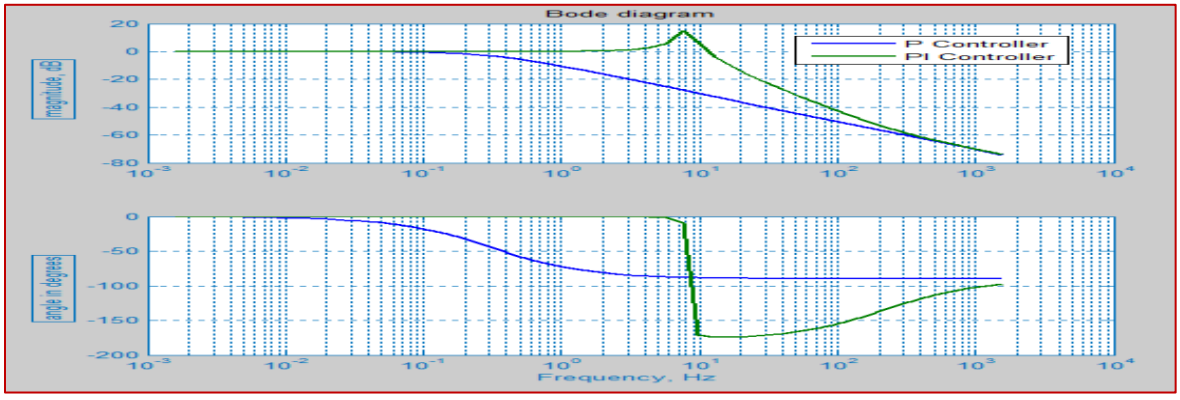

Figure 5.10 Bode diagrams of G'$_{vo\_Vref(s)}$ with P and PI controller

Figure 5.10 compares the voltage closed-loop transfer function with P and PI controller. With PI controller in which are considered for analysis are K_{po}= 0.3, K_{io}= 1,800, there is a peak at frequency about 10Hz. It raises the portion of the harmonics in the output voltage. The peak magnitude decreases as K_i decreases and it decreases to zero when K_i=0. Also with only P controller, the magnitude gain keeps around 0 dB thus the steady-state error stays in a reasonable range. So using a single proportional controller can reduce the harmonic components in the output voltage and still track the reference voltage very well.

5.5.2. Controller design

5.5.2.1. Inner Current Controller Design

The inner loop controller design of multi-loop with capacitor differential feedback is consistent with the controller design of capacitor current feedback. The compensated open-loop transfer function of the inner current loop can be obtained as:

$$G_{c\_op}(s) = \frac{K_{p2} C_f e^{-sTs} s}{L_f C_f s^2 + R_f C_f s + 1} \tag{5.5}$$

Where, K_{p2} is the gain of current controller.

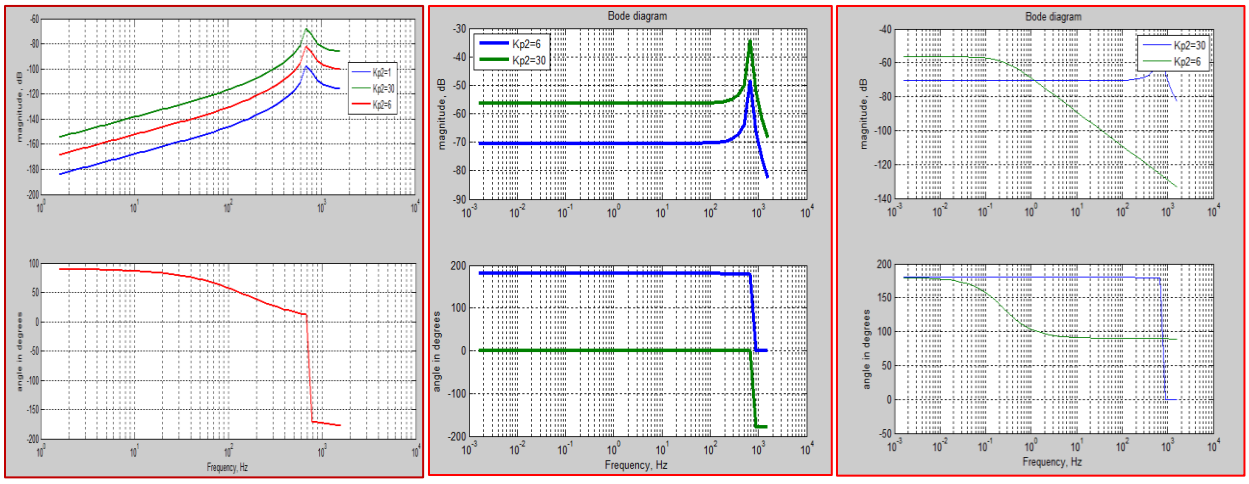

(a) (b) (c)

Figure 5.11 Bode diagrams of inner loop transfer function (a) open loop without delay (b) open loop with delay (c) closed-loop without delay at different K_{p2}

Inner current open-loop at proportional gain K_{p2}=6, 30 for no load case (worst case condition). As K_{p2} increases, the high resonant peak increases which make it hard to design the outer voltage control loop to achieve good system stability and dynamic response. However, the resonant peak can be eliminated by closed-loop control. The compensated closed-loop transfer function of the inner current loop is:

$$ic = \frac{K_{p2} e^{-sTs} C_f s}{L_f C_f s^2 + (K_{p2} e^{-sTs} + R_f) C_f s + 1} i_{cref} - \frac{L_f C_f s^2 + C_f R_f s}{L_f C_f s^2 + (K_{p2} e^{-sTs} + R_f) C_f s + 1} i_o \qquad (5.6)$$

Where i_{cref} is current reference generated by voltage loop, i_c is capacitor current and i_o is the load current.

The design goal of inner current closed-loop in a multi-loop control is to obtain a high loop bandwidth to achieve enough stability margins rather than to obtain a small tracking error. So the current controller is designed to be a single proportional controller. Figure 5.11 (a) shows the bode diagrams of current closed-loop transfer function at different K_{p2} values without considering the control delay. As indicated, the bandwidth can be widen and also the phase error can be reduced through increasing the proportional gain K_{p2}. Ideally, the bandwidth of I_C/I_C^* should be maximized by using a higher K_{p2}, to achieve perfect reference tracking at all input frequencies, a faster dynamic response and the complete blocking of disturbance input from feeding forward to the output (I_C/I_{load}=0). In order to obtain unity gain from output frequency to half of the switching frequency, the gain value should be designed to be 30. However, in practice, a digital control implementation for above multiple-loop control method introduces a time delay, usually equal to one switching period T_s, which strongly limits the system bandwidth and affects the dynamic performance [21]. A high gain would degrade the control loop stability. This can be further verified by the bode diagrams of the current open loop with control delay at different K_{p2}, as shown in Figure 5.11(b). When K_{p2} =6, the phase margin is above 0^o; when K_{p2} =30, the phase angle at crossover frequency and the system become unstable. Based on this gain selection criterion K_{p2} is set as 6, which will give a reasonable closed-loop current gain I_C/I_{Cref} and negligibly small I_C/I_{load} gain at the fundamental frequency [42].

5.5.2.2 Outer Voltage Controller Design

For the outer voltage regulation loop, a PI controller is used to maintain high loop gain at low frequency and zero steady state error. The compensated open-loop voltage transfer function is:

$$G_{vop} = (K_{p1} + \frac{K_{i1}}{s}) \frac{K_{p2} e^{-sTs}}{L_f C_f s^2 + (K_{p2} e^{-sTs} + R_f) C_f s + 1} \tag{5.7}$$

, where K_{P1} and K_{i1} are parameters for PI controller. K_{p1} and K_{i1} are selected to obtain unit gain at this crossover frequency. Also, the zero of the PI compensator is set the same as the corner frequency of LC filter, resulting in the following equations:

$$\frac{K_{p1}}{K_{i1}} \approx \frac{1}{\sqrt{LC}}, \left| G_{vop(s)} \right|_{s=j2\prod fc1} = 1 \tag{5.8}$$

Which leads to K_{p1}=0.05, K_{i1}=300.

5.5.3. Advantage of Design

Compared to inductor current feedback strategy, capacitor current feedback has better disturbance rejection capability. If capacitor voltage differential term is used as inner current feedback variables, the closed-loop transfer function of the outer voltage loop can be expressed as

$$\begin{aligned} V_o = & \frac{(K_{p1}s + K_{i1}) K_{p2} e^{-sTs}}{L_f C_f s^3 + (K_{p2} e^{-sTs} + R_f) C_f s^2 + (K_{p1} K_{p2} e^{-sTs} + 1)s + K_{i1} K_{p2} e^{-sTs}} V_{ref} \\ & - \frac{L_f s^2 + R_f s}{L_f C_f s^3 + (K_{p2} e^{-sTs} + R_f) C_f s^2 + (K_{p1} K_{p2} e^{-sTs} + 1)s + K_{i1} K_{p2} e^{-sTs}} io \end{aligned} \tag{5.9}$$

Where V_{cref} is the given voltage reference and V_o is the output voltage. If inductor current is used as inner current feedback variables, the closed-loop transfer function of the outer voltage loop can be expressed as,

$$V_o = \frac{(K_{p1}s + K_{i1})K_{p2}e^{-sTs}}{L_f C_f s^3 + (K_{p2}e^{-sTs} + R_f)C_f s^2 + (K_{p1}K_{p2}e^{-sTs} + 1)s + K_{i1}K_{p2}e^{-sTs}} V_{ref}$$
$$- \frac{L_f s^2 + (K_{p2}e^{-sTs} + R_f)s}{L_f C_f s^3 + (K_{p2}e^{-sTs} + R_f)C_f s^2 + (K_{p1}K_{p2}e^{-sTs} + 1)s + K_{i1}K_{p2}e^{-sTs}} io \quad (5.10)$$

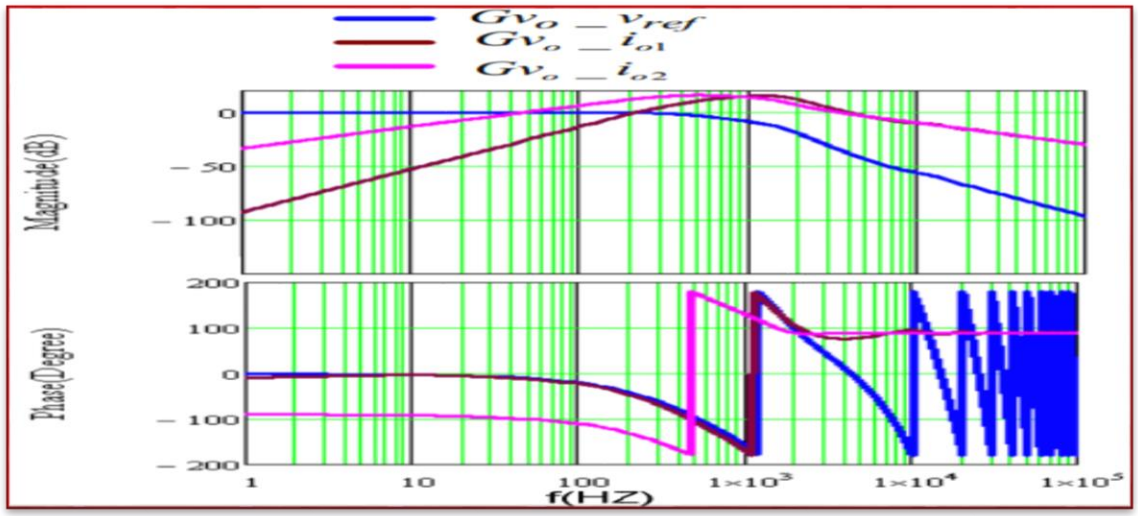

Figure 5.12 Bode diagrams of the outer voltage closed-loop transfer function with capacitor current or inductor current feedback as inner loop.

From equation (5.7) and (5.8), it is notable that in the capacitor current feedback and inductor current feedback, the output voltage-to-reference voltage transfer function G_{vo} is exactly the same, while the voltage-to-output current transfer function $G_{vo\_vref(s)}$ different from each other, where $G_{vo\_io1(s)}$ and $G_{vo\_io2(s)}$ are corresponding to (5.7) and (5.8) respectively. Figure 5.12 shows the bode diagrams of closed-loop voltage transfer function using two control schemes respectively. Obviously, capacitor current feedback strategy has lower gain at low frequency range for output voltage to load current than inductor current feedback strategy, which means it has much better disturbance rejection capability.

5.6 Multi-Loop controller with both voltage differential feedback and voltage and current decoupling through only output voltage feedback

5.6.1. Control Block Diagram

In [42], output voltage decoupling and output current decoupling by only using the output voltage feedback. The decoupling of output voltage and current makes the inner loop equivalent to a first order system. Thus the system will exhibit a fast dynamic response to load disturbance. With considering the control delay, the inner loop gain has to be designed smaller than the design value from pole placement technique, in order to raise the system stability margin. This scheme possesses very fast dynamic response at load step change and can also achieve good steady state performance at both linear and nonlinear loads. In addition, it only uses the output voltage as the feedback variable, which reduces the system complexity. This method is proved to be an effective solution for voltage control in standalone mode of grid-tie three phase voltage source inverters. The proposed new control block diagram has been shown in Figure 5.13.

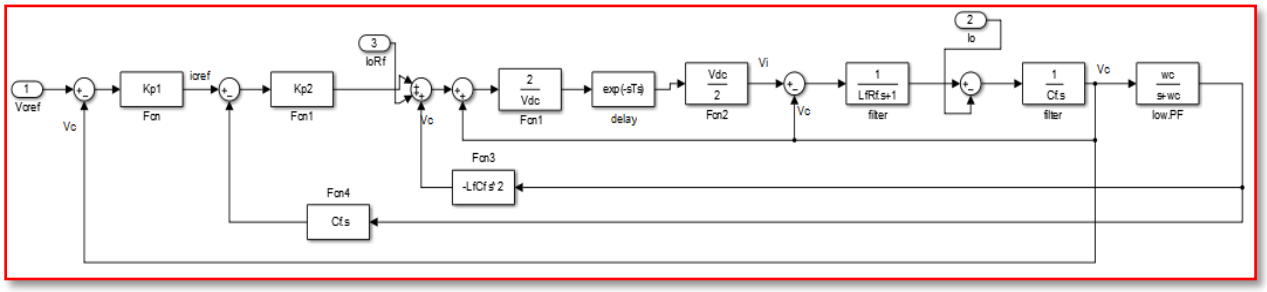

Figure 5.13 Control block diagram of proposed multi-loop controller

5.6.1.1 Output Voltage Decoupling

Except for the voltage differential feedback, in the inner loop, the sensed value of output voltage is positively feedback to decouple the output voltage in the augmented control plant in order to improve the system dynamic performance. It is also equivalent to feedback the integration value of capacitor current scaled by C_f .With this decoupling, only the voltage across the output inductor needs to be commanded. This will cause a relatively small voltage variation at load step change because the filter inductor impedance is small. In addition, since most of the inverter command v_i is constructed from the output voltage decoupling, the inner loop gain can be designed more robust.

Thus, the effect of phase delay introduced by the filtering in the capacitor current feedback will be reduced. In a word, system dynamic response will be faster with this output voltage decoupling. This can be further verified by comparing the root locus of the system with and without output voltage decoupling as follows [42].

Without v_C decoupling, the inner current closed-loop transfer function can be written as:

$$G_{ic\_icref} = \frac{sK_{p2}C_f}{s^2 L_f C_f + sC_f(r_f + K_{p2}) + 1} \tag{5.11}$$

With V_c decoupling, the transfer function becomes:

$$G_{ic\_icref2} = \frac{i_c}{i_{cref}} = \frac{K_{p2}}{sL_f + R_f + K_{p2}} \tag{5.12}$$

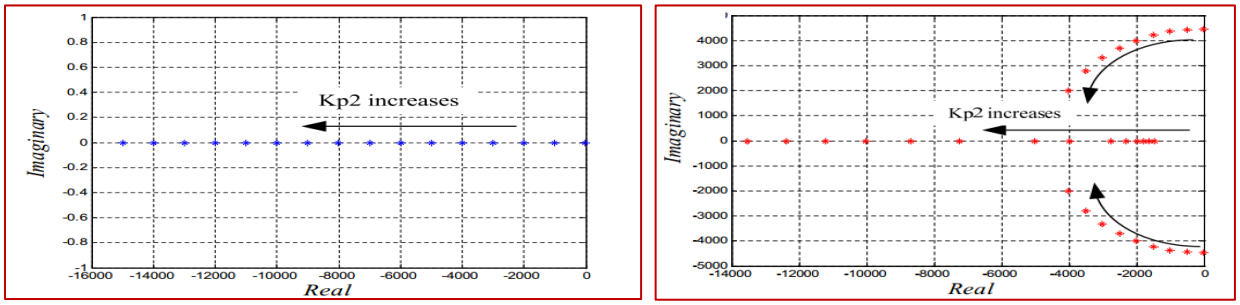

(a) (b)

Figure 5.14 Root locus of inner closed-loop when K_{p2} increases from 0 to 15 with step equal to 1 for System (a) With output voltage decoupling (b) Without output voltage decoupling .

The root locus of two systems when K_{p2} increases from 0 to 15 with step equal to 1 has been shown in Figure 5.14 (a) and (b). G_{ic_icref2} is a first order transfer function and all of its poles are on the negative real axis. Its biggest pole locates at s=-1 when K_{p2} =0. As K_{p2} increases, the poles are approaching infinity. G_{iC_iCref} is a second order transfer function, thus it has two poles at a fixed K_{p2} value. When K_{p2} is small, one pole moves far away from the imaginary axis on the real axis; another pole moves towards the real axis and far away from the imaginary axis from a location which has a big imaginary absolute value. Obviously, at the same K_{p2}, the poles of un-decoupled one locate closer to the y axis than the decoupled one, and with the same step, the dominant pole of the un-decoupled system moves less distances for real axis than the decoupled one. So it has

longer response time and higher overshoot value at step response. Also its large imaginary part of the dominant pole will cause the oscillation in the dynamic response. Simply saying, the additional zero at the nominator of the un-decoupled system reduces the damping ratio of the system and increases the system overshoot at step response. So the decoupling term can improve the system dynamic response.

5.6.1.2 Load current decoupling

The load current decoupling is implemented by the negative capacitor voltage second differential feedback, as shown in Figure 5.13, which is also equivalent to negative capacitor current differential feedback. It is an approximation to the positive load current differential feedback which can fully decouple the load current in the inner loop. The reason of this approximation is: the capacitor current, inductor current and load current satisfies the equation $i_L=i_C+i_O$; and the inductor current will keep almost constant at the load step change. So the derivative of load current is identical to the negative derivative of capacitor current $\frac{di_o}{dt} = -\frac{di_c}{dt}$. In addition, the observe value of output current could be used to decouple the resistance term in the feedback, considering that the resistance in the inductor is very small and the inaccurate observe value will not affect much. The estimated load current used here is shown in the following expression:

$$\hat{i_o} = (v^*_i - v_c)/(sL_f + r_f) - i_c \tag{5.13}$$

, in which v_i* represents the control command for the inverter.

This decoupling term provides an additional current loop command to produce the needed load current without waiting for errors in the voltage to occur, thus the system exhibit infinite dynamic stiffness up to the band width of the voltage modulator, provided that the estimation of the inductance L is accurate. It brings the load current in the closed loop thus increases the rejection gain for the load current disturbance. This also can be verified by the bode plot of disturbance to output transfer function of inner loop as shown in Figure 5.15. Without load current decoupling, the disturbance to output transfer function is:

$$G_{ic\_io1} = \frac{i_c}{i_o} = -\frac{sL_f + R_f}{sL_f + (R_f + K_{p2})} \tag{5.14}$$

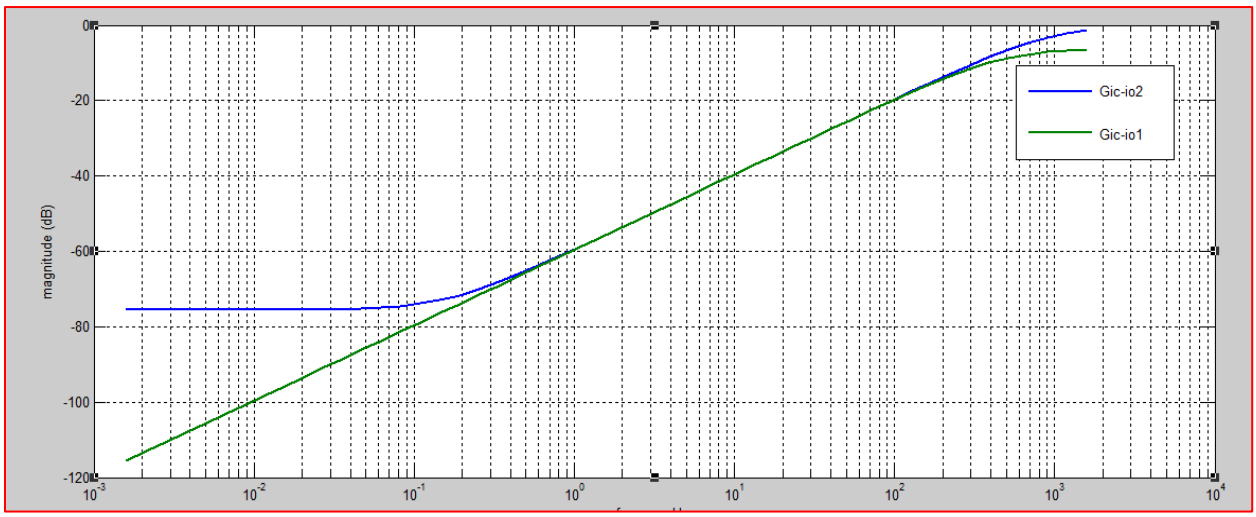

Figure 5.15 Bode plot for load current disturbance to output of inner current loop with and without load current decoupling

With load current decoupling, the transfer function becomes

$$G_{ic\_io2} = \frac{i_c}{i_o} = -\frac{sL_f}{s.2L_f + K_{p2}} \tag{5.15}$$

From the bode plot of these two transfer functions shown in Figure 5.15, it can be seen that at low frequency, two methods have the same output stiffness to the load current disturbance; while at higher frequency range, the controller with load current decoupling has higher dynamic stiffness, in another word, a unit change of io will cause less i_C change. This can also be recognized by observing the pole in the denominator of the transfer function. The pole has been shifted towards the imaginary axis by adding a load current decoupling loop, which also decreases the rate of change of i_C caused by io because the damping factor has been reduced.

5.6.1.3 Steady state performance

With the designed steady state error compared to others. Without capacitor current inner loop while with outer voltage loop by using PI controller, the closed loop transfer function is

$$Vc = \frac{K_{p2}(K_{p1} + K_{i1}/s)}{s^2 L_f C_f + sC_f r_f + ((K_{p1} + K_{i1}/s)K_{p2} + 1)} V_{cref} = G_{vI}(s)V_i(s) \tag{5.16}$$

With current inner loop while without output voltage and load current decoupling, the closed loop transfer function is

$$V_c(s) = \frac{K_{p1}K_{p2}}{s^2 L_f C_f + sC_f(r_f + K_{p2}) + (K_{p1}K_{p2} + 1)} V_{cref}(s) = G_{II}(s)V_i(s) \tag{5.17}$$

With current inner loop and also with output voltage decoupling and capacitor current negative decoupling:

$$V_c(s) = \frac{K_p 1 K_{p2}}{s^2.2L_f C_f + s(2r_f + C_f K_{P2}) + (K_{p1}K_{p2})} V_{cref}(s) = G_{vIII}(s)V_i(s) \tag{5.18}$$

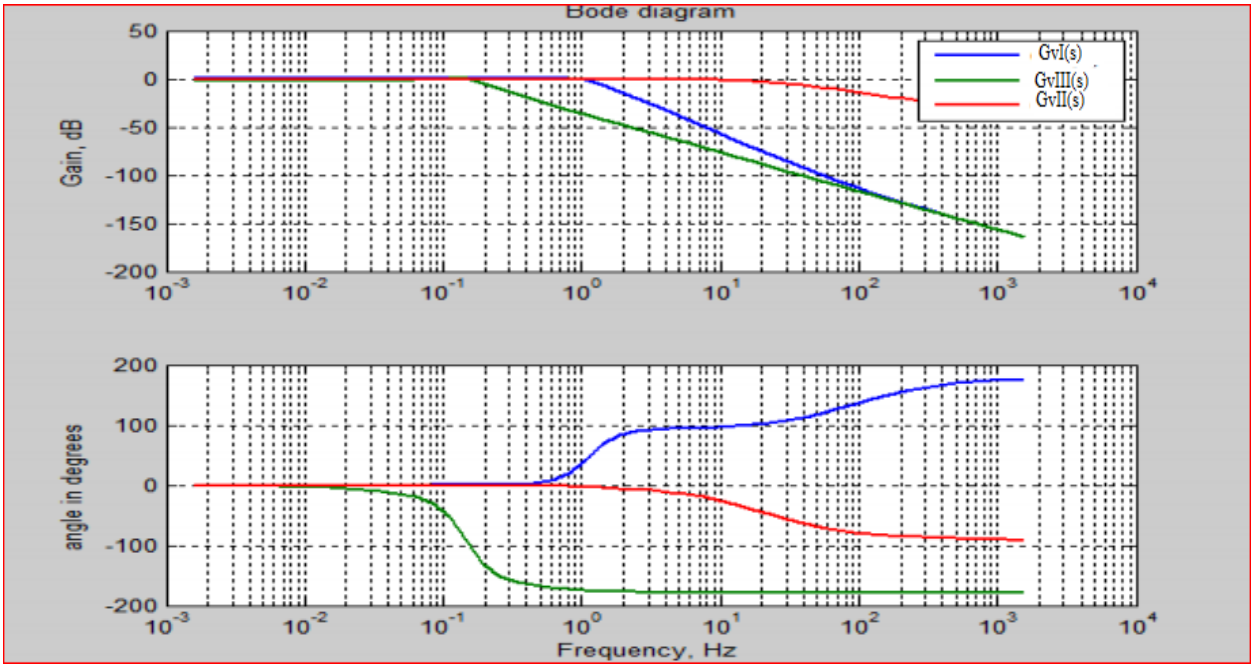

Figure 5.16 Bode plot of the closed-loop transfer function from voltage reference to output voltage with three control strategies

The bode plot of the control to output transfer function has been shown in Figure 5.16. Table 5.1 lists the controller gain used for the outer and inner loop. If estimated value of L_f, r_f and C_f are accurate, the controller will exhibit perfect tracking capability up to the bandwidth of the outer voltage loop. Without capacitor current loop, there is resonant peak at the corner frequency of L-

C filter. Without V_C and Io decoupling, the output cannot track the reference well. Also both of them have relatively high gain at high frequency. The proposed control method exhibits very small tracking error at both low frequency and also exhibits low gain at high frequency. So it can reduce the tracking error and lower the THD component in the output voltage very small tracking error at both low frequency and also exhibits low gain at high frequency. So it can reduce the tracking error and lower the THD component in the output voltage waveform.

5.6.1.4 Output Impedance

The closed-loop output impedance depends on the circuit configuration and also the control strategy. In this proposed controller, the output impedance can be expressed in equation (5.19) and the bode plot is shown in Figure 5.17.

$$\left|\frac{V_c}{i_0}\right| = \frac{sL_f + R_f}{s^2.2L_fC_f + s(K_{p2}C_f + r_fC_f) + K_{p1}K_{p2}} \tag{5.19}$$

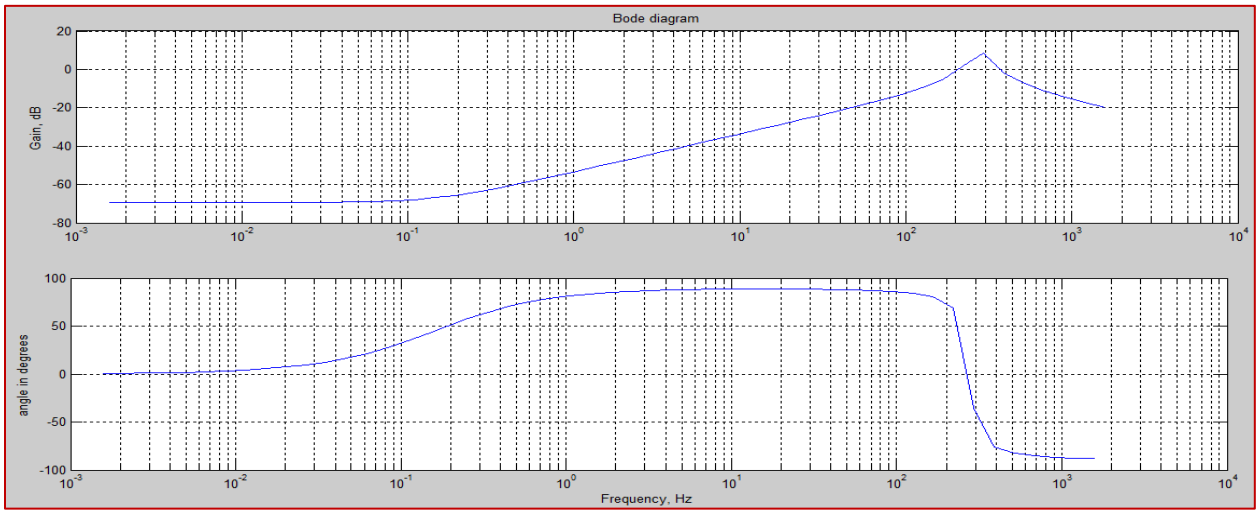

Figure 5.17 Output impedance of stand-alone system

The impedance phase at fundamental frequency 50Hz is 90 degrees. It means it has nearly pure inductance characteristics.

Table 5.1The considered constants for control system analysis (specifications)

Switching frequency	10kHz
Rated output frequency	50Hz
Dead time	1.5µs
Dc-link voltage	400V
Output phase voltage(rms)	400V(peak-to-peak)
Filter inductor and resister	
(L_f,Rf)	1mH,1mΩ Y_{con}
Filter capacitor(Cf)	50µF Ycon
Controller gains and parameters	
Inner loop gain Kp2	6
Integerator constants Ki	300
Load	*PF=0.5: R= 5Ω or 100 Ω, L 23mH*
Outer loop gain Kp1	0.05
Low pass filter cut off frequency ωc	6280rad/s

5.7 Simulation Results

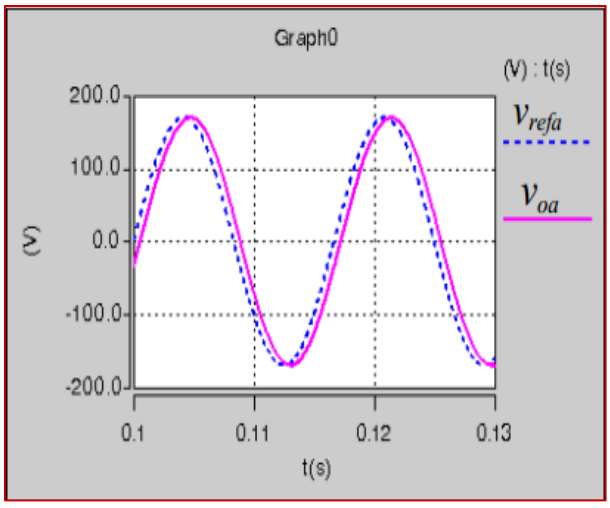

(a) $R =$ 100Ω (Y con.) with CVDF

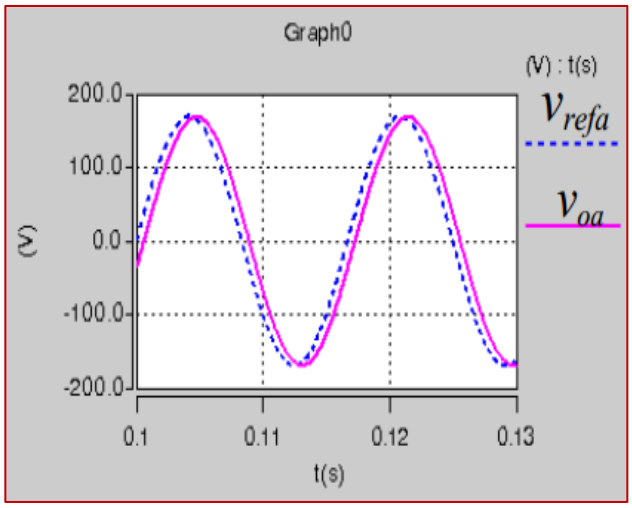

(b) $R =$ 5Ω (Y con.) with CVDF

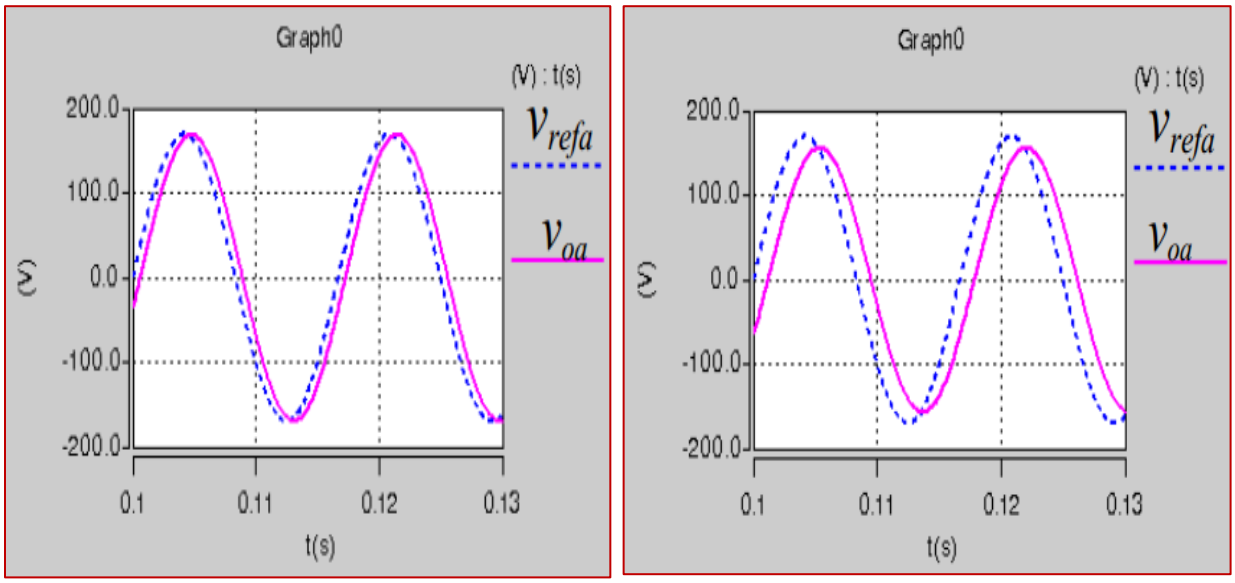

(c) R =100Ω (Y con.) with ICF (d) R = 5 Ω (Y con.) with ICF

Figure 5.18 Simulation results for output voltage (pink one) and reference voltage (blue one) at (a-b) capacitor voltage differential feedback (CVDF) (c-d) inductor current feedback (ICF)

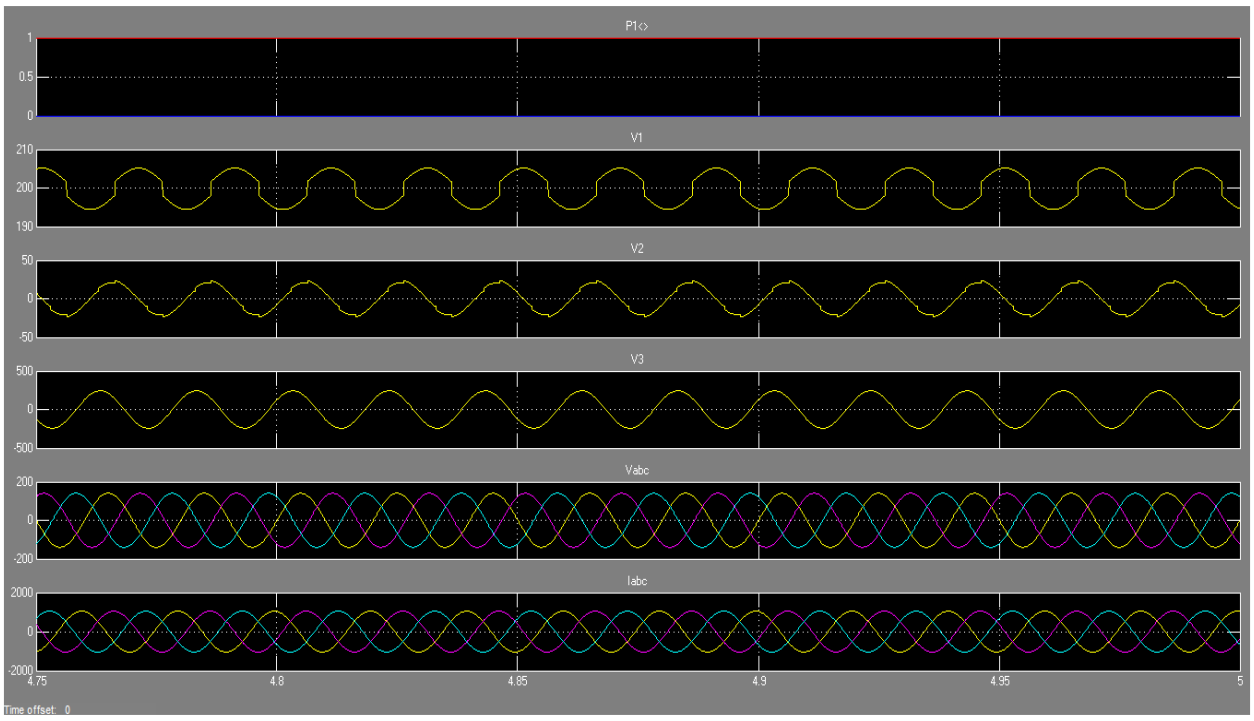

Figure 5.19 Output voltage and current with RL load with the multi-loop controller with voltage differential and load voltage current decoupling with only output voltage feedback

Figure 5.19 shows the simulated output voltage at various load condition at different point of the model. It shows that the control loop has much better stiffness to the load disturbance. The simulation performances of the multi-loop controller which has both voltage differential feedback and voltage and current decoupling in the inner loop have been shown in Figure 5.19. Generally, this thesis proposes a multi-loop controller with voltage differential feedback, and with output voltage decoupling and output current decoupling by only using the output voltage feedback. The output voltage differential feedback loop actively damps the output LC filter resonance and thus increases the system stability margin. The decoupling of output voltage and current makes the inner loop equivalent to a first-order system and thus improves the system dynamic response to load disturbance. The pole placement technique has been used here to design the inner loop and outer loop gain, with considering the effect of system control delay. The proposed control scheme possesses very fast dynamic response at load step change and can also achieve good steady-state performance at both linear and nonlinear loads. In addition, it only uses the output voltage as the feedback variable, which reduces the system complexity. The theoretical conclusion has been verified by simulation results. This method is proved to be an effective solution for voltage control in stand-alone mode of three-phase micro-grid inverters.

CHAPTER SIX

6. CONCLUSION AND RECOMMENDATION

6.1 Conclusion

This study concerned on three specific objectives. The first is assessing renewable energy source potential, identifying options and modeling of DG feasible RES to provide electricity for Adama city- Ethiopia by harnessing power from renewable energy resources for sustainable energy supply to the area. The second is selecting the source type based on their optimization since the modeling of each energy source must be focused on the market available cost of source. The third is designing of the control system when distributed generators is working with utility grid system of the area. Therefore, based on the study the conclusion of each is here.

Electrifying the area is now and will remain as challenging assignment for developing countries like Ethiopia. To meet the energy requirement of the nation hybridizing renewable energy technologies can cater sustainable solutions. Currently, comparing renewable energy systems with conventional fuel powered plants and grid connected power systems, renewable hybrid schemes are not cost effective. Nonetheless, the necessity of environmental protection, farseeing the current living standard of the communities forced to bring wise solutions that are environmental friendly technologies, hence hybrid of PV/Wind/Fuel cell technologies are in the frontier. In Adama the current COE is much lower than the value obtained from hybrid DGs system considered in this thesis ($0.196/kWh) because the main source of energy in the country is hydro power, however due to economic constraints hydropower potential is not exploited fully to cover the electricity demand of the country. Thus, the implementation of other renewable energy sources like solar, wind and PEM fuel cell energy power systems can elevate the country's electric shortage. During the design of the DG hybrid system set-up it is done an optimization process based on the electricity load, climatic data sources, and economics of the power components in which the NPC has to be minimized to select an economic feasible power system. HOMER simulation result displayed the most economical feasible system sorted by NPC from top to down, the prime system ranked first has renewable fraction of 15 unit wind turbines with 100kW each rating power, 1000kW photovoltaic panel, and, 500kW fuel cell using 955,000kg hydrogen tank and 500kW converter are part of the system to fulfill the required estimated load demand per day.

In addition to modeling of micro-grid distribution generators, the grid connected of DG with smart controlling system is the good solution of the frequently interruption of the area. The proposed design control strategy for grid-connected inverter is capable to achieve high-quality dynamic and steady state performances under both linear and non-linear loads. Moreover, its design is also simple and requires only an accurate knowledge of output filter parameters. In general, a voltage & current controller is designed with interfacing control techniques one for grid-connected operation and the other for intentional islanding operation. An islanding-detection, which is responsible for the switch between the two controllers, is presented. In addition, it is shown that the response of the proposed control schemes is capable of maintaining the voltages and currents within permissible levels during grid connected and islanding operation modes. The simulation results show that the proposed control schemes are capable of maintaining the voltages within the standard permissible levels during grid-connected and islanding operation modes.

6.2 Recommendation

Comparing the current study and giving the direction for future work

- In this study efficiency of components, temperature and pressure effects both wind and solar resources are not considered, thus studying with the inclusion of these two parameters could be done in the future.
- The estimated load are taken for modeling each distributed generation. Thus, the exact number of households and appliances used by all the community services and households should be studied by interviewing the villagers.
- The accurate electricity load consumption by the specific community exposed to the study has to be calculated based on the availability of appliances in each household.
- Renewable energy technology components accurate cost data has to be obtained
- Further optimization analysis should be required when considering various sensitivity cases.
- For parallel inverter operations, the power sharing between several inverters should be taken into account. So an outer power loop should be added to both of the voltage loop in standalone mode and current loop in grid-connected mode.
- Also the droop control law needs to be adopted according to the output impedance of the inverter

- The effect of the transition from grid mode of operation to standalone operation should require further study
- Detail study of grid connected distributed generation also will require more analysis and design

References

[1] Worku, Solomon Derbie Gont and Getachew Biru, "ASSESSMENT OF POWER RELIABILITY AND IMPROVEMENT POTENTIAL BY USING SMART RECLOSERS," *Journal of EEA*, vol. 31, 2014.

[2] R. D. Patidar and S. P. Singh, "Active And Reactive Power Control And Quality Management In DG-grid Interfaced System," vol. 4, no. 3, pp. pp.81-90, May 2009.

[3] EEPCO, "Power Sector Market Report," Ethiopia, Adiss Ababa, 2013.

[4] Samuel Tesema, GetachewBekele, "Resource Assessment and Optimization Study of Efficient Type Hybrid Power System for Electrification of Rural District in Ethiopia," *International Journal of Energy and Power Engineering*, vol. 3, no. 6, pp. 331-340, 2014.

[5] M. M. Tefera, "food security attainment role of urban agriculture: a case study from Adama town, central Ethiopia," *Journal of Sustainable Development in Africa*, vol. 12, no. 3, 2010.

[6] F. Mohamed, "MICROGRID MODELLING AND SIMULATION," March 2006.

[7] H. Musa, "A Review of Distributed Generation Resource Types and Their Mathematical Models for Power Flow Analysis," *Published online,* pp. 174-18, July 1, 2015.

[8] M. F. Akorede, H. Hizam, and E. Pouresmaeil, " "Distributed energy resources and benefits to the environment,Renewable and Sustainable Energy Reviews," vol. 14, pp. 724-734, 2010.

[9] T. J.H., "Modeling distributed generations in three phase distribution load flow," *IEE Proceeding Generation Transmission Distribution,* vol. 2, no. 3, p. 330–340, 2008.

[10] L. Priyadarshanee, "modeling and control of hybrid ac/dc micro grid," Rourkela, 2012..

[11] Omeje, C.O., Esobinenwu, C.S, "Simulation Study of A Grid Connected Hybrid PulseWidth Modulated Multi-Level Converter for A Distributed Power Generation," vol. 3, no. 10, 2014.

[12] Sougata Sen, Indrajit Koley, Pritam Chowdhury, Dr.Pradip Kumar Saha, Dr.Gautam Kumar Panda, "modelling,simulation and control of a non conventional fuel cell power generation system by varying oxygen pressure using matlab," *International Journal of Advanced Research in Electrical,*

Electronics and Instrumentation Engineering, vol. 2, no. 4, pp. 1231-1239, Vol. 2, Issue 4, April 2013.

[13] Maria Outeiro and A.Carvalho, "MatLab/Simulink as design tool of PEM Fuel Cells as electrical generation systems," in *European Fuel Cell Forum,* Switzerland, July 2011.

[14] Mpatzelis Stratis, Modelling and Optimal Design of a Fuel Cell Energy Storage System using rejected energy by Wind Parks in isolated Electric Grids, Chania : epartment of Electronic and Computer Engineering,Technical University of Crete, 2009.

[15] Omessaad Elbeji, Mouna Ben Hamed, Lassaad Sbita, "PMSG Wind Energy ConversionSystem: Modeling and Control," *Department of Electric Automatic, National EngineeringSchool of Gabes, Gabes, Tunisia,* July 2014.

[16] J. W. &. S. T. Ackermann, " Wind Power in Power Systems.," *Ltd, Royal Institute of Technology, Stockholm Sweden,* 2005.

[17] J. Slootweg, *Wind Power: Modelling and Impact on Power System Dynamics,* Netherlands: PhD thesis,Technische Universiteit Delft, December 2003.

[18] "matlab/Simulink," 2010,2013.

[19] M. S. Panda, "fault analysis on maximum point power tracking based grid connected," 2013.

[20] J.G. Slootweg, S.W.H. de Haan, H. Polinder, and W.L. Kling, "Modeling wind turbines in power system dynamics simulations.," *In Power Engineering Society Summer Meeting, 2001.IEEE, Vancouver,Canada, 15-19,* vol. 1, p. 22 – 26, July 2001.

[21] Q. Lei, " high performance control of inverter interfaced distributed generation," *Michigan State University,* 2012.

[22] Cornelis A. Plet, Maria Brucoli, John D.F. McDonald and Timothy C. Green, "fault models of inverter-interfaced distributed generators: experimental verification and application to faultanalysis," 2012.

[23] Zhixin Miao, Alexander Domijan, Lingling Fan, "investigation of Microgrids with Both Inverter Interfaced and Direct AC Connected Distributed Energy Resources," 2011.

[24] T. Suman, "Modelling and Simulation of Micro Grid Equipped Based on Photo Voltaic /Fuel Cell Equipped with Power Electronic Interfaces," *International Journal of Research Studies in Science, Engineering and Technology,* vol. 1, no. 8, pp. 110-118, November 2014, .

[25] A. A. Salam, A. Mohamed and M. A. Hannan, "technical challenges on microgrids," vol. 3, no. 6, DECEMBER 2008.

[26] M. Jamil, S. M. Sharkh, M. Abusara, R. J. Boltryk, "robust repetitive feedback control of a three-phase grid connected inverter," *School of Engineering Sciences, University of Southampton,Highfield,Southampton SO17 1BJ,United Kingdom,* 2010.

[27] R. D. Patidar and S. P. Singh, "Active And Reactive Power Control And Quality Management In DG-grid Interfaced Systems," vol. 4, no. 3, pp. 81-90, MAY 2009.

[28] K.Jaganmohangoud,P.Varaprasada Reddy, "Power Quality Improvement of Load Connected Grid Interfaced Inverter by Using FLC Merged Cascaded Current–Voltage," *SSRG International Journal of Electrical and Electronics Engineering (SSRG-IJEEE)* , vol. 1, no. 9, November 2014.

[29] Tomas Hornik and Qing-Chang Zhong, Senior Member, IEEE, "A Current-Control Strategy for Voltage-Source Inverters in Microgrids Based on H∞ and Repetitive Control," *IEEE transactions on power electronics,* vol. 26, no. 3, pp. 943-952, March 2011.

[30] Juan C. Vasquez, Josep M. Guerrero,, "Adaptive Droop Control Applied to Voltage Source Inverters Operating in Grid-Connected and Islanded Modes," *IEEE transactions on industrial electronics,* vol. 56, no. 10, pp. 4088-4095, October 2009.

[31] Daniele Menniti, Ciro Picardi, Anna Pinnarelli and Domenico Sgrò, "Application of a suitable control strategy for grid-connected inverters to the power management of a Microgrid," *University of Calabria Italy* , vol. 11, pp. 250-265, February, 2010.

[32] Ashna Mohan, Dinto Mathew, Vidya M Nair,, "A Control Strategy for a Distributed Power Generation Microgrid Application," vol. 2, no. 1, pp. 395-402, 2013.

[33] I. R. E. A. (IRENA), THE POWER TO CHANGE:SOLAR AND WIND COST REDUCTION POTENTIALTO 2025, June 2016.

[34] Omar Hazem Mohammed, Yassine Amirat, Mohamed Benbouzid, Adel Elbast, "Optimal Design of a PV/Fuel Cell Hybrid Power System for the City of Brest in France," *IEEE ICGE,* pp. 119-123, 2014.

[35] PAUL GILMAN and PETER LILIENTHAL, "MICROPOWER SYSTEM MODELING WITH HOMER,Integration of Alternative Sources of Energy," *National Renewable Energy Laboratory,* 2006.

[36] F. Fazelpour, "Economic analysis of standalone hybrid energy systems for application in Tehran, Iran," *International Journal of Hydrogen Energy,* vol. 41, no. 19, pp. 7732-7743, 25 may 2016.

[37] M. H. Kebede, "dynamic modeling and techno-economic analysis of pv-wind-fuel cell hybrid power system: the case study of nifasso," July 2014.

[38] Anton Andonov, Lyubomir Antonov, "Modeling of an electrolyzer for a hybrid power supply system," *Science, Engineering & Education,Mathematics and Technical Sciences,University of Chemical Technology and Metallurgy, 8 Kl. Ohridski, 1756 Sofia, Bulgaria,* vol. 1, no. 1, pp. 36-38, 5 September 2016.

[39] S. Shokoohi, H. Bevrani,J. Moshtagh,S. Ahmad,, "Transient Stability Enhancement in Microgrids Including Inverter Interfaced Distributed Generations," vol. 12, 2015.

[40] G. Ofualagba, S.O. Otuagoma, "The Modeling of a Hybrid Wind-Microturbine Generation System," *International Journal of Scientific & Engineering Research ,ISSN2229-5518,* vol. 3, no. 6, June-2012.

[41] T. Haneyoshi, A. Kawamura, and R. G. Hoft,, "Waveform compensation of PWM inverter with cyclic fluctuating loads," *in Proc. IEEE IAS Annu. Meeting, Denver, CO,* p. 744–751, 1986.

[42] J. M. Carrasco, L. G. Franquelo, J. T. Bialasiewicz, E. Galvan, R. C. P. Guisodo, M. A. M.Prats, J. I. Leon, and N. Moreno-Alfonso,, "Power-electronics systems for the grid integration of renewable energy source: a survey," *IEEE Trans. Ind. Electron.,* vol. 53, no. 4, pp. 1002-1016, Aug. 2006.

Appendix

Technical Specs for a Schott Mono-250 Watt Solar Panel

Model: Perform Mono 250
Brand: Schott Solar
Product Type: **Solar Panels**

Made in the USA

Item:	Price:
1202401	$365.00 Qty: 1 add to cart

With a proven field performance, Schott's Perform™ Mono 250-watt solar panel is appropriate for residential, commercial or utility scale solar power applications -- large or small. This particular solar panel is made of monocrystalline solar cells, the solar panel's first generation solar technology.

The Perform Mono 250 is manufactured in the US, in their facility in Albuquerque, New Mexico, and qualifies for:

Model	Watts	Amps	Volts	Size LxW (Inches)	Weight (lbs.)	Item
Per from Mono 250	250	8.0	31.1	66.34 X 39.09 x 1.97	41.5	1202401

Technical Data Data at Standard Test Conditions (STC)	
Module type	250
Nominal power [Wp] † Pmpp	≥ 250

Voltage at nominal power [V] Vmpp	31.1
Current at nominal power [A] Impp	8.0
Open-circuit voltage [V] Voc	37.3
Short-circuit current [A] Isc	8.5
Module Efficiency [%] η	14.9
STC (1,000 W/m2, AM 1.5 cell temperature 25ºC)Power sorting tolerance (as measured by flasher): -0 Watts / +4.99 Watts	

Data at Normal Operating Cell Temperature (NOCT)	
Nominal power [Wp] Pmpp	178.3
Voltage at nominal power [V] Vmpp	27.7
Open-circuit voltage [V] Voc	33.7
Current at nominal power [A] Impp	6.4
Temperature [ºC] TNOCT	48
NOCT (800 W/m2, AM 1.5, wind speed 1 m/s, ambient temperature 20ºC)	

Data at Low Irradiation
At a low irradiation intensity of 200 W/m^2 (AM 1.5 and cell temperature 25ºC) 96% of the STC module efficiency (1000 W/m^2) will be achieved.

Data at Low Irradiation
At a low irradiation intensity of 200 W/m^2 (AM 1.5 and cell temperature 25ºC) 96% of the STC module efficiency (1000 W/m^2) will be achieved.

Temperature Coefficients	
Power [%/ºC]	-0.44
Open-circuit voltage [%/ºC]	-0.33
Short circuit current [%/ºC]	+0.03

Cost of Wind Energy

The financial services company Lazard reports in their 2016 Levelized Cost of Energy Analysis that wind energy is now one of the most affordable options for new electricity generation.

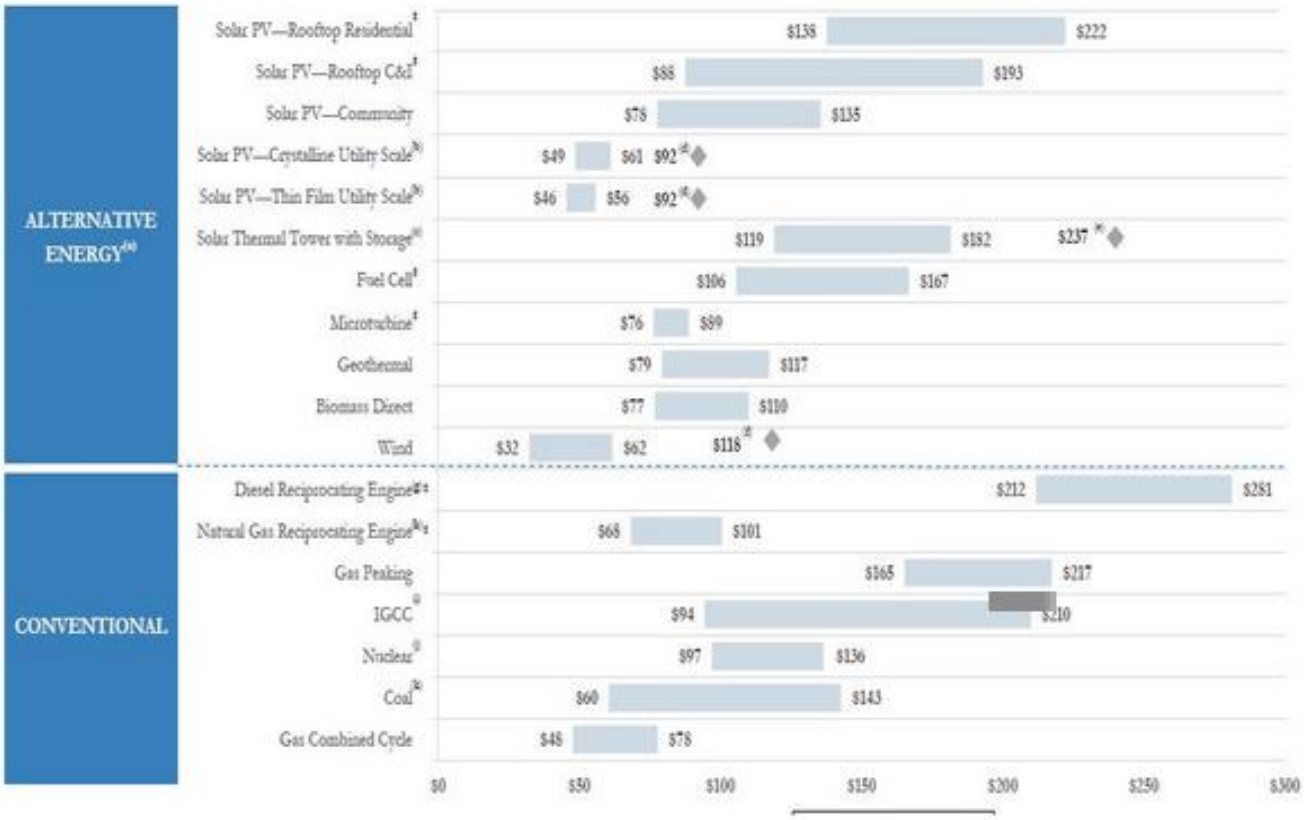

Source: Lazard's Levelized Cost of Energy Analysis - Version 10.0

HOMER SIMULATION OUTPUT

PV (kW)	FL100	FC (kW)	Conv. (kW)	Elec. (kW)	H2 Tank (kg)	Disp. Strgy	Efficiency Measures	Initial Capital	Operating Cost ($/yr)	Total NPC	COE ($/kWh)	Ren. Frac.	Capacity Shortage	FC (hrs)
1000	15	500	500	3400	955000	CC	No	$ 4,203,000	90,269	$ 6,942,790	0.196	1.00	0.00	1,780
1000	15	500	500	3400	955000	LF	No	$ 4,203,000	90,269	$ 6,942,790	0.196	1.00	0.00	1,780
1000	15	500	500	3400	955000	CC	Yes	$ 4,203,000	90,269	$ 6,942,790	0.196	1.00	0.00	1,780
1000	15	500	500	3400	955000	LF	Yes	$ 4,203,000	90,269	$ 6,942,790	0.196	1.00	0.00	1,780
1000	15	500	500	3400	955500	CC	No	$ 4,203,250	90,272	$ 6,943,131	0.196	1.00	0.00	1,780
1000	15	500	500	3400	955500	LF	No	$ 4,203,250	90,272	$ 6,943,131	0.196	1.00	0.00	1,780
1000	15	500	500	3400	955500	CC	Yes	$ 4,203,250	90,272	$ 6,943,131	0.196	1.00	0.00	1,780
1000	15	500	500	3400	955500	LF	Yes	$ 4,203,250	90,272	$ 6,943,131	0.196	1.00	0.00	1,780
1000	15	500	500	3400	955600	CC	No	$ 4,203,300	90,272	$ 6,943,198	0.196	1.00	0.00	1,780
1000	15	500	500	3400	955600	LF	No	$ 4,203,300	90,272	$ 6,943,198	0.196	1.00	0.00	1,780
1000	15	500	500	3400	955600	CC	Yes	$ 4,203,300	90,272	$ 6,943,198	0.196	1.00	0.00	1,780
1000	15	500	500	3400	955600	LF	Yes	$ 4,203,300	90,272	$ 6,943,198	0.196	1.00	0.00	1,780
1000	15	500	500	3400	956000	CC	No	$ 4,203,500	90,275	$ 6,943,472	0.196	1.00	0.00	1,780
1000	15	500	500	3400	956000	LF	No	$ 4,203,500	90,275	$ 6,943,472	0.196	1.00	0.00	1,780
1000	15	500	500	3400	956000	CC	Yes	$ 4,203,500	90,275	$ 6,943,472	0.196	1.00	0.00	1,780
1000	15	500	500	3400	956000	LF	Yes	$ 4,203,500	90,275	$ 6,943,472	0.196	1.00	0.00	1,780
1000	15	500	500	3500	955000	CC	No	$ 4,213,000	90,405	$ 6,956,935	0.197	1.00	0.00	1,780
1000	15	500	500	3500	955000	LF	No	$ 4,213,000	90,405	$ 6,956,935	0.197	1.00	0.00	1,780
1000	15	500	500	3500	955000	CC	Yes	$ 4,213,000	90,405	$ 6,956,935	0.197	1.00	0.00	1,780
1000	15	500	500	3500	955000	LF	Yes	$ 4,213,000	90,405	$ 6,956,935	0.197	1.00	0.00	1,780
1000	15	500	500	3500	955500	CC	No	$ 4,213,250	90,408	$ 6,957,276	0.197	1.00	0.00	1,780
1000	15	500	500	3500	955500	LF	No	$ 4,213,250	90,408	$ 6,957,276	0.197	1.00	0.00	1,780
1000	15	500	500	3500	955500	CC	Yes	$ 4,213,250	90,408	$ 6,957,276	0.197	1.00	0.00	1,780
1000	15	500	500	3500	955500	LF	Yes	$ 4,213,250	90,408	$ 6,957,276	0.197	1.00	0.00	1,780
1000	15	500	500	3500	955600	LF	No	$ 4,213,300	90,409	$ 6,957,344	0.197	1.00	0.00	1,780
1000	15	500	500	3500	955600	CC	Yes	$ 4,213,300	90,409	$ 6,957,344	0.197	1.00	0.00	1,780
1000	15	500	500	3500	955600	LF	Yes	$ 4,213,300	90,409	$ 6,957,344	0.197	1.00	0.00	1,780
1000	15	500	500	3500	956000	CC	No	$ 4,213,500	90,411	$ 6,957,617	0.197	1.00	0.00	1,780
1000	15	500	500	3500	956000	LF	No	$ 4,213,500	90,411	$ 6,957,617	0.197	1.00	0.00	1,780
1000	15	500	500	3500	956000	CC	Yes	$ 4,213,500	90,411	$ 6,957,617	0.197	1.00	0.00	1,780
1000	15	500	500	3500	956000	LF	Yes	$ 4,213,500	90,411	$ 6,957,617	0.197	1.00	0.00	1,780
1000	15	500	500	3600	955000	CC	No	$ 4,223,000	90,542	$ 6,971,080	0.197	1.00	0.00	1,780
1000	15	500	500	3600	955000	LF	No	$ 4,223,000	90,542	$ 6,971,080	0.197	1.00	0.00	1,780
1000	15	500	500	3600	955000	CC	Yes	$ 4,223,000	90,542	$ 6,971,080	0.197	1.00	0.00	1,780
1000	15	500	500	3600	955000	LF	Yes	$ 4,223,000	90,542	$ 6,971,080	0.197	1.00	0.00	1,780
1000	15	500	500	3600	955500	CC	No	$ 4,223,250	90,545	$ 6,971,421	0.197	1.00	0.00	1,780
1000	15	500	500	3600	955500	LF	No	$ 4,223,250	90,545	$ 6,971,421	0.197	1.00	0.00	1,780
1000	15	500	500	3600	955500	CC	Yes	$ 4,223,250	90,545	$ 6,971,421	0.197	1.00	0.00	1,780
1000	15	500	500	3600	955500	LF	Yes	$ 4,223,250	90,545	$ 6,971,421	0.197	1.00	0.00	1,780
1000	15	500	500	3600	955600	CC	No	$ 4,223,300	90,545	$ 6,971,490	0.197	1.00	0.00	1,780
1000	15	500	500	3600	955600	LF	No	$ 4,223,300	90,545	$ 6,971,490	0.197	1.00	0.00	1,780
1000	15	500	500	3600	955600	CC	Yes	$ 4,223,300	90,545	$ 6,971,490	0.197	1.00	0.00	1,780
1000	15	500	500	3600	955600	LF	Yes	$ 4,223,300	90,545	$ 6,971,490	0.197	1.00	0.00	1,780
1000	15	500	500	3600	956000	CC	No	$ 4,223,500	90,548	$ 6,971,762	0.197	1.00	0.00	1,780
1000	15	500	500	3600	956000	LF	No	$ 4,223,500	90,548	$ 6,971,762	0.197	1.00	0.00	1,780
1000	15	500	500	3600	956000	CC	Yes	$ 4,223,500	90,548	$ 6,971,762	0.197	1.00	0.00	1,780
1000	15	500	500	3600	956000	LF	Yes	$ 4,223,500	90,548	$ 6,971,762	0.197	1.00	0.00	1,780
1000	15	500	1000	3400	955000	CC	No	$ 4,223,000	90,881	$ 6,981,369	0.197	1.00	0.00	1,780